2015

Analytical and Numerical Validation of Nozzle Spray Measurement Data Obtained from a Newly Developed Production System

Iddrisu Seidu
Cleveland State University

ANALYTICAL AND NUMERICAL VALIDATION OF NOZZLE SPRAY MEASUREMENT DATA OBTAINED FROM A NEWLY DEVELOPED PRODUCTION SYSTEM

IDDRISU SEIDU

Bachelor of Mechanical Engineering

Cleveland State University

May, 2013

Submitted in partial fulfillment of requirements for the degree

MASTER OF SCIENCE IN MECHANICAL ENGINEERING

at the

CLEVELAND STATE UNIVERSITY

December, 2015

We hereby approve this thesis for

Iddrisu Seidu

Candidate for the Master of Science in Mechanical Engineering degree for the

Department of Mechanical Engineering

and the CLEVELAND STATE UNIVERSITY

College of Graduate Studies

Thesis Chairperson, Dr. Mounir Ibrahim

Department & Date

Thesis Committee Member, Dr. Vikram Shyam

Department & Date

Thesis Committee Member, Dr. Ralph J. Volino

Department & Date

Student's Date of Defense: August 6, 2015

ACKNOWLEDGEMENTS

First and foremost, I would like to thank the great coordination efforts from my advisory committee consisting of committee chair, Dr. Mounir Ibrahim of Cleveland State University, and committee members Dr. Vikram Shyam of NASA Glenn Research Center, and Dr. Ralph Volino of the US Naval Academy.

Secondly, I would like to thank the Parker Hannifin Corporation, Gas Turbine Fuel Systems Division for allowing me to conduct research and work on my experiments at their facility in Mentor, Ohio. Their expertise on atomization allowed me to absorb a lot of knowledge needed for this thesis. The following people have been immensely helpful –

- Raymond D'Arcy
- Georges El Helou
- Ravi Gudipati
- Amanda Kennard
- Wes Latuch
- Adel Mansour
- Tom Ray
- Ed Schanz
- Andy Sczypta
- Erlendur Steinthorssen
- Jeff Wovkulich
- Ed Zdankiewicz

and countless others who are not listed.

Finally, I would like to thank my loved ones, family, and friends for their very colorful, inspirational support of me throughout this entire process.

ANALYTICAL AND NUMERICAL VALIDATION OF NOZZLE SPRAY MEASUREMENT DATA OBTAINED FROM A NEWLY DEVELOPED PRODUCTION SYSTEM

IDDRISU SEIDU

ABSTRACT

A newly developed production test stand for measuring the spray angle of a pressure swirl atomizer was constructed and used to measure a product line of these pressure swirl atomizers – the macrospray atomizer. This new test stand, utilizing constant temperature hot wire anemometers, captures the spray angle data based on the voltage drop the hot wire probes see as they traverse the spray cone of the atomizer and as fluid droplets impinge upon the wire. Datasets acquired from the experiments are compared and correlated with computational fluid dynamics (CFD) simulation data. In addition, angles obtained from another type of spray characterization technique, the spray angle device, are also compared to see how closely CFD can predict the angle as captured by this new stand and how reliable and independent of human error it is. Another nozzle with a pressure swirl atomizer, the conventional atomizer, is also simulated to compare its agreement with experimental values obtained from the spray angle device. Finally, the datasets are compared to understand if the CFD results, when compared to the two spray characterization techniques used in this thesis for both the nozzle and atomizer can be utilized to assist in future atomizer designs. For the macrospray atomizer, it was found through the experiments that

the hot wire stand predicts the spray angle more accurately within 10% error. The spray angle device measured the spray angles within an error of 29% while the CFD introduced more error into the spray angle measurement obtained, within 7% to 93%. The conventional atomizer was found to have an error up to 18% with CFD results and up to 28% with the manual spray angle device.

TABLE OF CONTENTS

NOMENCLATURE

$2\theta_m$ = spray angle (cone angle) [º]

ε = turbulent kinetic energy dissipation rate [$dimensionless$]

μ = dynamic viscosity [$\frac{kg}{m \cdot s}$]

υ = kinematic viscosity [$\frac{m^2}{s}$]

ρ = density of liquid [$\frac{kg}{m^3}$]

σ = surface tension [$\frac{N}{m}$]

A_a = air core area [m^2] [in^2]

A_o = exit orifice area [m^2] [in^2]

A_p = swirl port area [m^2] [in^2]

A_e = effective area [m^2] [in^2]

C_d = coefficient of discharge [$dimensionless$]

D_s = swirl chamber diameter [m] [in]

d_o = exit orifice diameter [m] [in]

E, V = voltage [V]

FN = flow number [$dimensionless$]

h = heat transfer coefficient [$\frac{W}{m^2 K}$] [$\frac{BTU}{ft^2 R}$]

i = current [A]

K = atomizer constant [$dimensionless$]

k = turbulent kinetic energy [$\frac{J}{kg}$]

L_d = droplet diameter [m] [in]

l_o = exit orifice length [m] [in]

L_s = swirl chamber length [m] [in]

m = mass [kg] [lb_m]

$\dot{m}$ = mass flow rate [$\frac{kg}{s}$] [$\frac{lb_m}{hr}$]

P = power [W] [$\frac{BTU}{minute}$]

ΔP = pressure drop [kPa] [psi]

Q = heat energy [kJ] [BTU]

R = resistance [Ω]

Re = Reynolds number [$dimensionless$]

T = temperature [℃] [°F]

t = time [s] [hr]

t_f = film thickness [m] [in]

V = velocity [m/s] [ft/s]

VoF = volume of fluid

~~V~~ = volume [m^3] [in^3]

~~$\dot{V}$~~ = volumetric flow rate [$\frac{m^3}{s}$] [$\frac{in^3}{s}$]

We = Weber number [$dimensionless$]

X = air core area to exit orifice area ratio [$dimensionless$]

LIST OF TABLES

LIST OF FIGURES

CHAPTER I

INTRODUCTION

1.1 Fluid Conveyance

Fluid conveyance or the transportation of fluid is what drives many of our energy and power transfer mechanical systems today in our ever-changing world. Organizations and industries globally are dedicated to producing and manufacturing systems that enable or assist these energy transfers. In addition to fluid conveyance for energy transfer purposes, other manufacturers specialize in applying this technique in the coating and spraying industries.

Parker Hannifin is a global engineering organization that designs and manufactures products, systems, and custom solutions for its customers. One of the corporation's groups, the aerospace group, develops many products for aircraft, including fluid control and delivery components. More specifically, its Gas Turbine Fuel Systems Division, has many years of experience in developing and designing fuel nozzles, a critical component of fluid conveyance.

Nozzles are one method of transporting fluid. Nozzles operate by driving pressurized fluid through an orifice. Because of the effectiveness of a nozzle's fluid transport characteristics, they are used in multiple applications, including the power generation, coating and paint applications. Mechanical engines are a significant source of these energy transfers. For engines to transfer the maximum amount of energy, the delivery of fuel to the engine must be controlled through nozzles, increasing efficiency. In the coating and painting industries, the objective would be to use an even coating of paint, solvent, or other fluid on the desired object.

Nozzles, have been shown over time with a multitude of experiments that they are one of the most crucial components of an engine and in controlling the fluid distribution. Nozzles begin the process of atomization – the breakup of fluid into very small, fine spherical droplets.

Atomization is of great importance to manufacturers dealing primarily with fluid delivery systems in the power generation, aerospace, and coating industries. This process ensures the engine or environment receives the proper amount of fluid.

In addition, monitoring and understanding how the products – nozzles – perform, is of utmost importance. The data collected from measuring can be instrumental in determining the success of a product when it enters the industry. It is for this reason that measurement and machine vision systems are of interest to many organizations. Ensuring that one's product always performs well at the lowest design acceptability is what separates reliable products from unreliable ones.

At first glance, the nozzles produced for the variety of industrial and commercial applications may seem very straightforward in understanding how the fluid flows. However, upon examination of nozzles and the conveyance of fluid from point A to B, it is realized that they are inherently complex, with geometry being the biggest influence on that complexity. This has led for the need to understand how exactly the geometry of these complex subsystems truly affect the spray conditions at and downstream of the outlet orifice.

Due to the common place usage of Parker's fuel nozzles, this thesis examines two of Parker's production nozzles, a macrospray atomizer and the conventional atomizer to provide useful data utilizing the CFD simulations and correlation of that data to the marketing data provided to customers. The production test stand in use for this thesis is based around hot wire anemometry.

1.2 Importance of Measurement Systems

Measurement systems are instrumental in ensuring the validity of a method, product, or any type of solution. The ability to confirm the desired output of any method, product, or solution allows its developer to alter or improve the process and to ensure that output occurs one hundred percent of the time. This concept of achieving as close-to-perfect results as possible one hundred percent of the time, is what drives lean manufacturing practices in industries globally.

Lean manufacturing is the method of minimizing the amount of waste in a manufacturing process. Waste in this sense can be, but is not limited to, materials, time,

and money. This idea of improving processes comes at a time when much of the world's focus has been turned towards efficiency in the workplace, specifically in the manufacturing sector. Techniques used primarily for experimental and academic purposes have found their way into manufacturing production settings.

Measurement systems can be divided into many categories. A category of importance in today's manufacturing world can be classified as machine vision systems. These systems are becoming much more commonplace in industrial settings where many of the same products are being produced and shipped out to customers. Since the 1970s, vision systems began their industrial usage as a way of identifying whether or not a product was satisfactory. Today, vision systems are used to inform the operator whether or not something is wrong with not just the product, but also the process. The process is just as important as the product itself due to the time invested into ensuring optimal product validation procedures.

New techniques have been developed over the course of the past few decades including upgrades to high-speed digital cameras, laser sheet imaging, lighting systems, and various other areas. Because of these improvements, it is now possible for manufacturers to fully adopt lean manufacturing practices by utilizing machine vision.

It is for these reasons that in order to quantify and qualify the nozzles produced, Parker has decided to use a hot wire anemometry based production test stand.

When it comes to spray characterization, visualization and characterization of fluid flow measurement systems and machine vision systems are an area of interest due to the details it can provide on the physical phenomena occurring within and on the stream.

1.3 Objective

This thesis attempts to understand three problems; the first problem is how accurately does the newly designed manufactured hot wire anemometry production test stand capture the data of interest – spray angle of the nozzle – and its agreement with CFD predicted data. The second problem, a subset of the first, is to compare how accurately the spray angle is predicted from the test stand to other types of spray measurement techniques.

The last problem of interest to this thesis is to understand the difference between spray angle measurement techniques if it exists, and if it can be traced back to the specific nozzle being measured. This will give a good judgment on the fidelity of the measurement techniques used.

Two nozzles will be used to carry out the experiment. The Parker Hannifin Macrospray atomizer nozzle, with a hollow cone spray atomizer, will be used with the newly developed stand in addition to using a spray angle device utilizing mechanical probes. The Parker Hannifin conventional atomizer, also with a hollow cone spray atomizer, will also be tested using only the spray angle device.

Figure 1: Left – Parker Macrospray Atomizer; Right – Parker Conventional Atomizer (Images courtesy of Parker Hannifin Gas Turbine Fuel Systems Division)

Table 1. Operating Conditions of Selected Atomizers

Nozzle	Fluid	Testing Inlet Pressure (psi)	Outlet Pressure (psi)
Macrospray Atomizer	Water	145	0
Conventional Atomizer	MILPRF 7024	100	0

CHAPTER II

BACKGROUND INFORMATION AND THEORY

2.1 Basics of Combustion

To understand atomization, another concept must be introduced beforehand. Combustion is the process of breaking the chemical bonds of the combination of hydrocarbons or fuel molecules and an oxidizer via heat energy, thereby releasing the chemical energy of the fuel molecules. While combustion does not relate to the coating and spraying industries, combustion has been one of the primary drivers of atomization research, making its explanation relevant.

Combustion is very important to the conversion of energy in heat engines. An example of this is the diesel engine. Diesel engines use a direct injection method where fuel, in a liquid-vapor form, is injected into the combustion chamber, along with the oxidizer, or ambient air. Within this combustion chamber, the heat along with a combination of high pressure breaks the chemical bonds of the hydrocarbon molecules. The combination of the oxidizer and fuel, reacts and combusts, creating an expansion of gas. When speaking

specifically of the diesel engine, the expansion of gas pushes against the piston in the combustion chamber, producing mechanical work for the overall system to use.

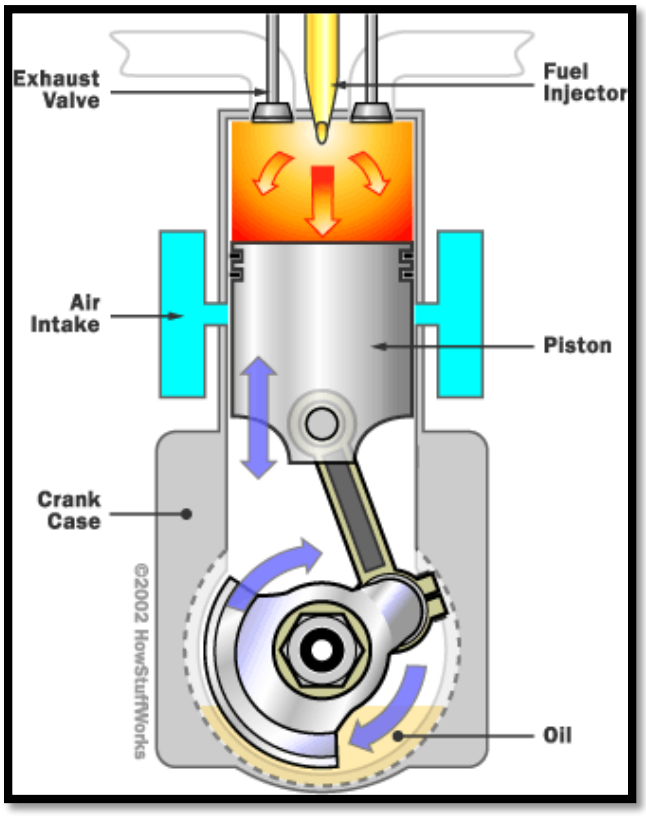

Figure 2: Combustion Process in Piston Cavity (Source: Howstuffworks.com)

Combustion is a process that has been refined over the years of its inclusion in work producing machines, or engines. Because of the release of chemical energy, the process can be inefficient and create soot and NO_X, having negative impacts on both the system and the outside environment. It is because of this that atomization became a topic of interest. Atomization has one of the greatest effects on the efficiency of the system when compared to other variables, including fuel type, oxidizer type, and oxidizer to fuel ratio.

2.2 Basics of Atomization

Since the creation of the internal combustion engine, research into fuels has been a large area of interest and in recent decades. That interest has morphed into using fuels outputting the least amount of by-products and harm to the environment. This shift in research has pushed the scientific community to evaluate how to use fuels more efficiently with atomization being one of the most important areas of study.

The research into droplet sizes became very prominent during the decades after the 1940s when popular usage of the gas turbine engine grew. Research into atomization provided information on how to burn fuels more lean, inject fuel at a range of pressures, and produce fewer by-products in the emissions of combustion systems. It is because of atomization that combustion systems achieve mixtures of fuel and air required by the design of the engine requiring its use.

Atomization is the primary purpose of nozzles. As defined earlier, atomization is the process of breaking up fluid into small droplets. In the case of power generation, fuel is more easily combusted and broken down when it has been fragmented into these small droplets, of which sizes typically range from 10 micrometers to 360 micrometers. It is the primary driver of energy transfer between the mechanical systems and energy storage, and thus needs to be very efficient. Nozzles conduct this process via a component called the atomizer. Atomizers are usually located near the tip of a nozzle, at the outlet orifice.

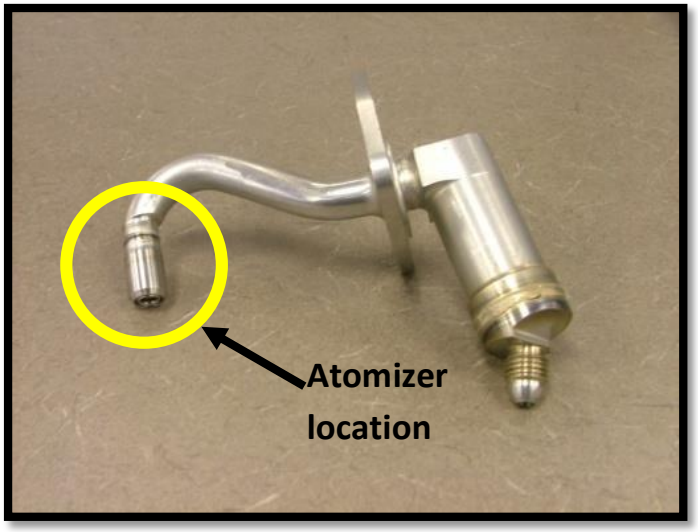

Figure 3: Atomizer Location Callout (Source: Parker Hannifin Gas Turbine Fuel Systems Division)

Fluid breakup through an atomizer is usually achieved through driving pressurized fluid across an atomizer or flowing high velocity air into the atomizer to assist the fluid breakup in conjunction with the pressurized fluid. Other methods for fluid breakup include mechanical component assistance. An example of this would be a rotating cup atomizer where fluid sits inside and is ejected from the cup due to the high angular velocity transferred from the rotational motion of the cup.

Previously stated, droplet sizes typically vary. For applications requiring small droplets (i.e. combustion, spray coating) the size of the droplets has a direct effect on the efficiency of the process. Therefore, it is pertinent to understand the steps in achieving small droplet sizes through dispersing the fluid.

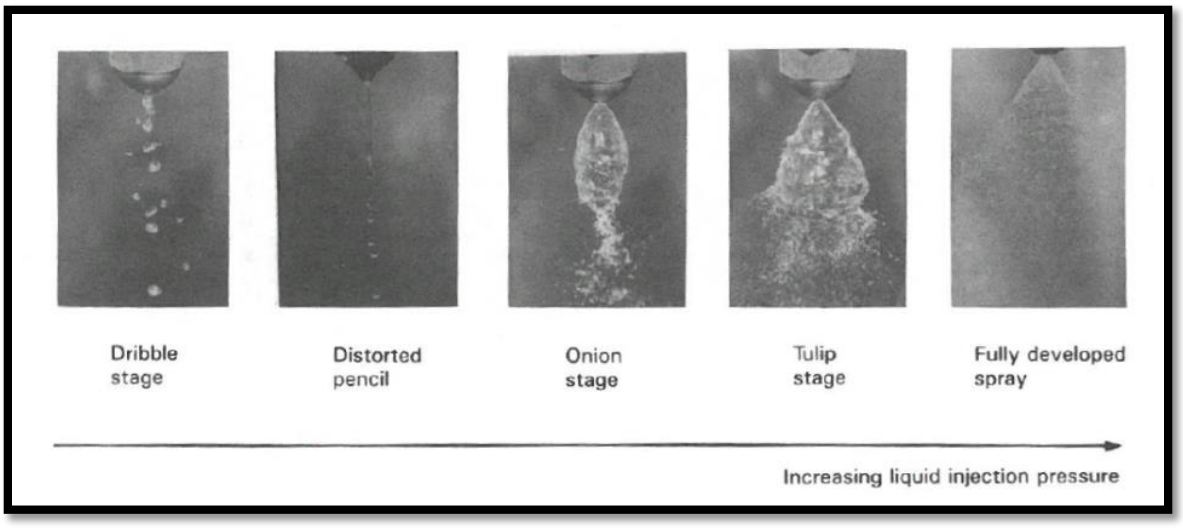

Figure 4: Atomization Process in Stages (Source: Atomization & Sprays)

The dispersion of a fluid medium through the process of atomization is as follows:

1. Dribble Stage
2. Distorted Pencil Stage
3. Onion Stage
4. Tulip Stage
5. Coarse Atomization Stage
6. Fine Atomization Stage

The previous terms for the different stages of atomization are colloquialisms used in industry and have no official names.

The primary physical phenomena driving the formation of the droplets, specifically, the differences between the onion stage and the fine atomization stage, is the surface tension driving the shape in the former, while momentum and inertia of the droplets drives the

latter stage. The tulip stage is the best representation of both phenomena occurring at the same time. The top half of the third frame in figure 4 shows the surface tension of the fluid driving the bulbous shape. The bottom half of the third frame of figure 4 shows how the inertia of the droplets is enough to break them away from the larger mass of fluid immediately above it. An increase in liquid injection pressure results in the successful completion of one stage and advancement to the next. It should be noted that during atomization, the stages cannot be seen as clearly as they are explicitly pictured in the previous figure. Due to the transient and turbulent processes occurring, the stages blend into one another.

Droplet size is a very significant area of research due to the effect fluid droplet sizes can have on the mixing of primary fluid into the secondary fluid medium, commonly air in most applications. Despite its significance on mixture of the primary fluid into the secondary fluid, droplet size will not be examined in this report as its effects cannot be measured directly due to the measuring capability of the test stand.

Interestingly, the dimensionless Weber number,We, is a ratio of the inertial forces to the surface tension forces.

$$We = \frac{\rho V^2 L_d}{\sigma} \quad \text{(Equation 2.1)}$$

Where ρ = flowing fluid density

V= fluid velocity

L_d = droplet diameter

σ= surface tension

Using this number gives insight into the formation of the stages of atomization and identifies the flow regimes.

2.3 Types of Atomizers

There are various methods to break up or atomize fluid and each fall under one of five categories. These categories include fixed orifice nozzles, variable orifice nozzles, airblast nozzles, air assist nozzles, and mechanically driven nozzles.

While the pressure differential of the fluid through the inlet port of an atomizer drives the fluid initially, the internal geometry of atomizers is the major influencer on the properties of fluid flow through an atomizer; however, the exit orifice determines the spray parameters downstream of the orifice. Fixed orifices induce an atomizer restriction on the exit orifice via a constant area. Variable orifices are usually mechanically driven designs where the outlet or inlet flow areas can be changed, typically using a spring or diaphragm to achieve this. This change in outlet flow area can affect the spray angle downstream.

Airblast atomizer nozzles use high velocity air to help the liquid break up as opposed to air assist atomizers which operate well at low fuel flow rates. Mechanically driven atomizers use mechanical devices such as rotating pistons or shafts to break up the fluid.

These atomizers can be further broken down into specialized categories based again on design intent and cost to manufacture. Notable examples include:

- Pressure atomizer
    - Plain orifice

    - Pressure swirl (simplex)
    - Duplex
    - Dual Orifice
    - Spill return
    - Fan spray
- Rotary
    - Spinning disk
    - Rotary cup
- Air Assist
    - Internal mixing
    - External mixing
- Airblast
    - Plain jet
    - Prefilming
- Ultrasonic
- Electrostatic

A brief overview of select atomizer types is given. However, due to the focus of this thesis, only pressure swirl atomizers are expanded upon. The reader is suggested to reference *Atomization and Sprays* by Arthur Lefebvre to gain an understanding of the basic physics and geometry of the other types.

2.4 Geometry of Atomizers

Pressure swirl atomizers, also called simplex atomizers, are typically designed with slots or "metering sections". These slotted sections impinge both a tangential and radial velocity on the fluid flowing through the channels. These additional velocity components give the fluid droplets at the outlet orifice added momentum to follow fluid path lines as designated by the internal geometry of the atomizer. Typical applications of these atomizers include diesel engine and gas turbine combustors. Many pressure swirl atomizers have metering sections at specified angles to produce the desired spray angle.

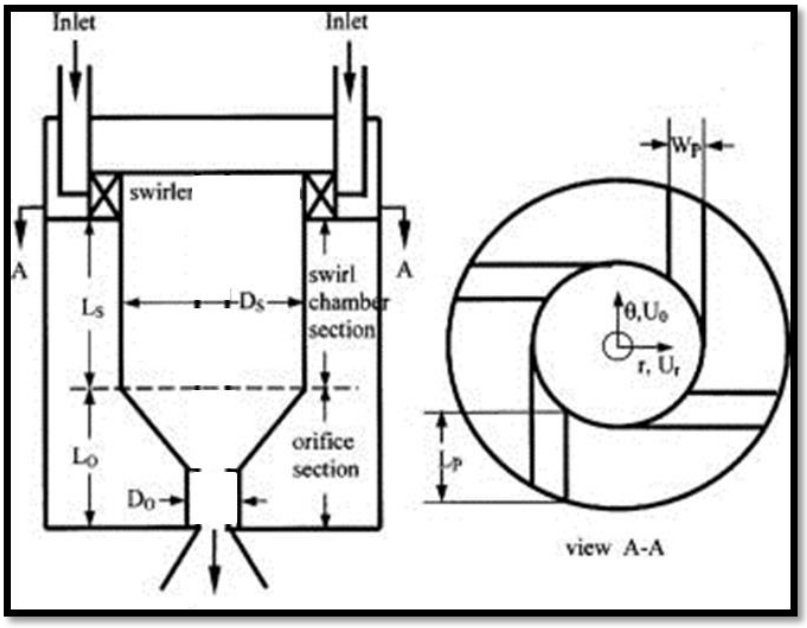

Figure 5: Pressure Swirl Atomizer Design (Source: Journal of Engineering for Gas Turbines and Power)

There are two types of pressure swirl atomizers – simplex and duplex nozzles. Simplex nozzles, similar to the previous figure, have one fluid path but have the disadvantage of a

10:1 flow range limitation. Flow range is the ratio of maximum flow output to minimum flow output of a nozzle.

Duplex nozzles have the advantage of reaching a 40:1 flow range. This feat is achieved by using two fluid paths versus one, each path having its own fluid supply. These types of nozzles have two metering sections, one with small slots and another with large slots. The small slots section is considered to be the primary, and the large slotted section is secondary. At low flows, the primary slots are used alone. After reaching a predetermined injection pressure, the secondary slots are opened, allowing for higher flow rates.

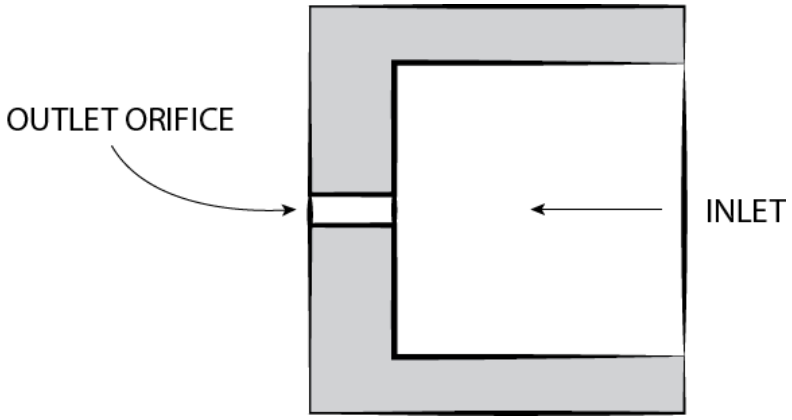

Figure 6: Plain Orifice Atomizer Design (Source: Wikipedia.org)

Plain orifice atomizers are popular in industry due to the simplicity of the design. As shown in figure 6, the diameters of the inlet and the outlet are the only two discernable features of interest and can be machined easily. Because of its simplicity, however, there are many drawbacks including the high supply pressure needed, its narrow spray angle, and it only being capable of producing a solid spray cone. Its applications include diesel engines, gas turbine engines, and various industrial applications such as furnaces.

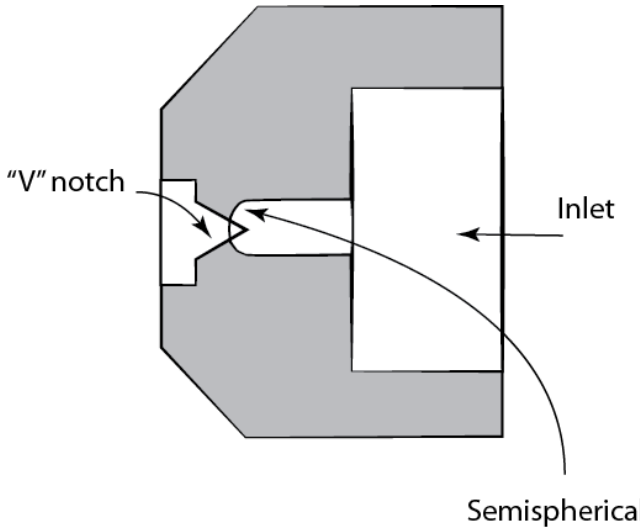

Figure 7: Fan Spray Atomizer Design (Source: Wikipedia.org)

Typical designs of fan spray atomizers are an adaptation of plain orifice atomizers as they include a "V" shaped notch that allows the exiting fluid to disperse at a wider angle. Fan spray atomizers are popular as they have very good atomization properties but come with the disadvantage of requiring high inlet pressures. These types of atomizers are used primarily in high pressure operations, such as coating processes.

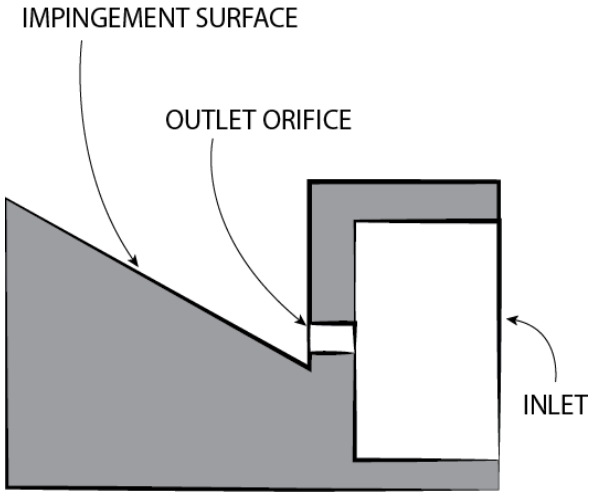

Figure 8: Surface Impinging Atomizer Design (Source: Wikipedia.org)

Surface impingement atomizers are of interest to designers who require spray angles to be within a certain range. Angles can easily be achieved based on the type of obstruction and geometry placed downstream of the outlet orifice. A huge disadvantage to these types of atomizers is the energy loss occurring from impinging the energized fluid onto an external orifice before it reaches its desired destination.

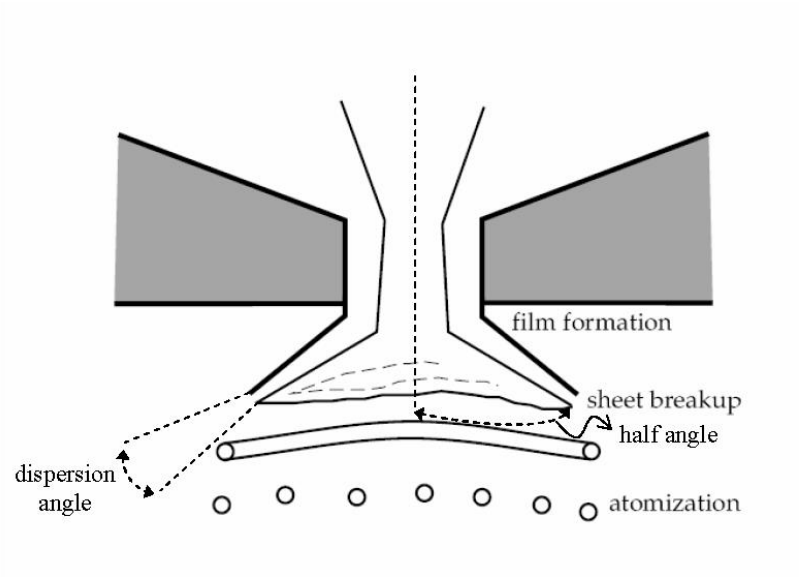

Figure 9: Pressure Swirl Atomizer Displaying Air Core and Dispersion (Source: Fluent Incorporated)

2.5 Theory of Pressure Swirl Atomizers

The design type of the atomizer will have geometric constraints based on the application and desired outlet conditions of the spray. For applications requiring a spray with both tangential and radial velocities, atomizers are designed with angled slots. The interrelations of these geometric dimensions can be inferred through ratios.

Examples of these ratios include outlet orifice diameter to chamber length, and inlet orifice diameter to outlet orifice diameter. There are several design charts on which dimensional ratios are most appropriate for a variety of design objectives. This is attributed to the multitude of variables possible to alter and designing for certain conditions over others. These design objectives may include achieving higher or lower spray angles, shorter or longer spray penetration, or higher mass flux distribution.

Table 2. Range of Values of Nondimensional Groups Covered by Jones [20] (recreated from Atomization & Sprays)

Table 5.1 - Range of values of nondimensional groups covered by Jones [20]			
Dimensionless group	Range covered	Typical value	
$l\_o/$	0.1 - 0.9	0.15	
L_s	0.31 - 1.26	0.7	
L_p	0.79 - 3.02	1.2	
$A\_p/($	0.19 - 1.21	0.52	
D_s	1.41 - 8.13	2.7	
$(d\_o\ \rho\_l$	11.5e3 - 3.55e5	Low Pressure 2.4MPa (350 psi) / 1.08e5	High Pressure 6.3 Mpa (900 psi) / 3.88e5
$(d\_o\ \rho\_$	1.913e3 - 21.14e3	6.45E+03	2.36E+04
μ_l	279 - 2235	750	
ρ_l	694 - 964	700	

Geometric ratios are of great importance to the design of nozzles as they are the driver of the flow conditions at the nozzle outlet. Design charts and parameters have been created to aid in the design of nozzles, based on the application. For pressure swirl atomizers, the primary ratios driving the spray angle are the following:

$$\frac{D_S}{d_o} \quad \frac{L_S}{D_S} \quad \frac{l_o}{d_o}$$ (Equations 2.2, 2.3, 2.4)

Where D_s = the swirl chamber diameter

d_o = exit orifice diameter

L_s = swirl chamber length

l_o = exit orifice length

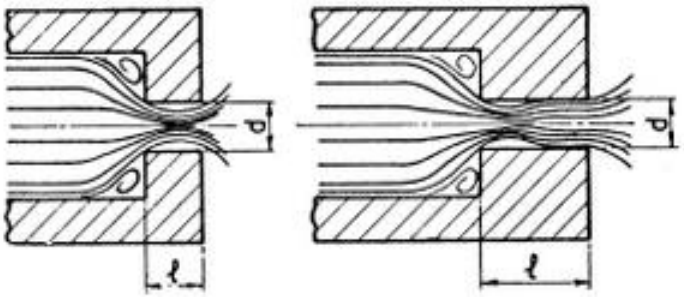

Figure 10: Effect of Geometry on Spray (Source: The Atomisation of Liquid Fuels)

2.5.1 Spray Cone Types

Depending on the design of the pressure swirl atomizer, sprays of different features are produced. There are two major types: The hollow cone spray and the solid cone spray. Hollow cone sprays are indicative of a pressure swirl atomizer, airblast, air assist, or dual type design. This hollow cone design produces a core of air further accelerating the droplets nearest it. Hollow cones project the atomized fluid in an annular shape. Solid cones do not have air cores and project the atomized fluid in a full circular area. This flow is produced by an injector internal to the spray. This injector near the exit orifice infuses fluid into the spray, changing the volume distribution of droplets. The selection of the spray cone type (dependent on the type of atomizer) is usually dependent on the application of the nozzle.

Solid cones usually have coarse atomization while hollow cones are preferred for fine atomization.

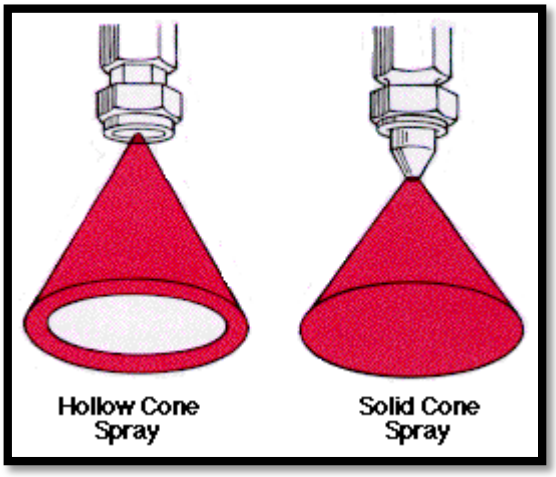

Figure 11: Hollow Cone Spray versus Solid Cone Spray (Source: Extension.org)

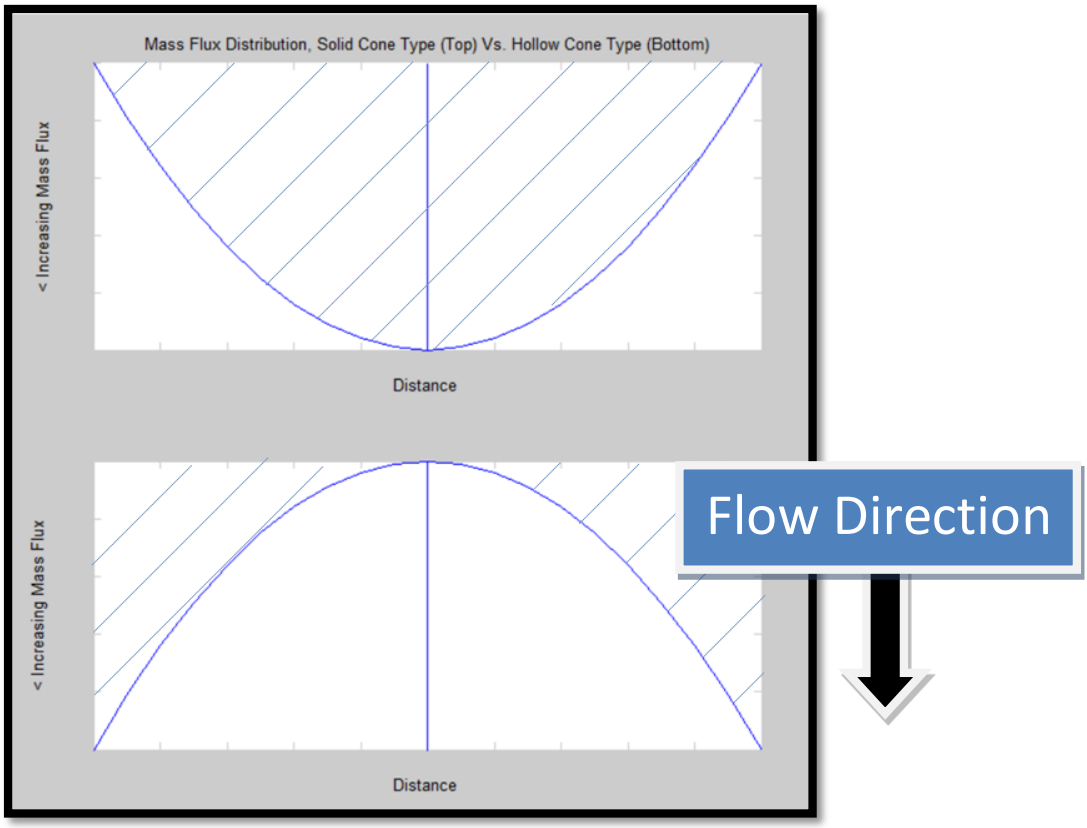

Figure 12: Mass Flux Distribution of Solid Cone versus Hollow Cone Type

Figure 12 shows the mass flux distribution of the solid cone spray type versus the hollow cone spray type, with the hatched region representing the fluid. The vertical line on both plots represents the centerline axis of the atomizer.

2.5.2 Spray Edge

When measuring the angle of a spray, it is necessary to distinguish the edge of the spray. Due to the process of spray formation, determining from which points the angle should be measured is not always straightforward. Mass flux distribution can also be desirable as this gives insight into the optimal location for measuring spray angle. There are a myriad of methods for finding the true edge of a spray cone. They can be broken down into two primary schools of thought: Theoretical spray edge and actual spray edge. Using either the theoretical spray edge or the actual requires basic trigonometric relations to be used to calculate the angle of the spray. The following figure shows the discrepancy between the theoretical spray and the actual spray. According to De Corso & Kemeny, this can be referred to as the “spray cone sheath”.

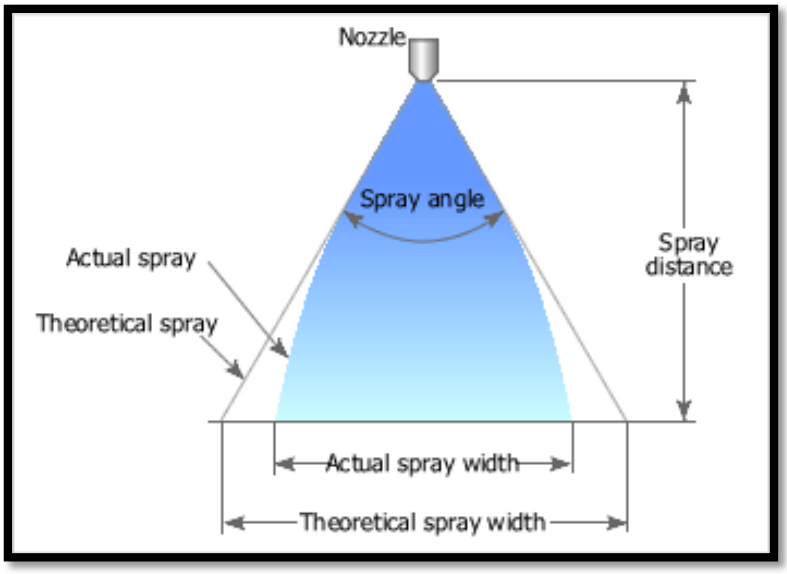

Figure 13: Spray Width Types (Source: Nozzle-Network.com)

The theoretical spray edge assumes a continuous vector in the direction of the flow extending from the selected vertex for the nozzle or atomizer up to the wetted region. This edge assumes no change in velocity and discounts any external fluid mechanic effects acting upon the spray. The actual spray width and spray edge take into account the change in momentum and velocity that the droplets undergo as they travel further from the orifice and, in shape, is more representative of tulip stage atomization.

By understanding which of these two parameters is better suited to the usage of the nozzle and atomizer, the designer will define spray angle based on what the application calls for. Equation 2.7 results in a the theoretical spray angle while equation 2.5 is more representative of the actual spray angle due to the influence of fluid parameters (viscosities and surface tension interaction of the injected fluid and the substance into which that fluid is injected).

The following is an example of the rational for choosing one "edge" over the other:

- An application requiring that the spray have a certain amount of mass flux reaching its destination would have its spray angle calculated via the actual spray edge.
- An application requiring that the spray angle of some nozzle is no larger than some selected value would be better suited for having its spray angle calculated using the theoretical spray edge.

2.5.3 Atomizer Constant, K

The atomizer constant, K gives a constant of performance for an atomizer.

$$K = \frac{A_p}{D_s d_o} \qquad \text{(Equation 2.5)}$$

Where K = atomizer constant

A_p= port area

D_s = swirl chamber diameter

d_o= exit orifice diameter

An atomizer constant is a ratio of measure comparing the axial momentum to the angular momentum. This is a critical ratio because it helps designers better create a nozzle depending on the required application. For example, a nozzle with an atomizer of a K_p greater than 1 is more inclined to have a deeper spray penetration length – that is, the distance a fluid jet enters into another fluid medium – with a narrow spray angle. However,

in the case of a nozzle with an atomizer of a K less than 1, the nozzle would produce a wider spray angle with a shorter spray penetration length. Depending on the type of application, the atomizer constant would be preferred to be higher or lower.

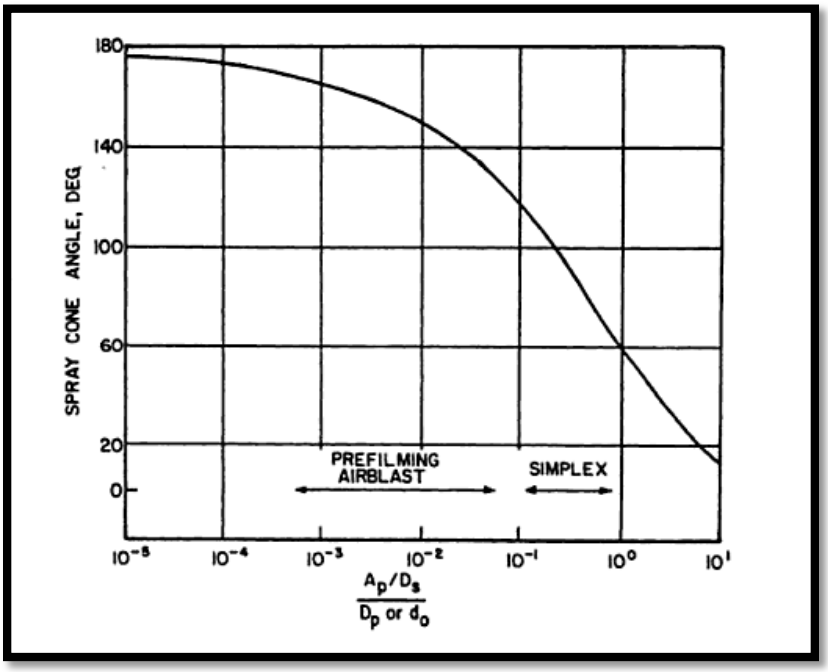

Figure 14: Theoretical Curve for Atomizer Constant (Source: Atomization & Sprays)

This constant is also desired to be in a particular range over another depending on the type of atomizer. In the case of pressure swirl atomizers are usually designed within a range of 0.1 to 1.

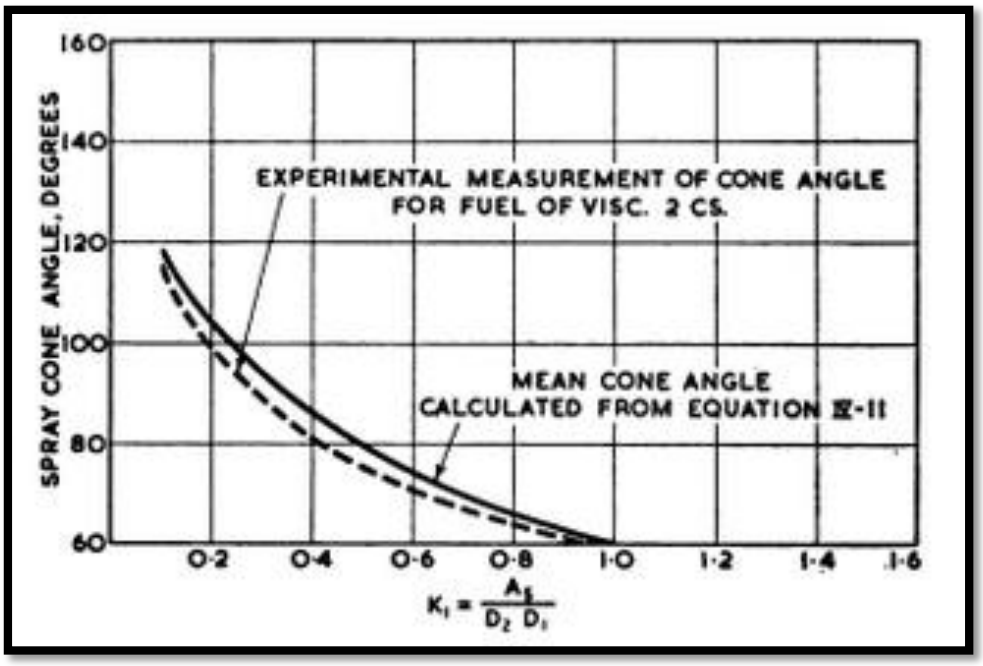

Figure 15: Effect of Atomizer Constant on Spray Angle (Source: Atomisation of Liquid Fuels)

2.5.4 Spray Angle

The spray angle of a cone is calculated from approximating the spray cone as a triangle. The vertex can be represented as point inside of the atomizer up to the surface from which the pressurized fluid exits. Spray angle is very important to pressure swirl atomizers as they are a function of the internal geometry of the swirler. Due to prior experiments, the behavior of sprays into another fluid medium is well understood. Previous experimentation and subsequent data and correlations assist current nozzle designers to achieve an appropriate spray angle based on the required application. Swirl atomizers have a different set of parameters that control and affect the angle downstream of the fluid injection point. Parameters primarily influencing spray angle of both the injection fluid and the penetrated

fluid include pressure differential, density, film thickness, viscosity and internal geometry ratios.

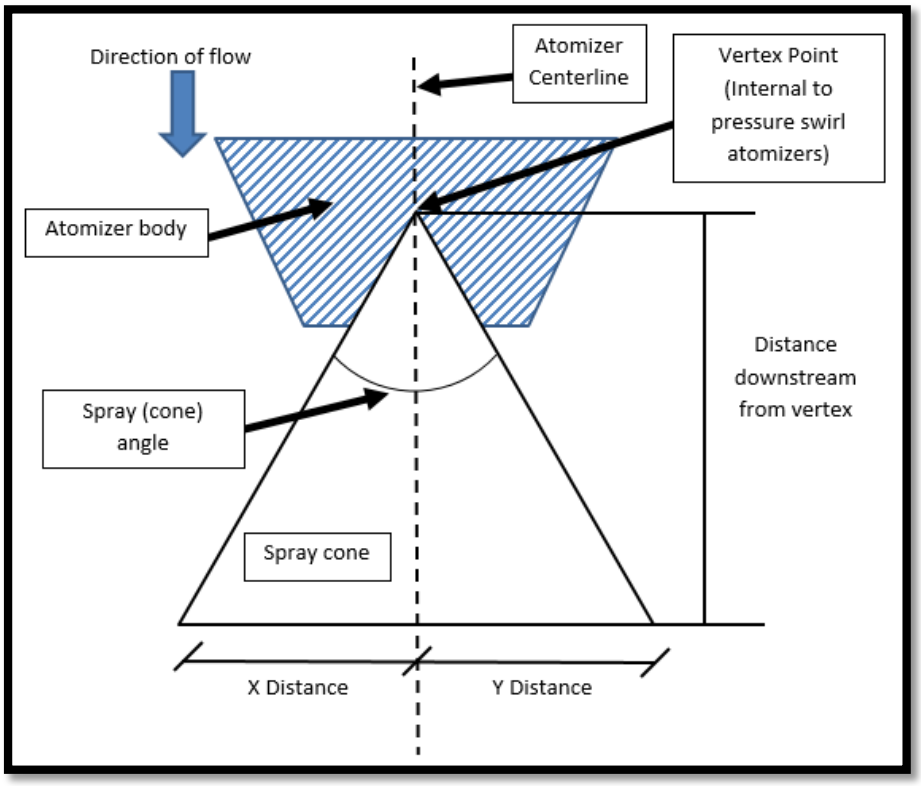

Figure 16: Basic Spray Cone Geometry

An empirical relation was obtained via experimentation of Rizk and Lefebvre -

$$2\theta_m = 6K^{-0.15} \left(\frac{\Delta P_L d_o^2 \rho_L}{\mu_L^2}\right)^{0.11} \qquad \text{(Equation 2.6)}$$

Where $2\theta_m$ = spray angle (cone angle)

K = atomizer constant

ΔP_L = fluid pressure drop

d_o = exit orificediameter

ρ_L = fluid density

μ_L = fluid dynamic viscosity

In the previous equation, $2\theta_m$ represents the spray angle versus the half spray angle, θ_m measured from the central axis of the atomizer. It is very vital to note the significance of each variable in the previous equation. When expanded to

$$2\theta_m = 6\frac{D_s^{0.15} d_o^{0.15}}{A_p^{0.15}} \left(\frac{\Delta P_L^{0.11} d_o^{0.22} \rho_L^{0.11}}{\mu_L^{0.22}}\right) \quad \text{(Equation 2.7)},$$

the effects of the orifice diameter,d_o are more easily seen. It has the most significant effect on the spray angle, while the fluid parameters are less influential.

Another way of calculating the theoretical spray angle is through the Giffen & Muraszew theory which states

$$\sin\theta = \frac{\left(\frac{\pi}{2}\right)(1-X)^{1.5}}{K\left(1+\sqrt{X}\right)(1+X)^{0.5}} \qquad \text{(Equation 2.8)}$$

Where θ_m= half spray cone angle

K= atomizer constant

X= air core area to outlet orifice area ratio

This theory is expanded upon later on in section 2.1.5.5, Theory of Pressure Swirl Atomizers – Discharge Coefficient, C_d

2.5.5 Discharge Coefficient, C_d

Pressure swirl atomizers are placed at the outlet of nozzles to convert the pressure of the fluid to kinetic energy, propelling and dispersing fluid into the medium surrounding the nozzle.

Pressure swirl atomizers produce air cores – thereby restricting the amount of flow at the exit orifice. Air cores are an area of the exit orifice blocked by a vortex of air, effectively limiting how much fluid can travel through the exit orifice area. Due to this limitation, these atomizers usually have small discharge coefficients. The discharge coefficient can be thought of as –

$$A_E = A_O \times C_D \text{ (Equation 2.9)}$$

Where A_E = fluid exit area (effective area)

A_O = exit orifice geometric area

C_D= discharge coefficient

Pressure swirl atomizers are placed at the outlet of nozzles to convert the pressure of the fluid to kinetic energy, propelling and dispersing fluid into the medium surrounding the nozzle.

There are many types of pressure swirl atomizers. They include a plain orifice and simplex nozzles with sub-designs under each type. As stated earlier, pressure swirl atomizers have tangential inlets to initiate the swirling velocity component in the flow imparting an angular momentum on the fluid in conjunction with the axial momentum.

Some designs of these tangential inlets use angled slots to further diversify the spray cone angle.

Table 3. Atomizer Types and Range of Discharge Coefficient (Source: Atomization & Sprays)

Atomizer Type	**Range of Discharge Coefficient**	**Angle Type**
Plain	0.8 - 0.95	Narrow, Hard
Swirl	0.2 - 0.6	Wide, Soft

A principal ratio for pressure swirl atomizers is the air core area to exit orifice area ratio X.

$$X = \frac{A_a}{A_o} \qquad \text{(Equation 2.10)}$$

Where X = air core area to exit orifice area ratio

A_a = air core area

A_o = exit orifice area

The preceding equation is important when analyzing a pressure swirl atomizer based using Giffen and Muraszew theory. This ratio,X, can be assumed to be any arbitrary number from 0 to 1. In this case, 0 represents maximum fluid flow through the exit orifice area while 1 represents no flow through the exit orifice area.

The discharge coefficient of a nozzle,

$$C_D = \left[\frac{(1-X)^3}{1+X}\right]^{0.5} \qquad \text{(Equation 2.11),}$$

identifies the effective area that a mass flow exits through versus the geometric area. Giffen and Muraszew determined that the above equation did not predict the discharge coefficient

obtained from experimental data. This led to their modified equation for discharge coefficient –

$$C_D = 1.17\left[\frac{(1-X)^3}{1+X}\right]^{0.5} \quad \text{(Equation 2.12)}$$

Taylor obtained yet another discharge coefficient for pressure swirl atomizers, but for inviscid (nonviscous fluid) flow –

$$C_D^2 = 0.225\frac{A_p}{D_s d_o} \qquad \text{(Equation 2.13)}$$

Giffen and Muraszew theory assumes nonviscous fluid (allowing for spray cone angle to be expressed in terms of geometry strictly).

The theory can be used to solve for the theoretical maximum spray angle of any atomizer using the following –

$$sin\theta = \frac{\left(\frac{\pi}{2}\right)C_D}{K\left(1+\sqrt{X}\right)} \text{ (Equation 2.14)}$$

Through substitution of equations 2.12, 2.13, and 2.14, it is easy to relate the atomizer constant, to the discharge coefficient and theoretical maximum spray angle.

Discharge coefficient helps to identify several characteristics about the flow through an atomizer. These characteristics include film thickness, and effective area. Knowledge of film thickness can assist designers in identifying which geometric constraints or even operational constraints, i.e. pressure differential, operating temperature, etc. might be needed. Coefficient of discharge also affects pressure swirl atomizers' working fluid velocity and swirl. Performance curves have shown that for swirl atomizers, a decreasing coefficient of discharge results in a higher fuel swirl and vice versa.

Based on true operating conditions of an atomizer, the discharge coefficient can be calculated from the following equation –

$$AC_d = \frac{\dot{m}_{tot}}{\sqrt{2\rho\Delta P}} \text{ (Equation 2.15)}$$

Where A = exit orifice area

C_d = discharge coefficient

$\dot{m}_{tot}$ = total mass flow through atomizer

ρ = fluid density

ΔP = fluid pressure drop

Atomizers have critical velocities which factor into the discharge coefficient. These critical velocities decrease as orifice diameter increases, and they increase as the orifice diameter decreases. The critical velocity for an atomizer assumes the fluid is flowing through a cylindrical volume and is entering the transition phase of the Reynolds number criterion. This critical velocity can be calculated via the following –

$$v = \frac{2000\nu}{d} \text{ (Equation 2.16)}$$

Where v critical velocity

2000 = transitional Reynolds number

ν= kinematic viscosity

d = characteristic length (exit orifice diameter)

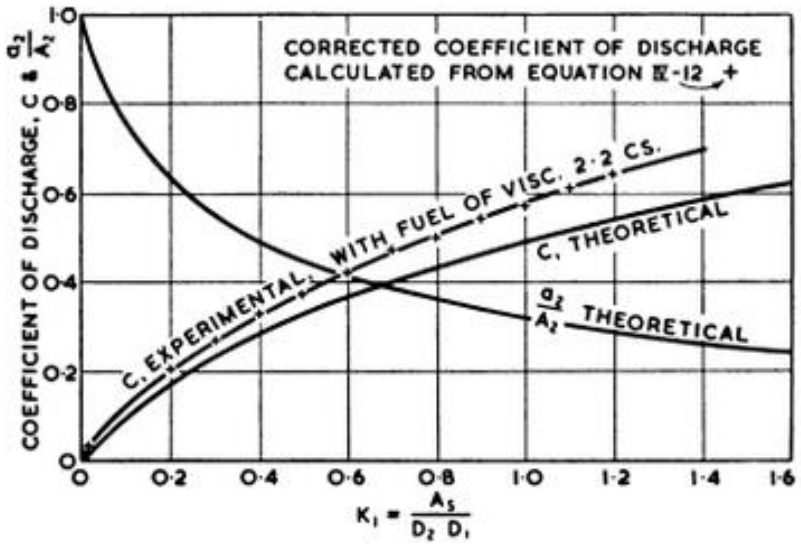

Figure 17: Effect of Discharge Coefficient with Atomizer Constant (Source: Atomisation of Liquid Fuels)

2.5.6 Effective Area, Ae

Effective area A_e is directly linked with the discharge coefficient. This characteristic is the indicator of how much area is actually used as the outlet orifice versus the geometric orifice. This number is always less than one as it is not physically possible to flow out of an area larger than the geometric constraints. Because of this, the conditions downstream of the outlet can vary based on this value. Equation 2.9 shows the relation between effective area and discharge coefficient.

The variable A_e is also dependent on the fluid type and geometric constraints. A fluid such as water with its lower viscosity, would be more likely to have a higher effective area over a more viscous fluid, such as hydraulic fluid. This can be figured intuitively from the shear stress that the accelerating fluid would have to overcome.

2.5.7 Flow Number, FN

Flow number is of primary importance to understanding atomization. It represents the effective exit area based on the mass flow and pressure drop across the atomizer.

$$FN = \frac{\dot{m}}{\sqrt{\Delta P}} \quad \text{(Equation 2.17)}$$

The importance of flow number is its usage as a benchmarking figure. For instance, when designing a fluid schematic where a nozzle has a small restriction and uses such as the macrospray atomizer studied in this thesis, one would find that the flow number of the atomizer is smaller than the orifice leading to the inlet of this nozzle. This means that the nozzle is properly sized for the fixture driving fluid to the atomizer. If the fixture providing fluid to a nozzle has a lower flow number versus the component it is flowing fluid to, this could be problematic as the nozzle would essentially view the fixture as an orifice and the proper flow would not be delivered.

Due to differences in systems of units, the formulation of flow number varies from SI units to US and British customary units. The corrected formulations are as follows —

$$FN_{UK} = 0.66 \times 10^{8} \times \rho_L^{-0.5} \times FN \quad \text{(Equation 2.18)}$$

$$FN_{US} = 0.66 \times 10^{6} \times \rho_L^{0.5} \times FN \quad \text{(Equation 2.19)}$$

In addition to these corrected values, the flow number can also be obtained for English units. The dimensionally correct form of the flow number equation can be used as —

$$FN = 0.395\left(\frac{A_p^{0.5} d_o^{1.25}}{D_s^{0.25}}\right) \qquad \text{(Equation 2.20)}$$

In an attempt to understand flow number across a range of nozzles, Kutty et al. manufactured simplex nozzles each with three pressure inlets. Each nozzle had a small change in design versus the others (i.e. inlet port length, inlet port diameter, etc.). The research conducted produced significant trends when discussing the volumetric discharge of simplex atomizers, in addition to effects on spray angle. The primary points of the research point towards volumetric discharge being greatly influenced by inlet port diameter and orifice diameter. More conclusions drawn from their experiments showed that the lengths of the swirler and inlet holes, also including the number of inlet holes, have minimal effects on the spray angle.

Analyses conducted by Rizk and Lefebvre on the experiments performed by Kutty et al. showed that for the nozzles used in the experiment, the recorded flow numbers did not match expectations per the basic flow number formulas when using the normal flow number relation. Through the analyses conducted, Rizk and Lefebvre found an empirical equation for flow number –

$$FN = 0.0308\left(\frac{A_p^{0.5} d_o}{D_s^{0.45}}\right) \qquad \text{(Equation 2.21)}$$

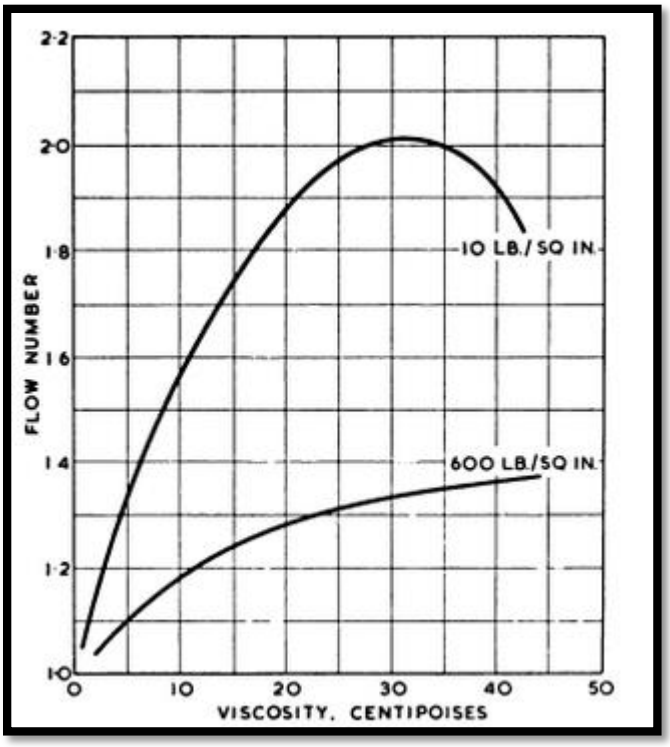

Figure 18: Effect of Flow Number versus Viscosity (Source: Atomisation of Liquid Fuels)

2.5.8 Film Thickness and Viscosity Effects on Spray Angle

There exists an inverse relation between radial distance within the swirl chamber of the atomizer and the fluid tangential velocity. Because of the friction force, tangential velocity is reduced. This leads to the correlation that with increasing viscosity, there is a decrease in tangential velocity.

The development of film thickness is crucial to fine atomization; if an adequate film thickness is not formed in the swirl chamber of the atomizer, atomization will not be of acceptable quality. Film thickness is a direct result of the viscosity and flow conditions of the fluid.

Viscosity can play a very important role in the development of film thickness and thereby, atomization. Very viscous fluids require more energy to move at a similar rate compared to fluids with lower viscosity. This difference, in conjunction with the operational pressure of the atomizer, contributes to the atomizer's spray angle.

The shear stress that the fluid must overcome increases with an increased velocity vector, parallel to the wall, as shown with the following equation –

$$\tau_x = \mu \frac{\partial u}{\partial x} \qquad \text{(Equation 2.22)}$$

Where τ_x = shear stress in x direction

μ = dynamic viscosity

∂u = velocity in x direction of differential unit x

∂x = differential unit length in x direction

Viscosity can have a small effect in the spray angle of other atomizer types. In the case of a plain orifice atomizer, the primary energy transfer occurs through pressure drop with frictional losses occurring at the liquid-wall interface. The major impedance to flow is the rapid change in diameter of the swirl chamber to the exit orifice (reference this from previous figure of plain orifice). Although pressure drop is the main driver, with a pressure swirl atomizer, frictional losses will play a larger role since the fluid must pass through channels with curvature and sharper angles.

2.5.9 Inlet Pressure Effect on Spray Angle

One variable that is influential on spray angle after reaching its steady state value is the supply pressure. Pressure drop primarily has its largest effect on the formation of the full cone angle. As mentioned previously, when the operational pressure of the nozzle is reached, a stable spray is seen. At this stage, any additional pressure added to the fluid does not have a major effect on the angle.

Based on experiments conducted by De Corso and Kemeny, spray angle is a function of fuel pressure drop and ambient gas density.

$$\theta = f(P\gamma^{1.6}) \quad \text{(Equation 2.23)}$$

The experiments performed by Ortman and Lefebvre showed that the spray angle formation is a transient process. Initial injection pressurization and flow of the fluid causes the angle to expand and then contract to its nominal steady state value after the constant operational pressure has been reached.

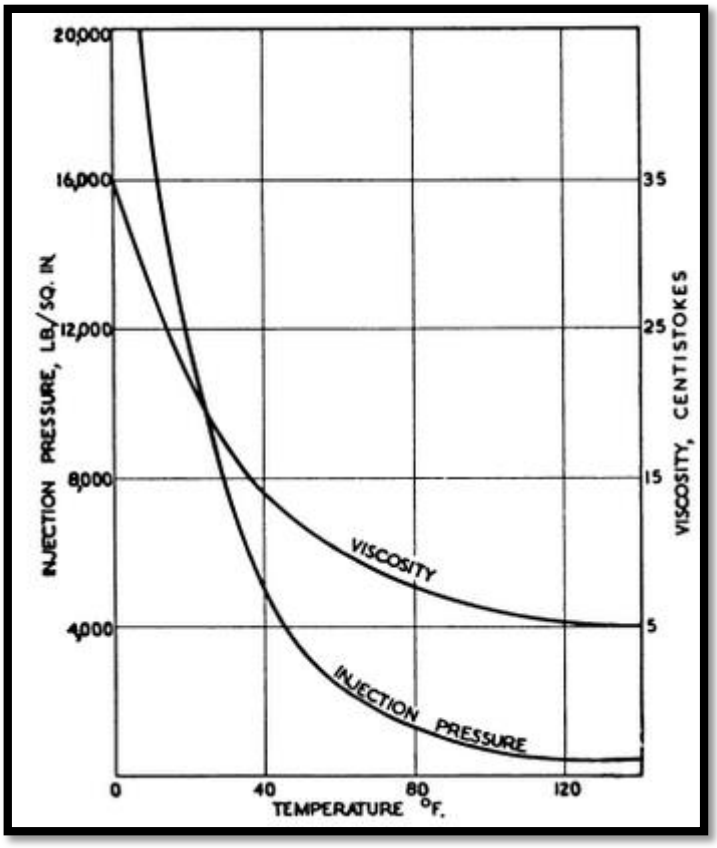

Figure 19: Effect of Injection Pressure on Viscosity (Source: Atomisation of Liquid Fuels)

2.5.10 Surface Tension Effect on Spray Angle

According to the empirical relation obtained by Rizk and Lefebvre, equation 2.6, surface tension is shown to have no relation to spray angle. An experiment performed by Giffen and Massey however, showed that while surface tension did affect spray angle, the effect was not appreciable. During this experiment, air core diameters, spray angles, and discharge coefficients were measured for liquids having a range of surface tension values. However, the viscosities of the liquids were approximately the same.

It is notable that many of the equations and correlations, specifically for discharge coefficient and spray angle, are empirical and have been obtained through experimentation. It is the opinion of the author that this trend shows that, in the field of atomization, the concepts and equations are still very theoretical and are more so empirical. For each empirical correlation obtained, there were specific sets of conditions used to derive the equations. This includes fluid properties, pressure drop, the fluid media being injected into, etc. The variance between the theoretical data and empirical data are further proof that the relationships between the fluid properties, atomizer geometry, and fluid mechanic principles can be better understood.

Through all of the research conducted on pressure swirl atomizers, it is seen that the spray angle tends to be influenced strongly by the outlet orifice diameter and atomizer constant more so than any other geometric dimension. In addition, dynamic viscosity and density tend to be the primary drivers of what makes or does not make a fluid atomize properly.

2.6 Measurement Systems

Through an extensive literature review, multiple measurement techniques are explored and researched to gauge which systems provide adequate results versus cost effectiveness.

2.6.1 Optical Methods

Machine vision systems are optical systems that utilize cameras to fully characterize sprays. There are several methods of making these characterizations when considering

spray applications. They include high speed imaging, laser Doppler velocimetry, particle Doppler interferometry (PDI), particle image velocimetry (PIV), laser induced fluorescence (LIF), planar laser induced fluorescence (PLIF), interferometric Mie imaging (IMI), and Shadowgraphy (shadow imaging).

The most basic and most commonly used system is the high speed camera imaging. Cameras with high speeds, high resolutions, and high sensitivities are coupled with software to analyze sprays. These software packages come with various algorithms to calculate spray angle and feed the information back to the user. Some programs work with still images while others can calculate the spray angle in real time and output data to the operator.

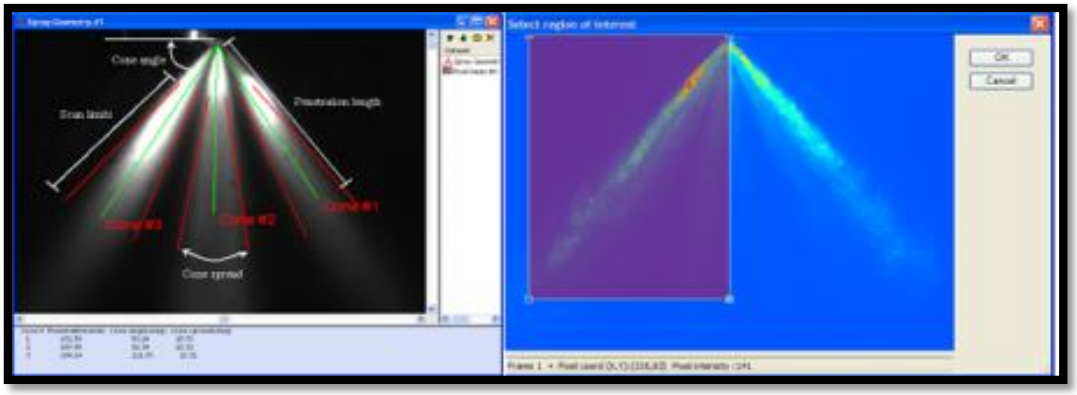

Figure 20: High Speed Camera Capturing (Source: Dantec Dynamics)

Laser Doppler Velocimetry (LDV) allows for the measurement of velocity at any point in the flow field. A laser is beamed into a flow, at which point, a droplet or particle passes

through the beam. The particle crossing through the beam gives off light. The intensity of the scattered light utilizes the Doppler Effect to derive the velocity of the particle or droplet.

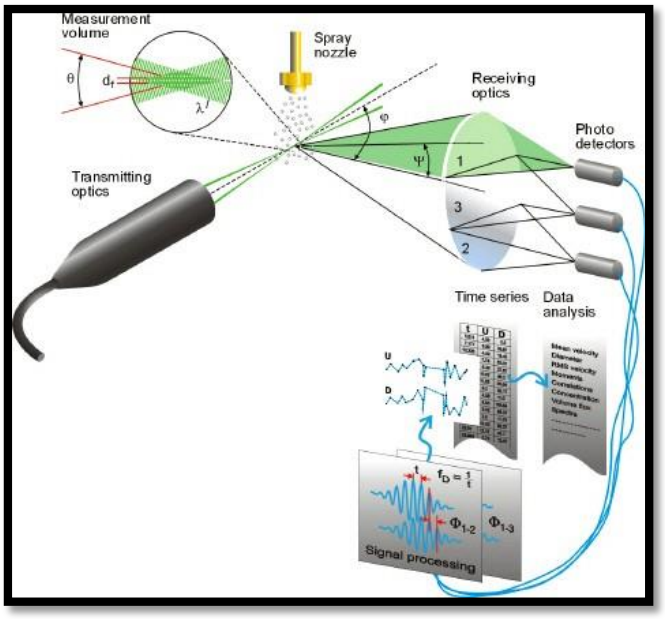

Figure 21: Overview of Particle Doppler Interferometry (Source: Dantec Dynamics)

Particle Doppler Interferometry (PDI) measures the velocity and diameter of small droplets based on a technique using laser light wavelength. The drop sizes over the entire spray cone are measured without the use of statistical distribution functions (i.e. Weibull, Student's t-distribution, etc.)

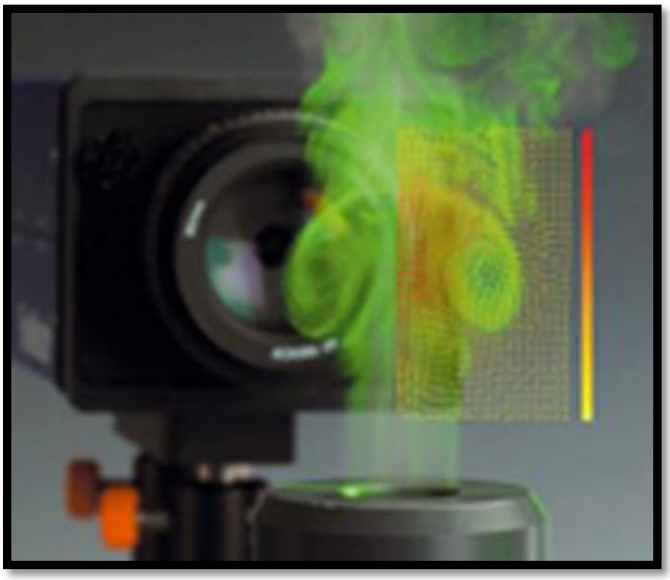

Figure 22: Particle Image Velocimetry (Source: LaVision)

Particle Image Velocimetry (PIV) measures the entire velocity field by taking two images within a short amount of time in conjunction with laser pulses. These images are then processed to find the time difference between two discrete points in two different frames, resulting in a calculated velocity vector.

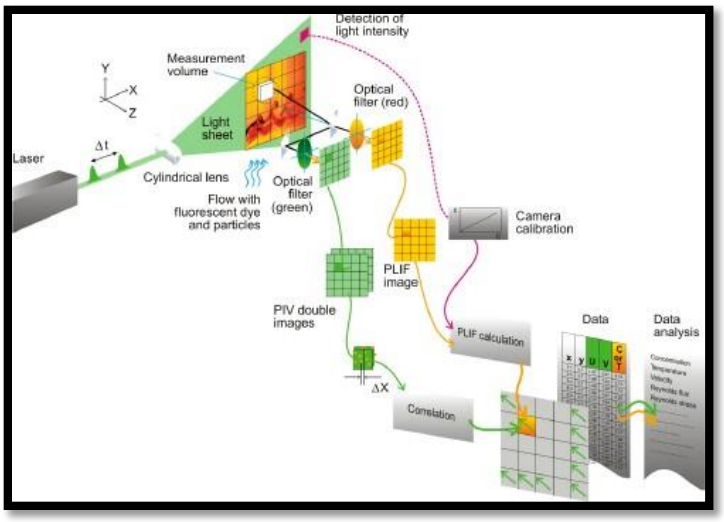

Figure 23: Planar Laser Induced Fluorescence (Source: Dantec Dynamics)

Planar laser induced fluorescence (PLIF) operates by beaming a sheet of laser light into a flow stream. This sheet interacts with the atoms to begin a change in the molecular structure. Some atoms and molecules absorb the incoming light while the other atoms/molecules emit light, becoming fluorescent. The emitted wavelengths of light are always longer than the wavelength of light initially absorbed. These fluorescent regions are then image captured. Laser induced fluorescence (LIF) operates on this same principle but uses a singular beam rather than a sheet.

Interferometric Mie Imaging (IMI) measures diameter of spherical droplets and operates by creating a region of overlap between a laser light sheet and a digital camera's viewing range.

Shadowgraphy (shadow imaging) uses high definition imaging and pulsed backlights. Utilizing optics (the focal length, focal plane, depth of field, etc.) the user is

able to calculate the diameter of the atomized droplet in addition to coordinates on the viewing plane. With a double pulsed light source, the user can freeze frames which results in easily seen velocity vectors between frames. This image is the shadow of the spray, as the name implies.

Each of the described methods is best suited for a specific application, depending on the desired outcome of the study. In some cases, a combination of the above imaging techniques can prove to be a powerful tool when characterizing sprays because not all techniques measure velocity, droplet size, etc. For instance, LaVision, a machine vision system vendor offers the SprayMaster product package which packages Shadowgraphy, IMI, LIF, and PIV techniques in one unit.

2.6.2 Patternation

Figure 24: Patternation (Source: Wikipedia.org)

Patternation is a popular way of characterizing sprays in regards to understanding the mass flow output of a nozzle or atomizer. As shown in figure 23, tubes are spread radially equidistant from one another. Once the nozzle is spraying at the nominal conditions and the spray cone is formed, the exiting fluid is collected into the tubes. When any of the tubes reaches a volume capacity of 75%, the supply line to the nozzle is cut off. The volume of fluid is measured from each tube and is plotted against its angular position from the center of the nozzle. This plot gives the "radial liquid distribution". This curve gives an informed estimate of where the nozzle may be deficient in its design, typically either in relation to its geometric constraints or boundary conditions (i.e., supply pressure, supply fluid temperature, etc.).

There are further corrective actions needed when obtaining the radial liquid distribution curves when wanting to compare angular position versus the volumetric flow rate of the nozzle. To acquire the true volumetric distribution, one must include an area weighting factor. Area weighting factor is the total number of collection tubes needed to measure all moving fluid a certain distance from the nozzle axis.

2.6.3 Hot Wire Anemometry

As stated earlier, visualization and characterization of fluid flow is an area of interest due to the details it can provide on the physical phenomena occurring within and on the stream. It is an industry which has been growing primarily since the early 1900s with the initial research papers and experiments written and conducted by scientists such as L.V. King (1915), Bordoni (1912), Gerdien (1913) and Kennelly and Sanborn (1914),

specifically on the side of hot wire anemometry. The 1970s brought on new concepts and techniques with the advent of computers - machine vision systems. There are machine vision systems that are tuned for spray characterization and utilize nonintrusive methods to identify various parameters of flow fields. Machine vision systems are preferred by some users over intrusive techniques, such as hot wire anemometry. Intrusive techniques and methodology can alter results of flow characterization in a negative manner, with the degree of impact depending on what process is used.

Even with the disadvantage of potentially disturbing the flow, intrusive methods can be desired over machine vision systems. This is due to the relative ease of setting up a test stand and collecting data instantly. Machine vision systems come with the disadvantage of needing advanced post-processing software with learning curves. These setups also require experience and knowledge dealing with lighting, environment setup and cameras in addition to the high costs associated with them.

As stated earlier, organizations dealing with flow characterization desire to detail the flow field of interest as best as possible within reasonable means. Gathering data on how, for instance, a spray exits a nozzle, helps its designers determine whether or not their tolerances are too loose or too tight on a product. It can help them minimize the amount of work needed from design engineers. Researchers gain a wealth of knowledge from detailed flow fields and are then able to use the data to better model physical phenomena affecting the problem of interest.

The initial designs and theory behind hot wire anemometry can be traced back to the early 1900s, as many thesis papers and experiments were conducted, with each subsequent set of results expanding upon the previous. However, many attribute L.V. King's 1915 paper to truly incorporate all aspects of design of hot wire anemometers and convection heat transfer. Hot wires operate using King's Law.

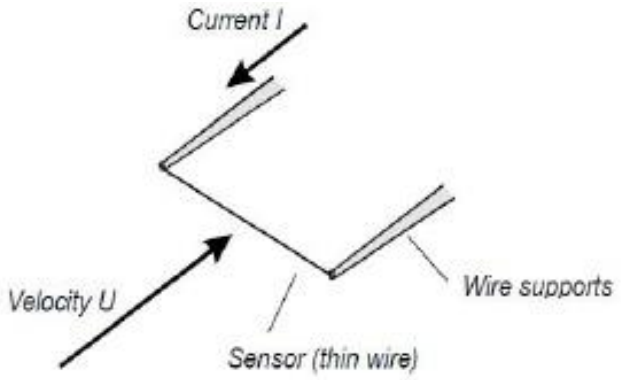

Figure 25: Hot Wire Operation & Construction (Source: Underwater Robotics Research Group)

$$I^2 Rw^2 = E^2 = (T_w - T_a)(A + B * U^n) \qquad \text{(Equation 2.24)}$$

Where I = current

R_w = wire resistance

E = voltage

T_w = wire temperature

T_a = ambient air temperature

A, B, n = calibration constants

U = velocity of flow stream

A pronged probe with a very thin conductive wire connecting the prongs is placed into a flow stream. Once in this flow stream, a current is run through the wire and a constant temperature is held by the wire. This is done by modulating the voltage from the source through the wire while keeping the voltage source the same.

A basic energy conservation relation for the hot wire is -

$$\frac{dE}{dt} = W - H \quad \text{(Equation 2.25)}$$

Where E= thermal energy of wire

W= power input to wire

H= heat transfer to surroundings

The preceding correlation is the relationship of power from convective heat transfer output from the corresponding electrical power input into the probe wire. Upon further expansion, this relationship is easily seen.

$$Q_{convection} = P_{wire,input} \text{ (Equation 2.26)}$$

Where $Q_{convection}$ = convective heat transfer from wire to surroundings

$P_{wire,input}$ = power input to wire

$$hA_s(T_w - T_f) = IV = I^2R \quad \text{(Equation 2.27)}$$

Where h = heat transfer coefficient

A_s = surface area

T_w = wire temperature

T_f = fluid temperature

I = current

V = voltage

R = wire resistance

There are two main kinds of hot wire anemometry techniques. They include constant current anemometry (CCA) and constant temperature anemometry (CTA).

CCAs operate with two equally sized resistors. The resistance value is set to that of the resistance of the wire when it is hot. It is generally assumed that the hot resistance value is 1.8 times the cold wire resistance. At zero flow speed, the supply current is then increased until the current output is balanced. Any change in flow speed will increase or decrease heat transfer, changing the temperature of the wire. This leads to a change in voltage, appearing at the output of the circuit.

CTAs' supply voltage is modified to maintain a constant wire temperature. The resistance in the circuit has a similar set up to CCAs; however, the output of the voltage modifier is a function of flow velocity.

CTAs are preferred to CCAs due to the lack of thermal inertia that has to be overcome. The measured temperatures are much lower than that of CTAs run with an already hot wire with almost negligible effects from thermal inertia.

2.6.4 Mechanical Probe Method (Spray Angle Device)

Another type of spray characterization is the probe method. A nozzle is placed into a chamber and is connected to the required supply fluid and supply air, if needed. The operator then moves two probes into the fluid, via rotating dials. When a "steady" stream of droplets begin impinging on both probe surfaces, the operator can then, through basic trigonometric relationships, calculate the spray angle. The following figure demonstrates the probe method, coupled with a patternation tool, known colloquially in industry as the "smiley face" tool. The tool collects fluid in the radial tubes and is a variant of the previous patternation method shown.

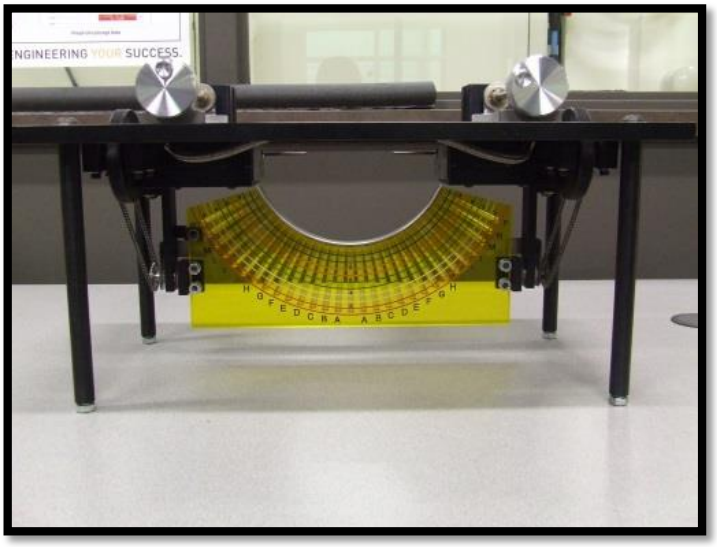

Figure 26: Manual Spray Angle Device (Source: Parker Hannifin Gas Turbine Fuel Systems Division)

The probe method can introduce error as there is no theoretical definition, equation, or categorization of a "steady" stream of droplets. Two operators, depending on how each

moves the probes towards the spray and counts droplets (based on different sizes), can find two different answers for the spray angle of a nozzle. Because there is no correlation between the probe distance and a constant parameter between different runs of the same nozzle product line, i.e. mass flux, there is no true way to say the mass flux between two identical nozzles are the exact same. However, due to manufacturing techniques having tolerances associated with them, it can be assumed that there is some tolerance band with the spray cone for any given nozzle and its atomizer.

This can be one of the least accurate methods of spray characterization as it can introduce human error, one of the highest sources of random error. The accuracy of the results utilizing this method can waver because of the training the operator must have to use the probes in addition to defining the edge of the spray. Another source of error introduced into this method is that the probes must be aligned with one another. If not, this introduces skew into the measurement.

2.7 Selection of HWA over Other Methods

In most experimental situations, the use of an optical system would be preferred over an intrusive method of measurement, hot wire anemometry included. However, in the case of the hot wire anemometry test stand, an adequate distance downstream of the nozzle outlet would have no large effect on the spray angle, making it an acceptable measurement technique.

Even with the capabilities of high speed cameras and lasers, hot wire anemometry has its advantages. Hot wire anemometry has the advantage of examining the spray from a very close proximity at a low cost. High speed cameras and lasers, if not focused exactly on the area of interest are only capturing a portion of the spray, commonly on a macroscopic scale. With hot wire anemometry, it is possible to obtain measurements very close to the exit of the nozzle. This distinction is of importance as this may provide two very different sets of data. The experiments explained in this report utilize CTAs due to their higher reliability and robustness over CCAs.

Due to its ease of use, along with excellent response time, hot wire anemometry, specifically constant temperature anemometry, is used as the primary method of characterizing the spray in the newly-designed test stand.

CHAPTER III

METHODOLOGY & EXPERIMENTAL DESIGN

In order to gain a comprehensive understanding of the capability of the hot wire anemometry approach in addition to the computational fluid dynamics (CFD) prediction, a top-down level approach is taken. The experimentation and analyses were conducted in the following order –

1. Design hot wire anemometry test stand
2. Implement hot wire test stand
3. Test macrospray atomizer nozzle
4. Test conventional atomizer nozzle
5. Use CFD code to ensure similarity of results based on selected models
6. Run CFD simulations of selected macrospray atomizer nozzles and compare results to results from test stand
7. Run CFD simulations of conventional atomizer nozzle to predict accuracy of probe method

3.1 Design & Implementation of HWA Test Stand

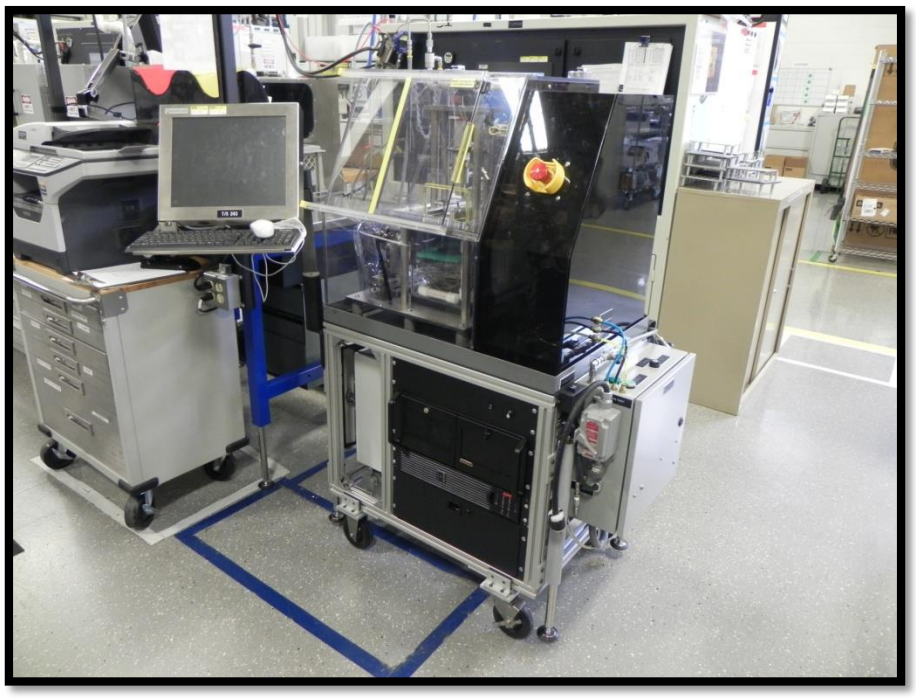

Figure 27: Hot Wire Test Stand Final Assembly (Source: Parker Hannifin Gas Turbine Fuel Systems Division)

Few vendors are involved in the manufacture of the precision equipment needed to produce hot wire anemometry measurement systems. As such, two Dantec Dynamics Mini CTA module systems were used in conjunction with two Parker Daedal traverses for the test stand. Two traverses and two hot wire systems were used in the stand to capture two linear measurements, orthogonal from each other. A basic fluid loop with a bleed valve was set up in conjunction with pressurized air supply line, and a supply line of deionized supply water. The test stand utilized a quick disconnect to the unit under test (UUT) to provide access to the nozzle being tested. A Parker Hannifin, two (2) inch stroke, low profile series (LP series) air cylinder was used to actuate the testing procedure by raising

and lowering the flow section. The following figure shows the CAD model of the stand with the traversing method of the hot wire probes also shown.

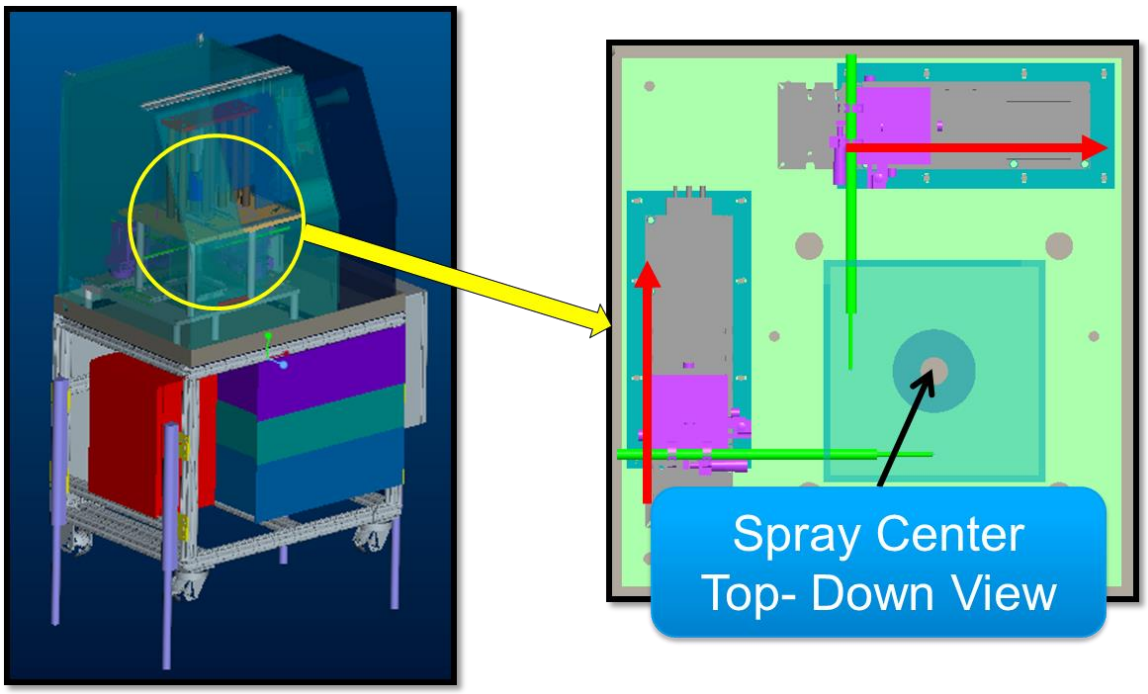

Figure 28: Traversing Operation of Hot Wire Test Stand (Source: Parker Hannifin Gas Turbine Fuel Systems Division)

For potential expanded usage of the test stand in the future, the bottom portion of the flow section was designed to be modular. This modular design allows for a wide range of button diameters and button heights to be tested on the stand.

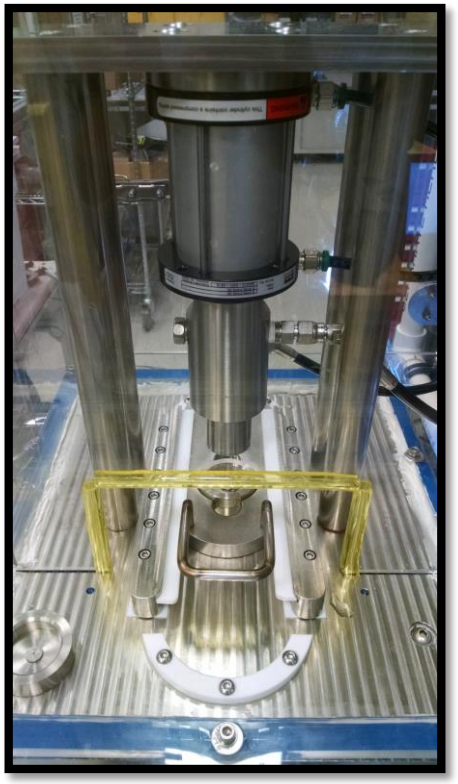

Figure 29: Flow Section of Hot Wire Test Stand (Source: Parker Hannifin Gas Turbine Fuel Systems Division)

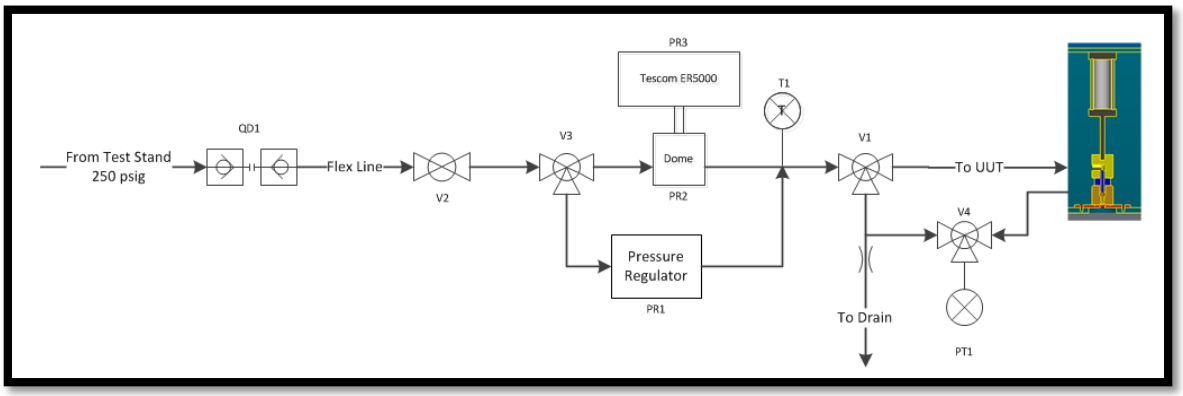

Figure 30: Fluid Schematic of Hot Wire Test Stand (Source: Parker Hannifin Gas Turbine Fuel Systems Division)

A Rosemount 3051C pressure transmitter and a Tescom ER5000 regulator were used in conjunction to control flow and ensure proper testing conditions throughout the entire testing process.

Basic operation of the test stand with a unit under testing is as follows:

1. Unit to be tested is placed in its designated location in stand.
2. Operator closes door to stand and presses the start button.
3. Safety checks are cleared and system alerts operator if any parameters are outside of desired ranges, (i.e. pressure, flow rate, temperature).
4. Flow fixture is lowered onto the unit under test and flow is sealed via an O-ring.
5. System engages fluid loop and flows water through fixture and unit under test.
6. Unit under test flows water and creates spray cone.
7. Hot wire probes traverse the spray cone in a predetermined movement. As hot wire probes traverse the spray, the voltage drop is captured as a voltage drop signal.
8. Data is exported to the on board computer for immediate post-processing.
9. A print out is displayed, showing the results of the scan (voltage versus distance). Button passes or fails depending on whether or not spray angle was within tolerance band.

3.2 Hot Wire Test Stand, Macrospray Atomizer

The macrospray atomizer nozzles were measured using the newly-developed hot wire anemometry test stand. This experiment doubles as a validation run of the test stand, in addition to verifying the already-existing nozzle dataset.

Since the hot wire system gives an output of voltage, a process of identifying the spray angle is based on a normalization of output voltage. Once normalized, the "center" of the spray cone is identified. Because of the intensity of the spray differing along the travel in both directions (change in mass flux), both voltage versus distance charts generated from the scan procedure will have a portion of the scan where the voltage reading is highest. This highest intensity point is identified as the edge of the spray. The sampling rate of the probes is 10 kHz, allowing for a large number of data points captured per unit step of the probes. The hot wire probes are physically locked to optics mounts, while these mounts are fixed to linear traverses, located internal to the stand.

The acquired data from the probes is first averaged out over the 1000 samples obtained per unit step of the traverse. This averaging technique helps to create a smooth curve. Afterwards, a normalization process is used on the curve to obtain a constant of the spray profile. This constant is what all other atomizers tested on the stand must anchor to within some tolerance band of the spray angle.

Since the macrospray nozzle is always placed at the same location and that fixed height is known in addition to having the highest intensity distances known, spray angle is easily calculable at this point via basic trigonometric relations.

The action of traversing two probes across a spray is also capable of detecting skew. Skew can have an effect on how the spray angle is measured. An example of this would be if the surface from which the button is spraying from isn't flush with the button introducing error into the angle calculation. However, due to current manufacturing techniques and their tightest tolerances possible, the machined components are as geometrically close to the design drawings as possible.

3.3 Spray Angle Device, Macrospray Atomizer

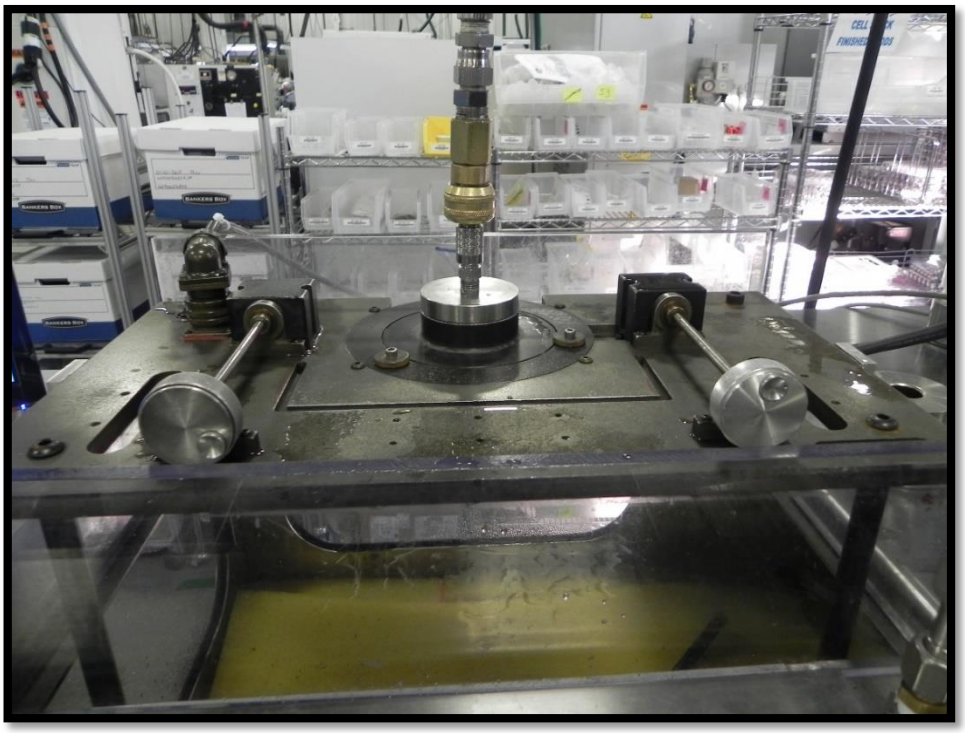

Figure 31: Fixture in Testing Setup, Macrospray Atomizer (Source: Parker Hannifin Gas Turbine Fuel Systems Division)

Figure 32: Fixture for Spray Angle Device, Macrospray Atomizer (Source: Parker Hannifin Gas Turbine Fuel Systems Division)

Since it is of interest to compare spray characterization techniques, the macrospray atomizer was tested on a spray angle device. Figure 31 shows the Parker Hannifin test stand used to gather spray angle data for the macrospray atomizer used for this study. The test stand uses typical hydraulic components including, valves, pumps, flow meter, pressure gauges and pressure regulators. The spray angle device shown in figure 25 is mounted on the top side of the enclosure or spray chamber. This spray chamber acts solely as a reservoir for capturing fluid exiting from the atomizer.

To acquire spray angle data, the atomizer was placed into its corresponding fixture (figure 32). The pressure was ramped up until the operating conditions of 145 psi (10 bar) were reached. A standard spray angle device was used to calculate the spray angle of the atomizer. The part was tested 30 times to acquire an adequate dataset.

3.4 Spray Angle Device, Conventional Atomizer

Since the atomizers of interest are production nozzles and are available on the market, there is an abundance of data available. However, acquiring more experimental data of these already available nozzles to enhance the accuracy of prior datasets is desirable. This extra data is another comparison criterion in addition to the CFD results. It is for these reasons an experimental set of data was obtained.

Because of the mechanical design differences, the conventional atomizer cannot be used on the hot wire test stand. However, to anchor the CFD data, an experiment was run using a different type of spray angle measurement. For these reasons, the mechanical probe method was deemed most appropriate.

An existing test stand was modified to accept the mechanical probe unit. The unit's main components consist of a base mounting plate, probes, and a volumetric distribution measurement tool ("smiley face" tool). The unit also contains a linear variable differential transformer (LVDT) to track linear movement of the probes. The nozzle is placed into its fixture and is then placed into a modified adapter plate. This assembly is then fixed to the mounting plate. Calibration of the unit is conducted by using a mechanical calibration gauge made for this specific type of probe patternator.

A typical testing procedure for the Parker conventional atomizer nozzle was followed to ensure accuracy of results. Jet engine calibration fluid, MILPRF-7024, was used as the flow fluid for the procedure. The experimental set up had an inlet pressure of 100 psi to the

primary nozzle circuit, while the outlet was discharged to a collection chamber at atmospheric pressure.

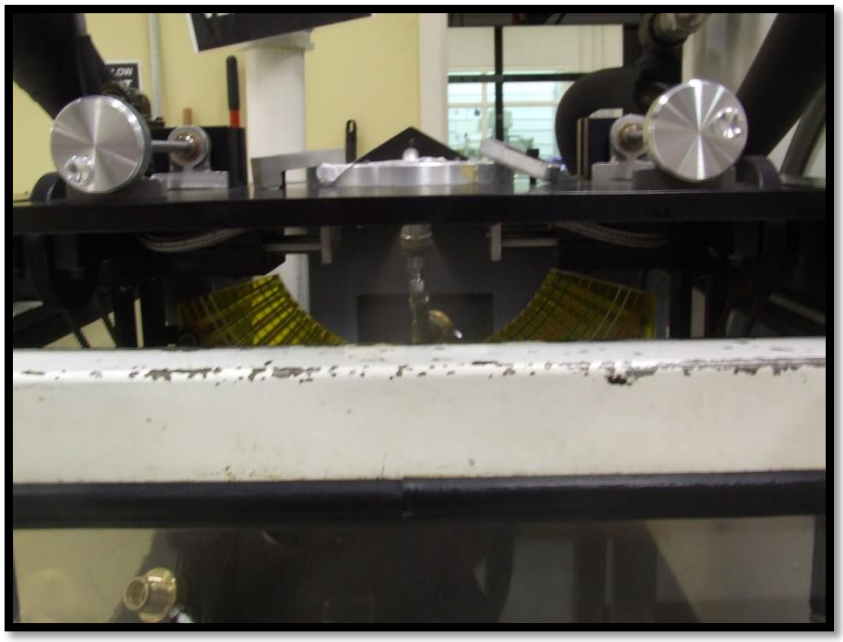

Figure 33: Rear View of Angle Device Setup, Conventional Atomizer (Source: Parker Hannifin Gas Turbine Fuel Systems Division)

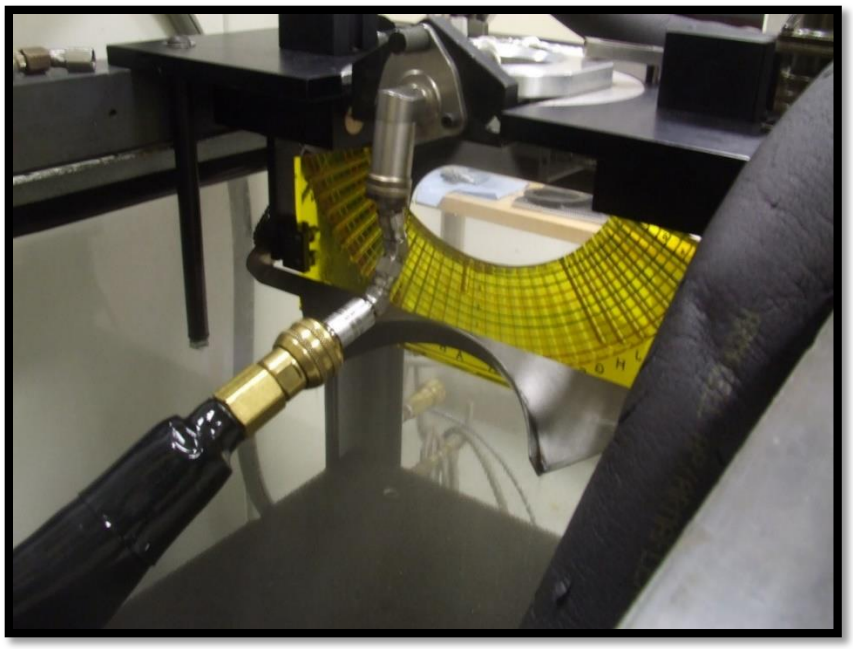

Figure 34: View of Test in Progress of Angle Device Setup, Conventional Atomizer

(Source: Parker Hannifin Gas Turbine Fuel Systems Division)

The nozzle was mounted to a modular mechanical adapter, allowing for this nozzle to be attached to the mechanical probe device.

CHAPTER IV

SIMULATION SETUP

4.1 Simulation Background Knowledge

Atomization through pressure swirl atomizers is an inherently turbulent process with pressure differentials and the fluid medium being two of the major variables factoring into the quality of the spray, shape of the spray, and droplet size of the fluid.

This highly turbulent process is based on the Reynolds number being very high in the small passages of the atomizer. Geometric surface imperfections are another variable that can factor in to the categorization of the flow. Based on the two nozzles studied in this thesis, the conditions of the simulations will vary. A basic overview of the potential choices selected in the simulations is required to understand how to accurately represent the true physics of the problem.

In the lifetime of computational fluid dynamics (CFD), multiphase flow models have helped to significantly increase the accuracy and predictability of simulating real world physics. Multiphase models are used to simulate the physics occurring within a system where two or more phases of one or two fluids are interacting. With both nozzles examined in this paper, a multiphase model will better predict a better set of results due to the interaction between the fluid (MILPRF-7024C and water) and the air it enters.

4.2 Code Anchoring (CFD boundary conditions, comparison with another case)

To gain an understanding of the underlying physical phenomena and their effects on the simulation, CFD code must be anchored to existing cases testing similar physics. The case used to ensure that ANSYS Fluent gives adequate results, is based a similar unpublished study conducted at Parker Hannifin, Gas Turbine Fuel Systems Division by E. Steinthorssen.

The simulation conducted uses the CFD code ANSYS Fluent, using the volume of fluid (VOF) method to simulate the air core, typical of pressure swirl atomizers. In this report, the authors simulated a manufactured pressure swirl atomizer and ran experiments to obtain the spray angle at different pressures in order to capture the air core at the outlet orifice. The same atomizer was created in CAD software and used in Fluent.

The CAD model which had an orifice diameter of about 0.040 inches was then imported into the simulation program. Since the purpose of the code anchoring/code validation is to identify if the Fluent code gives results within the real world operating conditions of the nozzle, the following parameters were set –

Table 4. Code Anchoring CFD Matrix

Fluid	Turbulence Model	Multiphase Model	Inlet Gauge Pressure (psi)	Outlet Gauge Pressure (psi)	Mesh Cell Count
Water	Realizable k-epsilon with enhanced wall treatment	Volume of fluid, explicit	100	0	Approximately 1.4 million

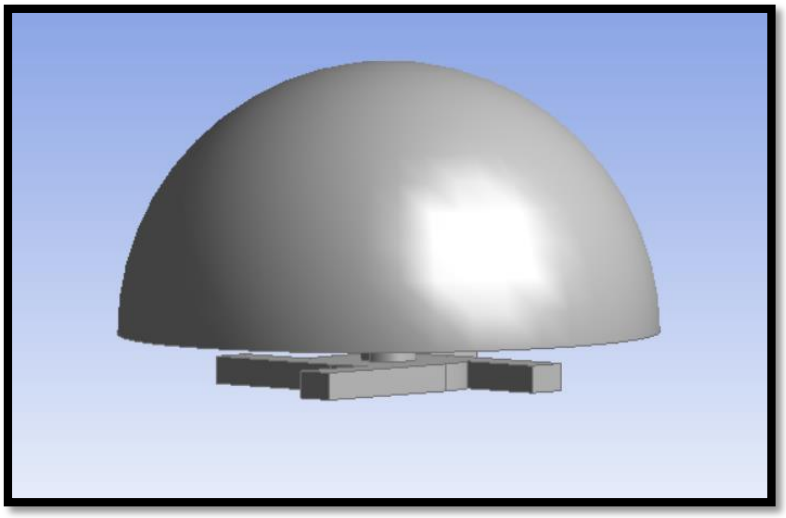

Figure 35: Code Anchoring Fluid Domain

The preceding figure, 35, is the model used in the code anchoring simulation. This swirler design is similar to the model used in the Parker Hannifin engineering report this code validation is based on. An inflation boundary layer is applied to the model to monitor the effects of the boundary layer on the spray formation, in addition to boundary film thickness.

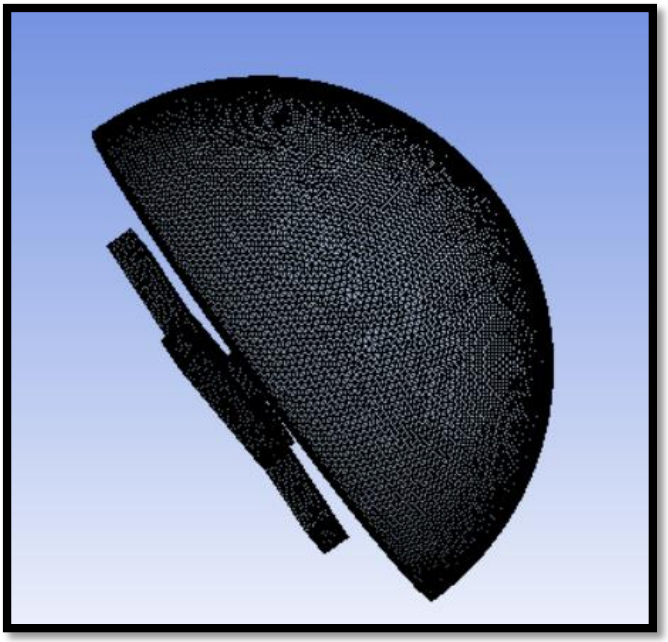

Figure 36: Meshed Code Anchoring Fluid Domain

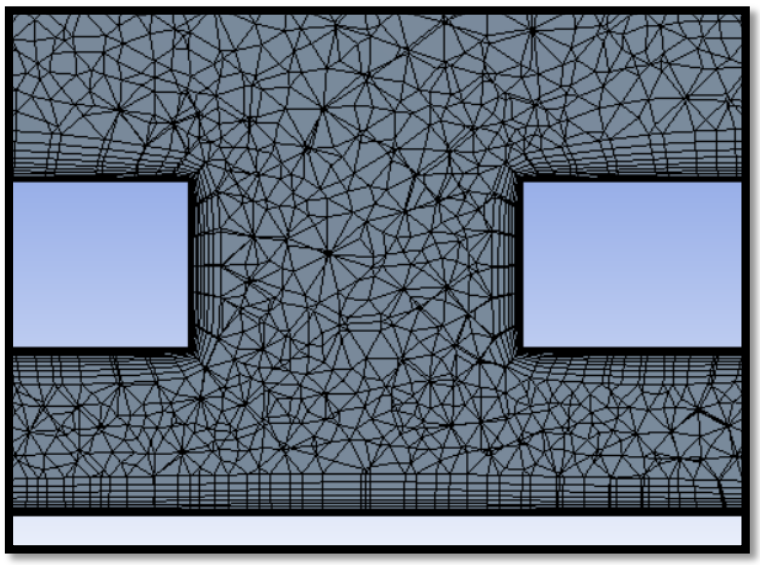

Figure 37: Code Anchoring Cross Section of Orifice

An inflation layer is applied to the walls of the inlet ports and the outlet orifice, as seen in figure 37. This is meant to capture film thickness and any fluctuations that may have on the spray characteristics.

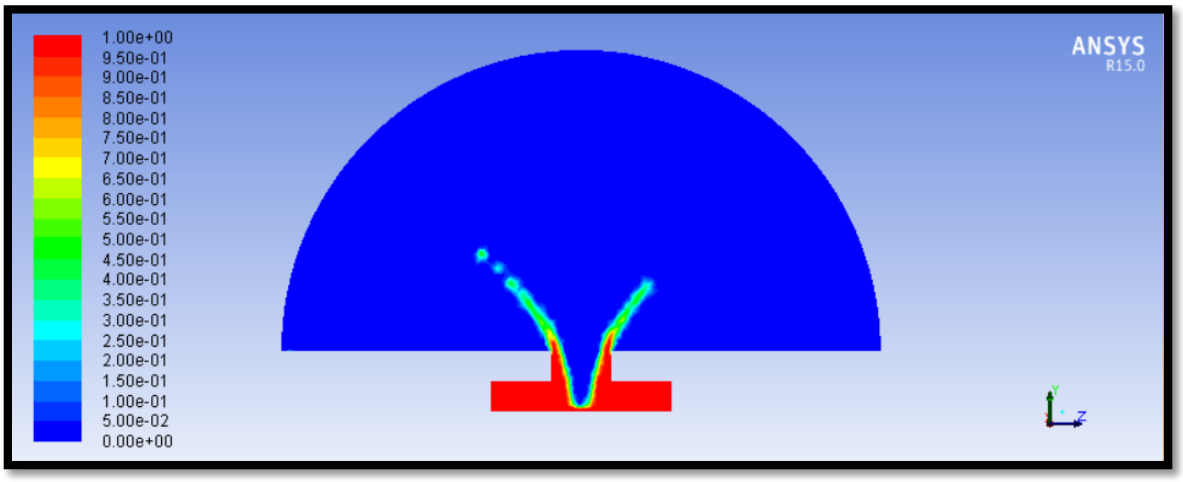

Figure 38: Code Anchoring Volume Fraction

Figure 38 shows the volume fraction of the entire model for water. Red represents water while blue represents air. Upon first glance, it is easily seen that the spray angle is fully displayed and the air core has fully formed. To verify this, pressure contours and velocity vectors must be correlated with the data obtained.

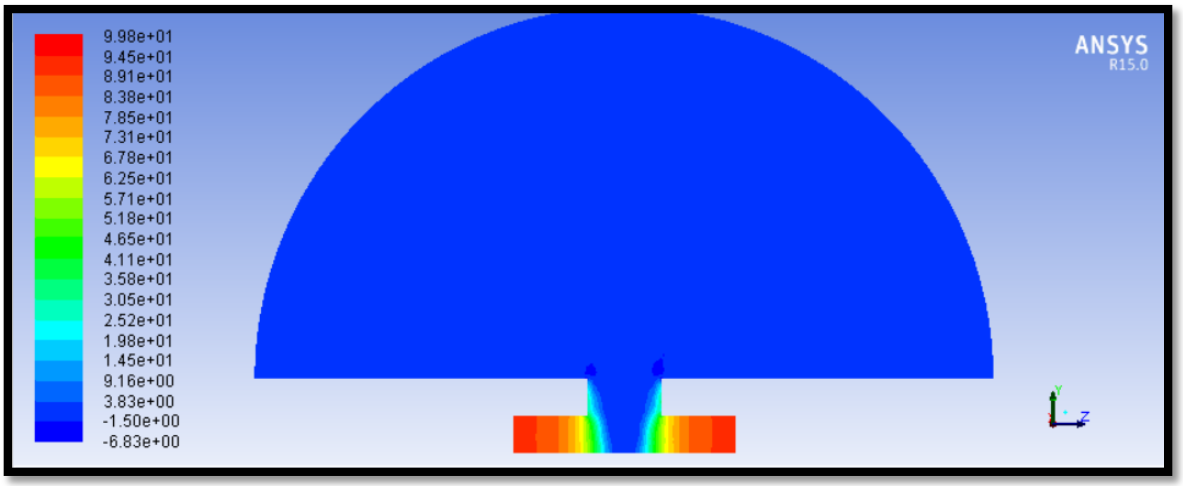

Figure 39: Code Anchoring Pressure Contours

The pressure contours of the geometry show the rapid pressure drop through the length of the inlet port as the fluid reaches the orifice. The low pressure region in the orifice is a good sign, as this is indicative of a low pressure-high velocity region.

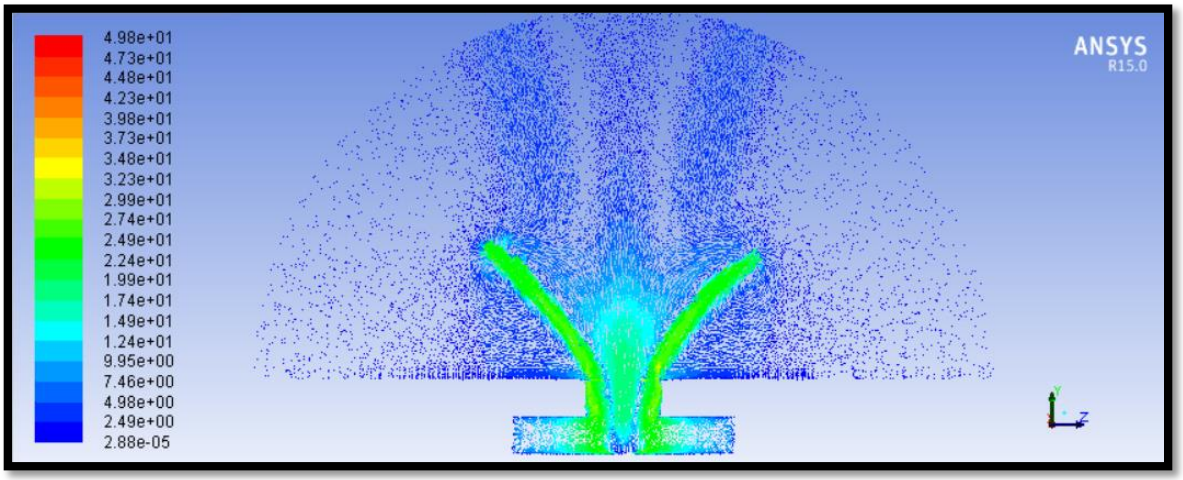

Figure 40: Code Anchoring Velocity Vectors

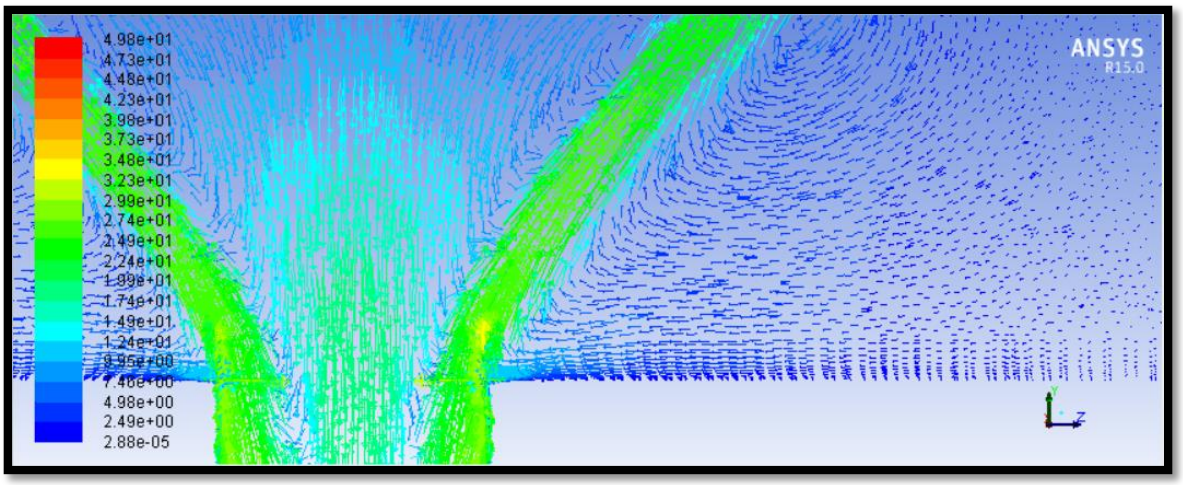

Figure 41: Code Anchoring Velocity Vectors, Orifice

The preceding figures, 40 and 41, show the velocity vectors in the air core and the region downstream of the orifice. Due to the required energy balance, you can see the fluid entrainment as the high speed vectors of the liquid jet force the surrounding stagnant air

into recirculation zones. Fluid entrainment is the process of trapping a fluid through another fluid's movement.

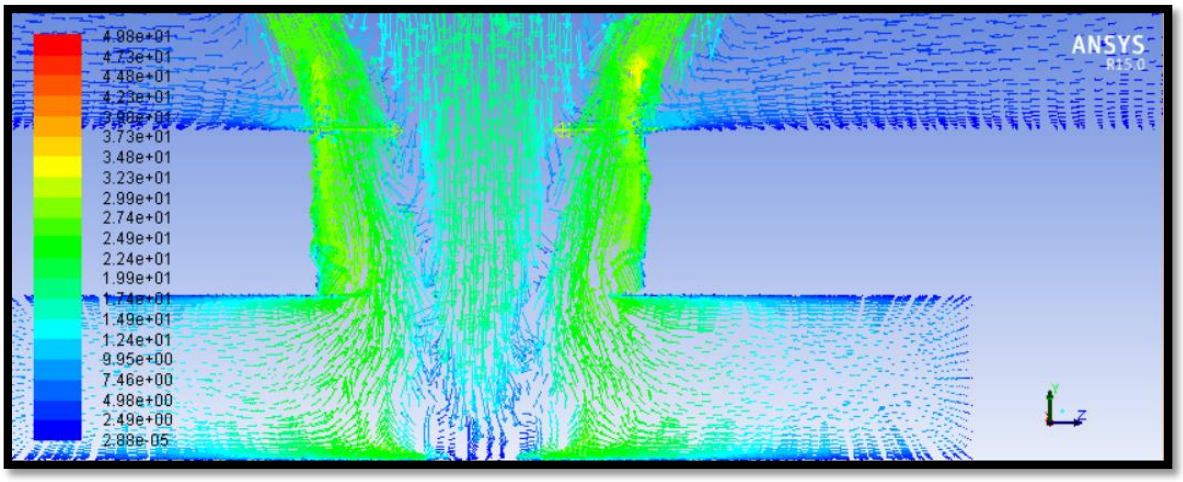

Figure 42: Code Anchoring Velocity Vectors, Air Core

Figure 42, the velocity vectors in the orifice, show the rushing of air into the air core vortex and back out again in the region between the air core and the film surrounding the wall thickness.

The results from the code validation process show that ANSYS Fluent has good agreement with real physical phenomena that occur with pressure swirl atomizers. The images show the film thickness against the outlet orifice wall. The air core formation is easily distinguishable from both the velocity vectors and volume fraction plots. The spray angle is also easily distinguishable in the volume fraction contours. These results give a strong showing of the accuracy of the models selected and utilized during simulations.

Before going on to run simulations of the model, it is critical to understand the impact of mesh resolution on the accuracy of the results and capturing of the physical phenomena occurring. Because of this, it is necessary to run a grid independence study, separate from the code validation, utilizing the model of the atomizers studied in this thesis.

4.3 Grid Independence Study

When conducting a CFD study, it is crucial to keep in mind the good practices and techniques that help ensure solution accuracy. Through this thinking comes the technique of grid independence studies. By identifying the mesh with an adequate amount of cells, extra computational time and processing power are eliminated, meaning that a solution is obtained in the shortest possible time with the fewest resources and a high degree of accuracy. To understand the effect of the mesh resolution on the solution stability and accuracy, a grid independence study was conducted for both the macrospray and conventional atomizer nozzles.

Four meshes were used for the study with a testing order of coarse > finer > finest. With this in mind, it was decided to refine the entire mesh, but to focus primarily on the outlet orifice region.

This region is of interest due to the film thickness and air core formation. Proper tracking of the multiphase interaction is very important in this region.

A set of criteria must be established to understand if a solution is considered to be accurate enough. The criteria to move from one mesh to another include –

1. The multiphase interaction was easily distinguishable with expected flow features of the spray.

2. The current solution was more stable versus the previous.

Once the two criteria have been met, a finer mesh was generated and was used in a simulation. Upon reaching solution stability, the solution was interrogated to see what gains, if any at all, were made from moving from a coarser mesh to a finer mesh.

Table 5. Macrospray Atomizer Grid Independence CFD Matrix

Mesh Count (cells, approx.)	**Turbulence Model**	**Fluid**	**Inlet Pressure (psi)**	**Outlet Pressure (psi)**
1 million	k-epsilon realizable w/ enhanced wall treatment	Water	145	0
3.5 million	“	“	“	“
7 million	“	“	“	“

Table 6. Conventional Atomizer Grid Independence CFD Matrix

Mesh Count (cells, approx.)	**Turbulence Model**	**Fluid**	**Inlet Pressure (psi)**	**Outlet Pressure (psi)**
1.5 million	k-epsilon realizable w/ enhanced wall treatment	MILPRF 7024	100	0
2.8 million	“	“	“	“
3.7 million	“	‘	“	“
3.8 million	“	“	“	“

The grid independence study showed that a mix of mesh resolutions was the best fit for the studies. The coarser cells were more concentrated near the inlet (discounting the boundary layer cells) and throughout the body of the inlet region. The orifice region required a highly dense mesh including the region immediately downstream of the outlet, in an attempt to capture the air core formation. In addition, the increase of cell count size from the second mesh to the third mesh did not improve the appearance of any physical events, such as the air core formation or the interfacing between the air and fluid. The 3.5 million cell mesh was selected as the best mesh for the macrospray atomizer, while the 3.7 million cell mesh was adequate in its solution for the conventional atomizer. For more information on the results of the grid independence study, the reader is suggested to reference appendix D.

4.4 Setup for Macrospray Atomizer Simulation

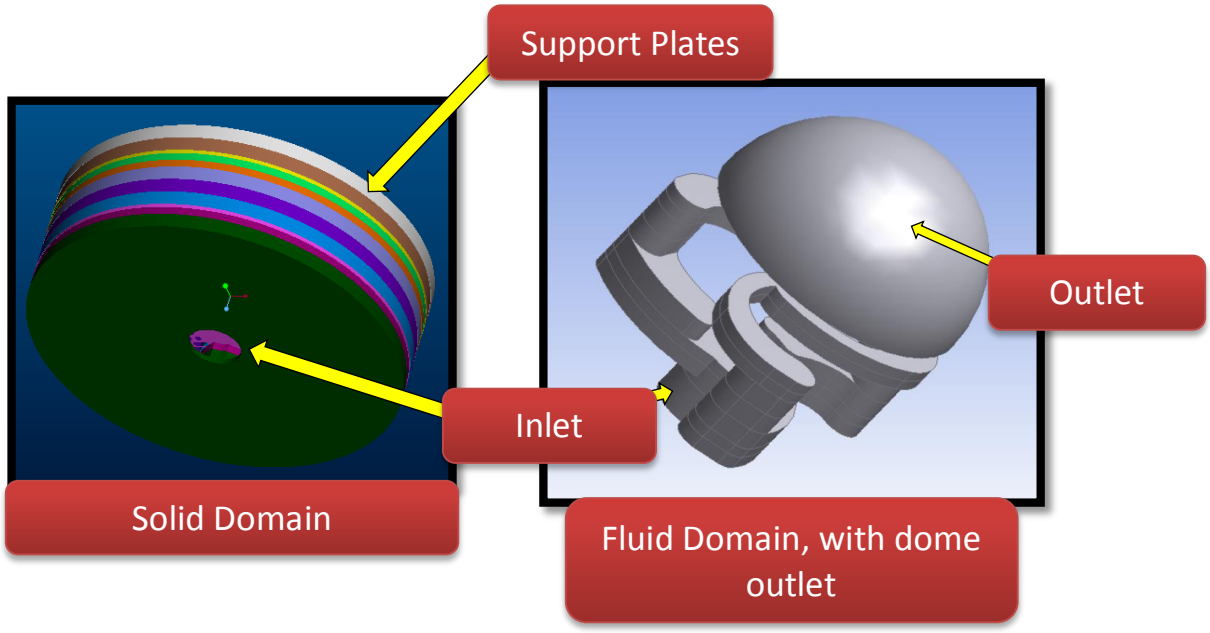

Figure 43: Macrospray Atomizer Solid and Fluid Domains

CAD geometry of the nozzles was generated and imported to ANSYS Fluent and meshed. The micro-atomizer's exit orifice is the area of interest. With this being the focus of the CFD simulation, the grid at this location must be very fine. The production component has a diameter at the exit orifice on the scale of a thousandth of an inch (0.001"). Approximately 3.4 million cells were used for the mesh as shown in figure 44.

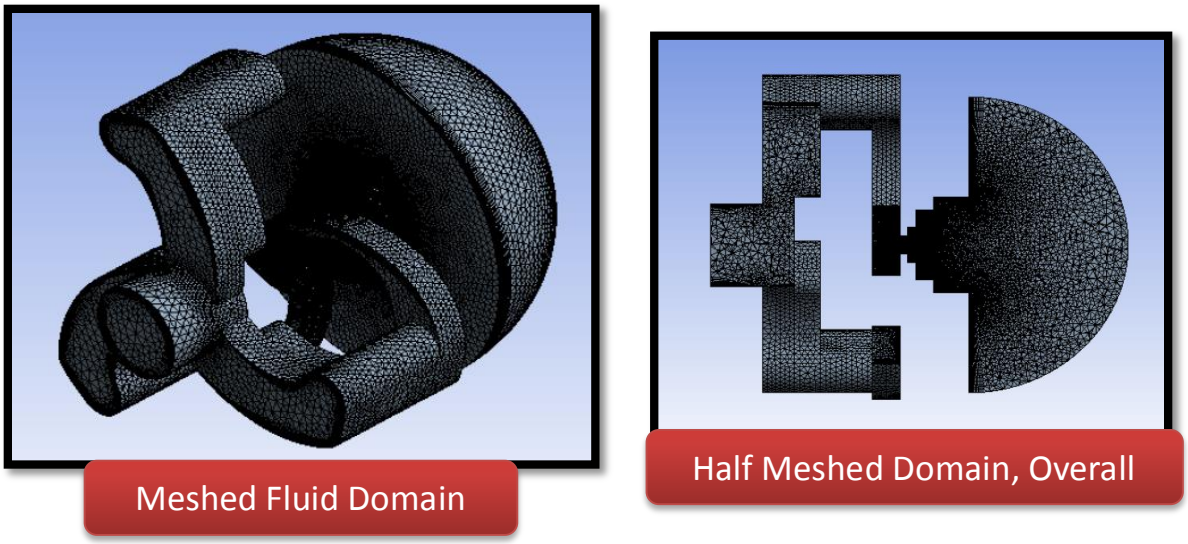

Figure 44: Meshed Fluid Domain

With the results from the code anchoring, the final mesh was used for the remaining simulations. The refinement process allowed for the capture of the air core formation in the outlet orifice and the spray angle downstream the orifice.

Each button model was simulated using its real world conditions. Because of the high injection pressures associated with the buttons, a step up approach was used. Simulations set with high inlet pressures are more predisposed to diverge the solution or result in a solution that does not settle or stabilize. All simulations began with low inlet pressures

beginning at 10 psi increasing by a factor of 2 for the next pressure until the operating condition of 145 psi was met.

During each pressure stage, the multiphase model was enabled. As mentioned previously, the volume of fluid multiphase model must be used to observe the interaction between the MILPRF-7024 calibration fluid and the air it is injected into. By identifying the boundary interface between the two fluids, an understanding of the viscous effects and velocity of the injection fluid on the surrounding medium is gained.

Table 7. Inlet Pressure Selections for CFD Runs, Macrospray Atomizer

Inlet Pressure Conditions (psi)
10
20
40
80
145

Enabling the multiphase model changes the simulation to a transient problem. Because of the transience of atomization, a very small time step on the order of 1e-7 is used and is slowly scaled up as the solution stabilizes. Upon the completion of a run and obtaining an adequate solution, the mesh was further refined.

4.5 Setup for Conventional Atomizer Nozzle Simulation

The conventional atomizer geometry was generated using Pro-E/Wildfire and was exported into ANSYS Workbench. The mesh generated for the model was at least 3.7 million cells with boundary inflation layers to capture the wall interactions.

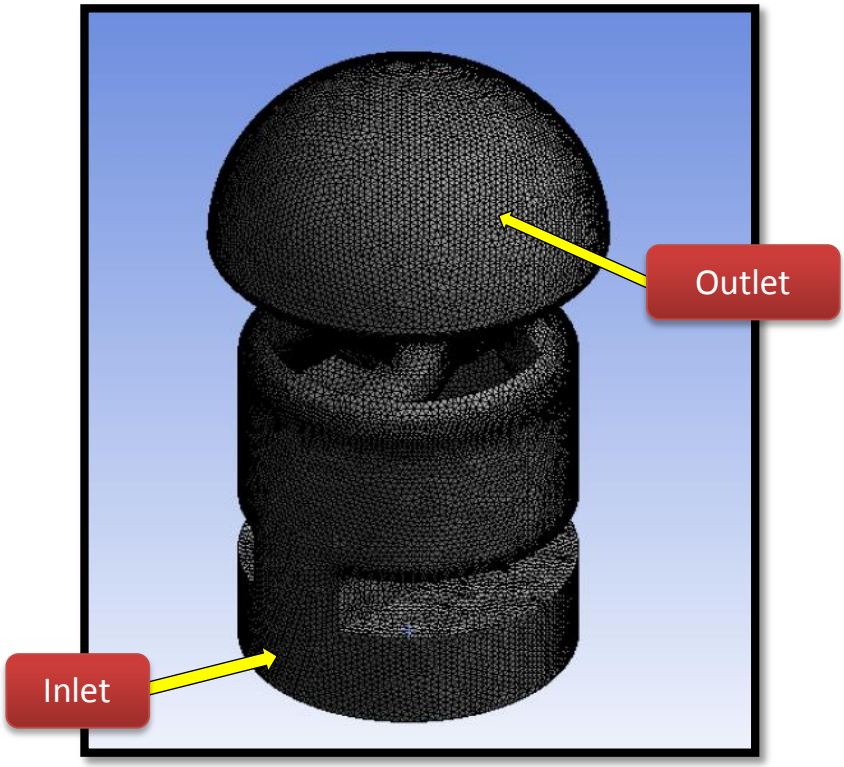

Figure 45: Meshed Conventional Atomizer Fluid Domain

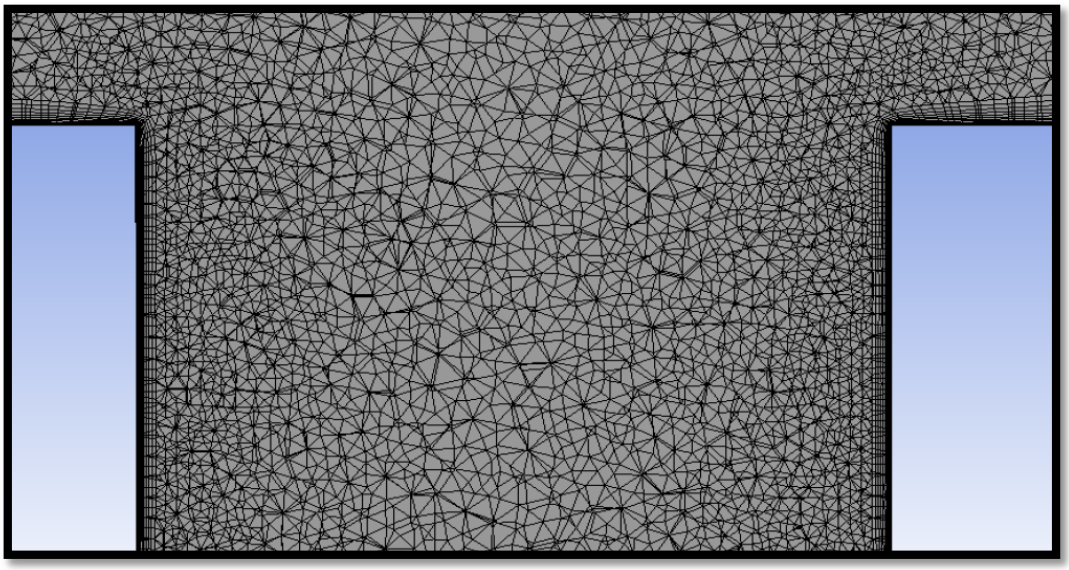

Figure 46: Meshed Conventional Atomizer, Orifice Close Up

In Fluent, a pressure-based solver was used to simulate the fluid flow, while the boundary conditions were modeled after the real world conditions of the atomizer. Due to the transience of atomization, the simulations were slowly increased from 10 psi up to 100 psi. This process was used to prevent the solution from diverging. After settling at 100 psi, the simulations were tweaked further. The selected residuals for the x,y and z velocities, in addition to the continuity, were 1e-3; a parameter selected based on the transience of the atomization. Mass flow and static pressure monitors were set to ensure solution stability and convergence.

Due to the real world physics of the problem, the k-epsilon turbulence and volume of fluid (VOF) multiphase models were enabled. The k-epsilon turbulence model was required to simulate the turbulent flow through the atomizer and to capture the wall effects. This simulated the fluid injection into the surrounding air medium.

Similar to the simulation parameters for the micro-atomizer, the large atomizer is also modeled with the volume of fluid multiphase model. The boundary interface is of great interest with the MILPRF-7024 and surrounding air medium.

Due to typical meshing practices, cells a certain length downstream of the outlet are usually larger cells since these areas are not commonly of interest. However, after completing a run in Fluent, the mesh was further refined to give a higher resolution for the boundary interface. This is needed due to the potentiality of a coarse grid losing track of what occurs downstream of the outlet orifice. Refinement with the VOF model helps to track boundary interface between the fluids.

Upon completion of the simulations, data were exported to ANSYS CFD-Post to post-process the data. Still-images were exported from Fluent. Spray angles were calculated using the image analysis software, FIJI (Fiji Is Just ImageJ). The angle tool functionality in FIJI allows the user to set the midpoint and endpoints to calculate an angle.

CHAPTER V

RESULTS

5.1 Results for Macrospray Atomizer Simulation

The volume fraction plots henceforth follow the legend scheme of red representing the flowing fluid, with blue representing air. The macrospray atomizer plots use red to represent water.

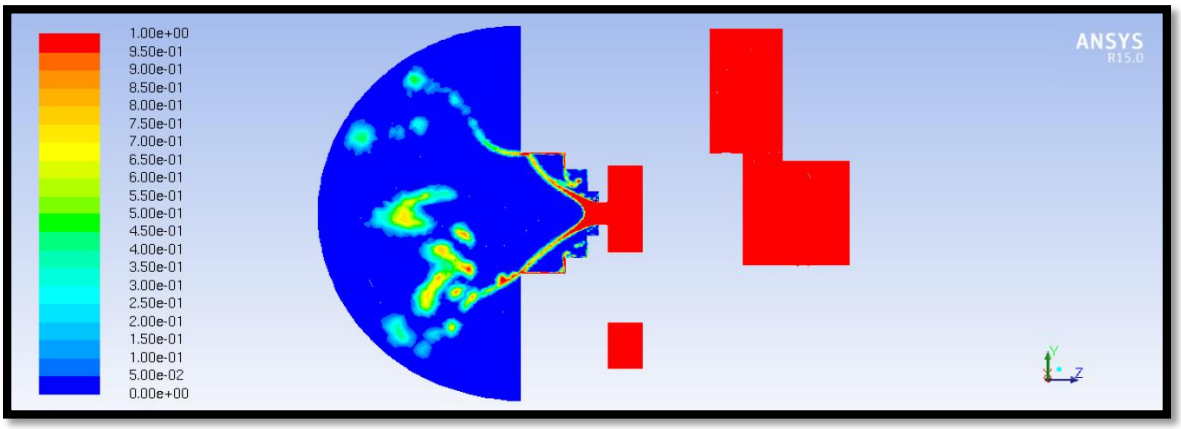

Figure 47: 145 psi, Macrospray Atomizer, Volume Fraction

Figure 47 shows the volume fraction plot of the macrospray atomizer under operating conditions. Downstream of the orifice, one can see the coalescing of water on to itself in addition to misting. This occurs in normal operation of the atomizer as pressure can fluctuate during the atomization process. This fluctuation affects the fluid dynamics of the observed system. Downstream of the orifice, the dispersing fluid is impinging upon the corners of the atomizer geometry, having an effect on the angle downstream after entering the hemispherical outlet domain.

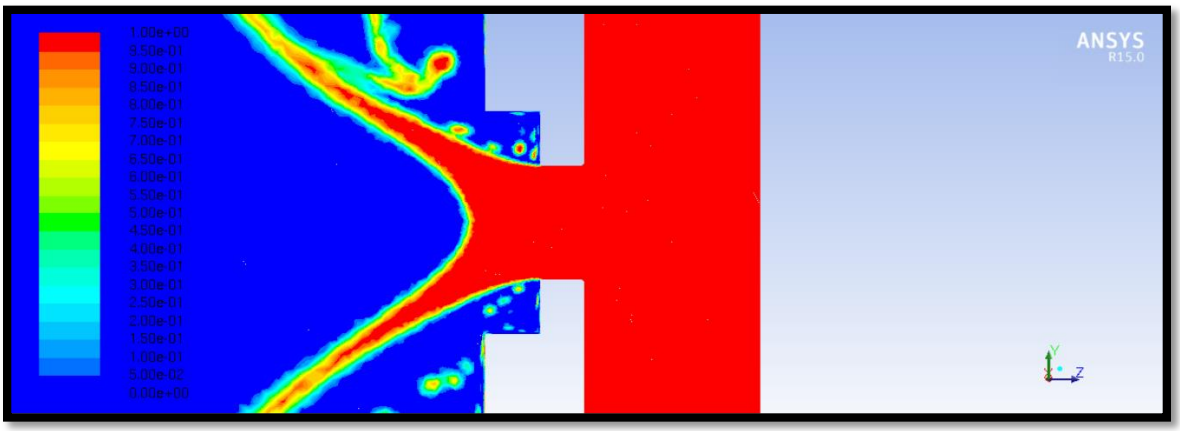

Figure 48: 145 psi, Macrospray Atomizer, Volume Fraction, Orifice

Figure 48 is a close up view of the orifice. The smaller droplets near the exit of the orifice appear due to occasional ejection of fluid that occur due to fluctuations of the flow, both upstream and downstream of the orifice.

The volume fraction plots are best suited for measuring the spray angle. After using FIJI (Fiji Is Just ImageJ) software, the spray angle was calculated to be approximately **65°**.

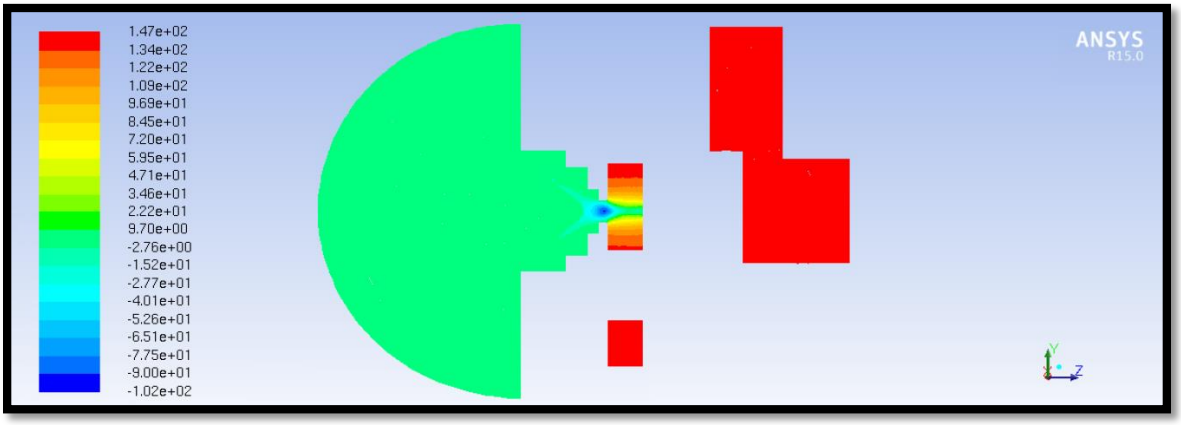

Figure 49: 145 psi, Macrospray Atomizer, Pressure Contours

Figure 49 is an overview of the macrospray fluid domain with its corresponding pressure contours. Upon first glance, the contours seem to follow the trend with the physical phenomena occurring in the atomizer.

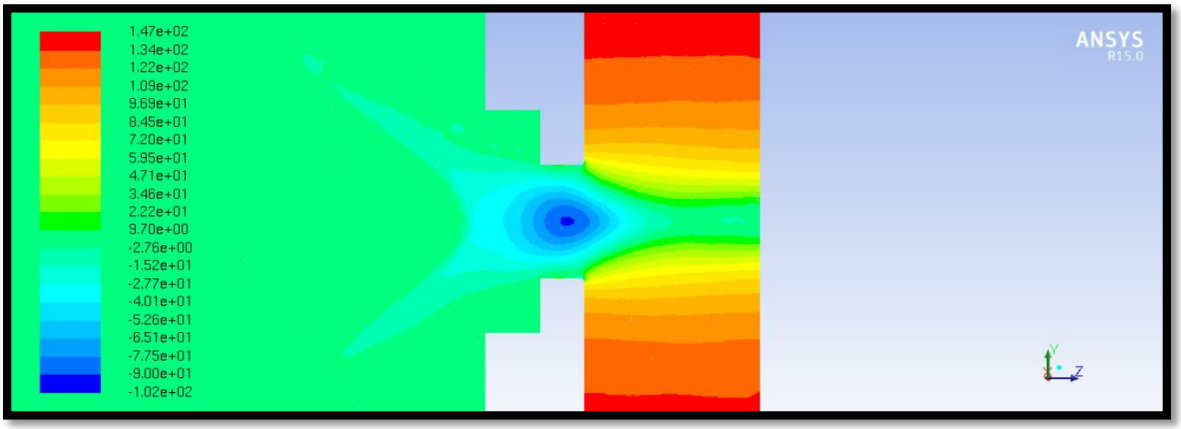

Figure 50: 145 psi, Macrospray Atomizer, Pressure Contours, Orifice

Figure 50 is a close up view of the orifice with its corresponding pressure contours. A low pressure region has appeared in the center of the orifice. This is indicative of pressure swirl

atomizers as previously stated in this report, which have a low pressure region in the center of the spray and atomizer, resulting in an air core.

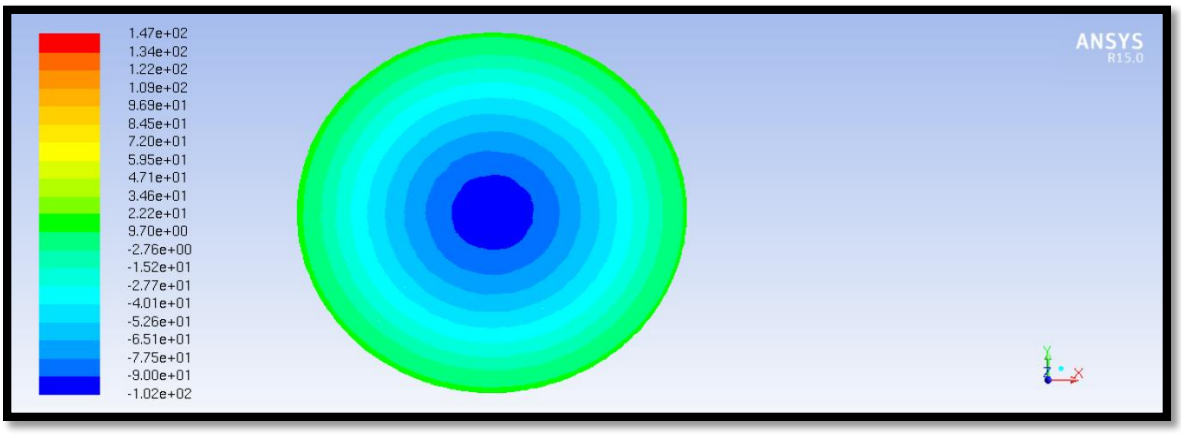

Figure 51: 145 psi, Macrospray Atomizer, Pressure Contours, Orifice Cross Section

The next figure, 51, shows a cross sectional cut of the orifice with the direction of flow being into the page. This figure provides further evidence of the low pressure region in the orifice of the atomizer.

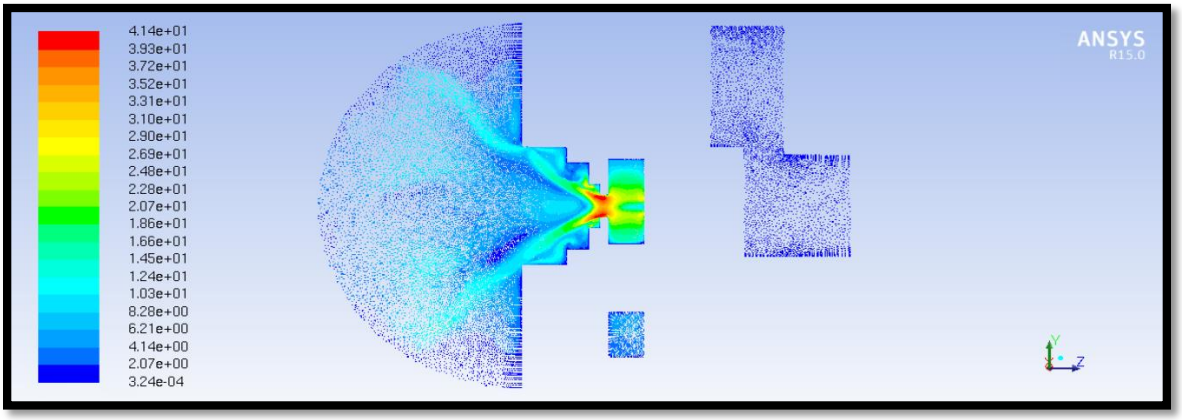

Figure 52: 145 psi, Macrospray Atomizer, Velocity Vectors

This overview of the velocity vectors, figure 52, is in accordance with both the volume fraction plots and velocity vectors. The fluid path is easily seen with the jets following the same path as those of the volume fractions shown in figures 47 and 48.

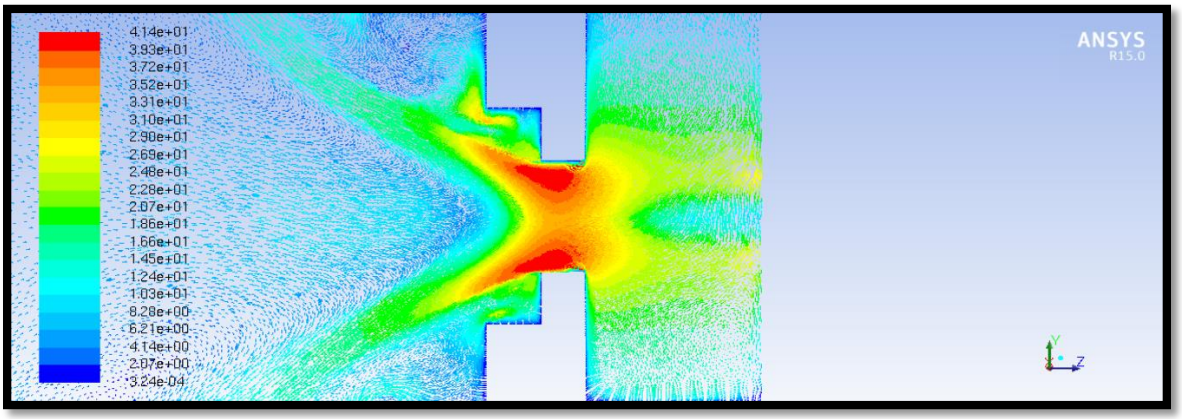

Figure 53: 145 psi, Macrospray Atomizer, Velocity Vectors, Orifice

This close up view, figure 53, of the orifice is in accordance with the pressure contours from figures 50 and 51. This relation can be understood as Bernoulli's principle where

high velocity regions are indicative of low pressure zones and low velocity regions are indicative of high pressure zones.

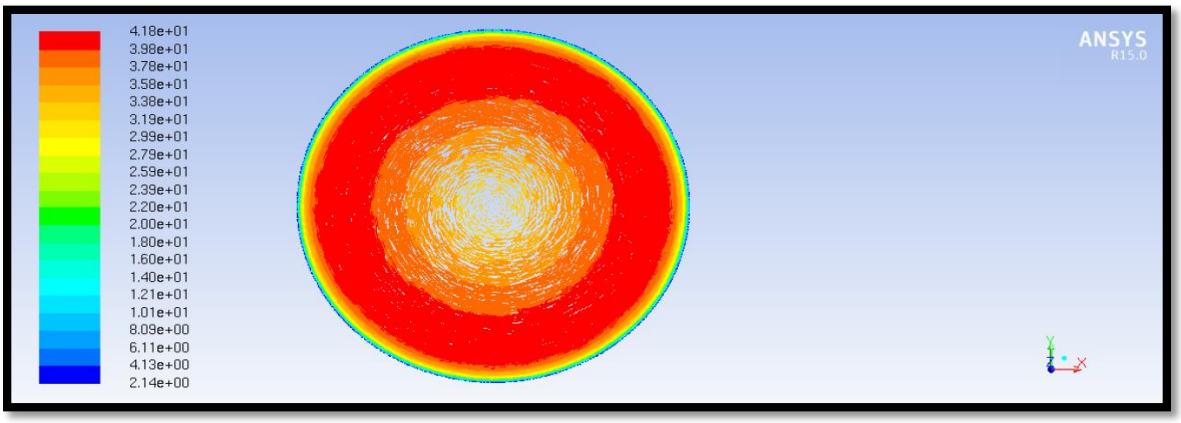

Figure 54: 145 psi, Macrospray Atomizer, Velocity Vectors, Orifice Cross Section

Figure 54 provides further evidence of the air core in the center of the orifice. This cross sectional cut of the orifice shows the flow having a direction into the page.

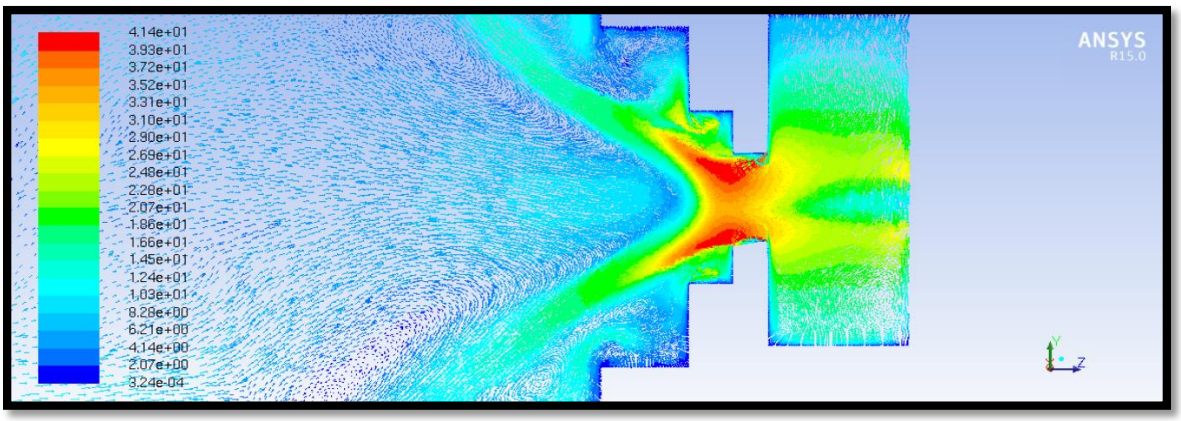

Figure 55: 145 psi, Macrospray Atomizer, Velocity Vectors, Air Core

The vectors in figure 55 show more of the downstream region to highlight how large of an air core is being created. Also seen is the fluid entrainment interaction of the jet of water entering the downstream air domain. This fluid entrainment follows the conservation of energy.

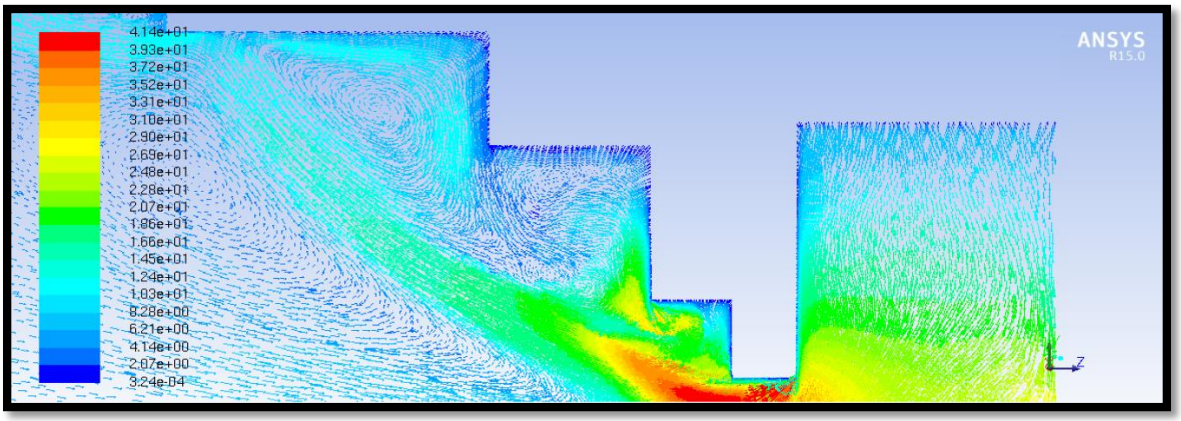

Figure 56: 145 psi, Macrospray Atomizer, Velocity Vectors, Recirculation Zones

Figure 56 shows the heavy recirculation zones being created due to the sharp corners of the geometry and the flow stream impingement.

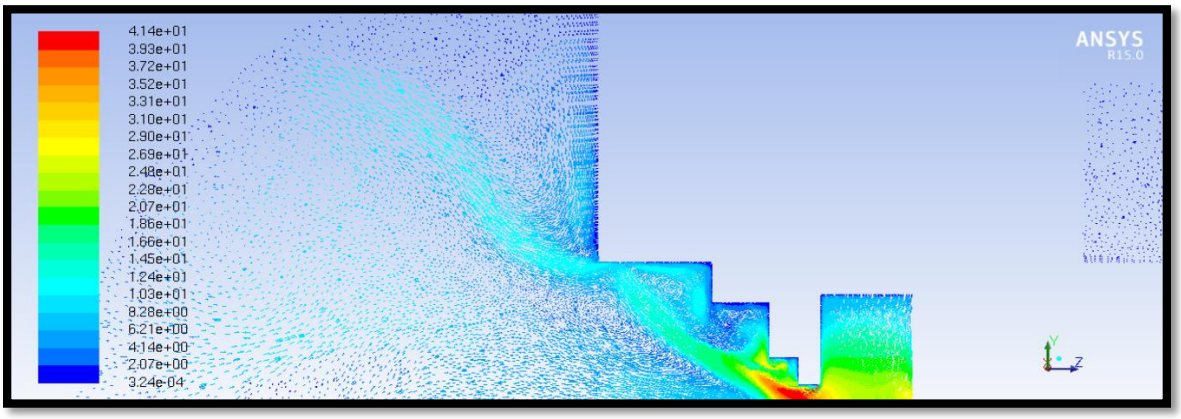

Figure 57: 145 psi, Macrospray Atomizer, Velocity Vectors, Jetstream Top

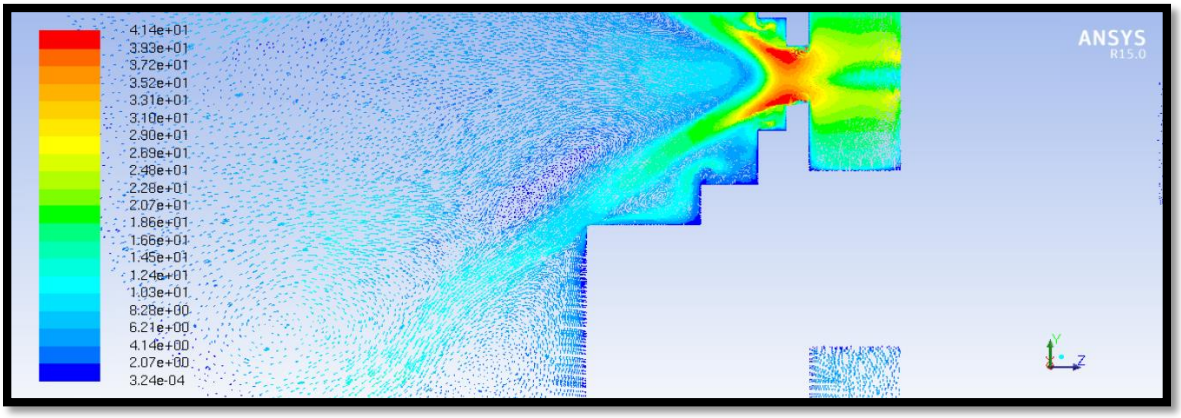

Figure 58: 145 psi, Macrospray Atomizer, Velocity Vectors, Jetstream Bottom

Figures 57 and 58 show the top and bottom jets of fluid entering the domain and their impingement on the corners of the fluid domain. The effect of the impingement is seen in the angle and the direction of the flow immediately downstream of the collision.

5.2 Results from Hot Wire Stand Experiment, Macrospray Atomizer

The following table lists the results from the thirty (30) runs on the hot wire stand. All scans were taken from tests that passed the criteria for a successful run as specified in the experimental setup section of this thesis.

Table 8. Hot Wire Stand, Macrospray Atomizer, Spray Angle Results

Run	X Angle (°)	Y Angle (°)
1	49.38	49.57
2	46.17	48.02
3	48.24	47.64
4	46.47	47.94
5	48.47	49.68
6	46.47	48.02
7	48.24	48.24
8	49.68	48.24
9	47.34	49.38
10	46.47	45.26

Continued from page 87		
11	49.88	46.47
12	47.94	48.17
13	47.64	46.58
14	49.26	47.34
15	48.78	47.94
16	49.42	47.94
17	48.78	49.38
18	48.47	49.38
19	49.38	49.68
20	49.38	46.17
21	46.76	46.47
22	48.78	47.94
23	46.47	48.24
24	49.08	49.38
25	47.94	47.64
26	49.38	48.47
27	48.24	48.24
28	45.86	47.94
29	47.94	48.24
30	47.94	48.17
Averages	**48.14**	**48.06**
Standard Deviation	1.17	1.09
Max	49.88	49.68
Min	45.86	45.26

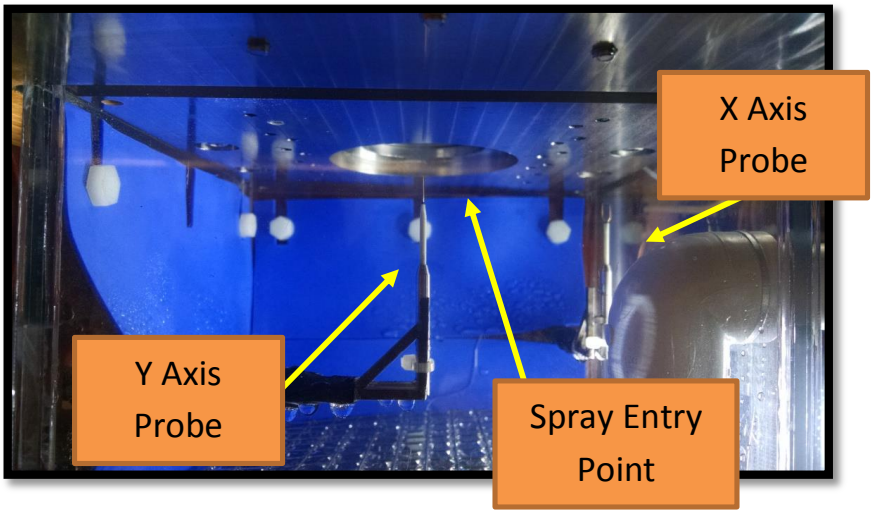

Figure 59: Hot Wire Stand, Test in Progress (Source: Parker Hannifin Gas Turbine Fuel Systems Division)

The macrospray atomizer tested for the duration of this test had an averaged spray angle of about 48° in orthogonal orientations. The table also shows spray angles that widely vary within a band of approximately 4°, as seen with the maximum and minimum spray angles recorded. Figure 59 shows an image of a test in progress, highlighting the orientation of the probes.

5.3 Results from Spray Bench Test Stand Experiment, Macrospray Atomizer

Table 9. Spray Angle Device, Macrospray Atomizer, Spray Angle Results

Run	Angle (°)	Skew (°)
1	45.2	1.8
2	34.4	-1.4
3	39.7	1.3
4	38.6	-0.9
5	39.9	0.7
6	44.8	1.3
7	42.5	2.7
8	41.1	2
9	37.5	0.2
10	39.3	1.1
11	43.7	1.8
12	39.6	1.3
13	45.4	0.8
14	40.9	1.4
15	42.0	0.9
16	39.1	1
17	42.5	2.3
18	43.0	3
19	41.8	2.3
20	40.5	1.7
21	47.3	2.5
22	37.9	0.4
23	42.2	2.6
24	41.7	2.3
25	44.7	3.8
26	45.5	4.2
27	45.6	4.1

Continued from page 89		
28	42.8	2.9
29	43.4	3.2
30	42.8	2.2
Averages	**41.8**	**1.8**
Standard Deviation	2.87	1.31
Max	47.3	4.2
Min	34.4	-1.4

For the thirty (30) tests run using the spray angle device, the macrospray atomizer had an averaged spray angle of about 42°. The table also shows spray angles that widely vary, even more than that of the hot wire stand within a band of approximately 13°. An averaged skew angle of approximately 2° was obtained. Skew is defined as the angle at which the bottom face of the atomizer is offset from the theoretically horizontal plane on which the measuring probes are located to.

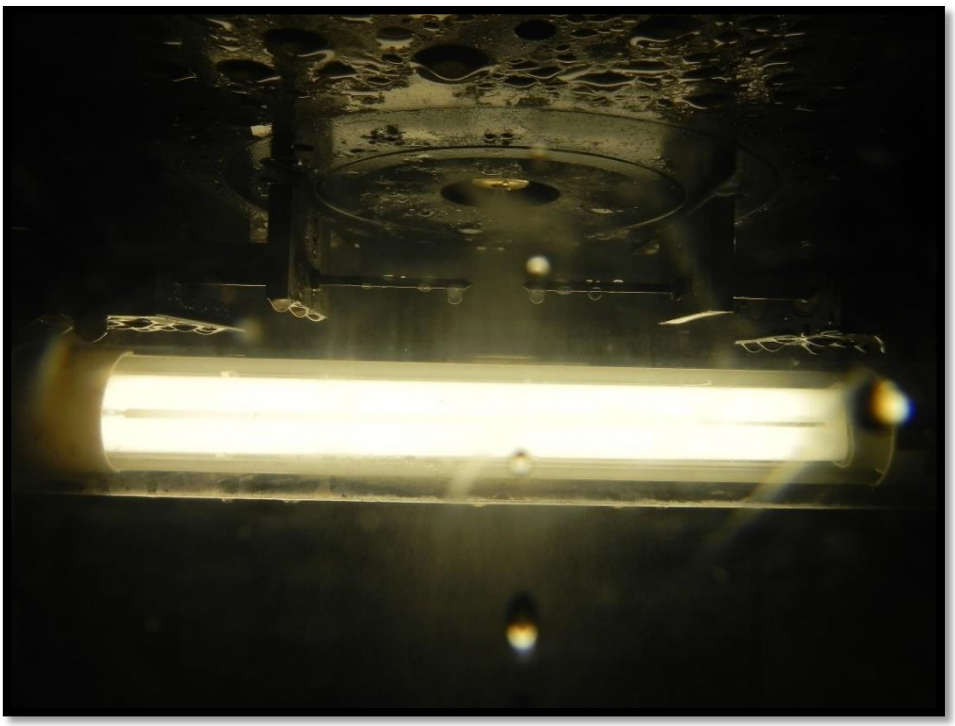

Figure 60: Spray Angle Device, Test in Progress (Source: Parker Hannifin Gas Turbine Fuel Systems Division)

5.4 Results for Conventional Atomizer Nozzle Simulation

After running the simulation for the conventional atomizer with the most optimal mesh resolution, expected results were obtained. Similar to the macrospray atomizer, the phase plots, pressure contours, and velocity vectors must be interrogated to understand the accuracy of the simulation.

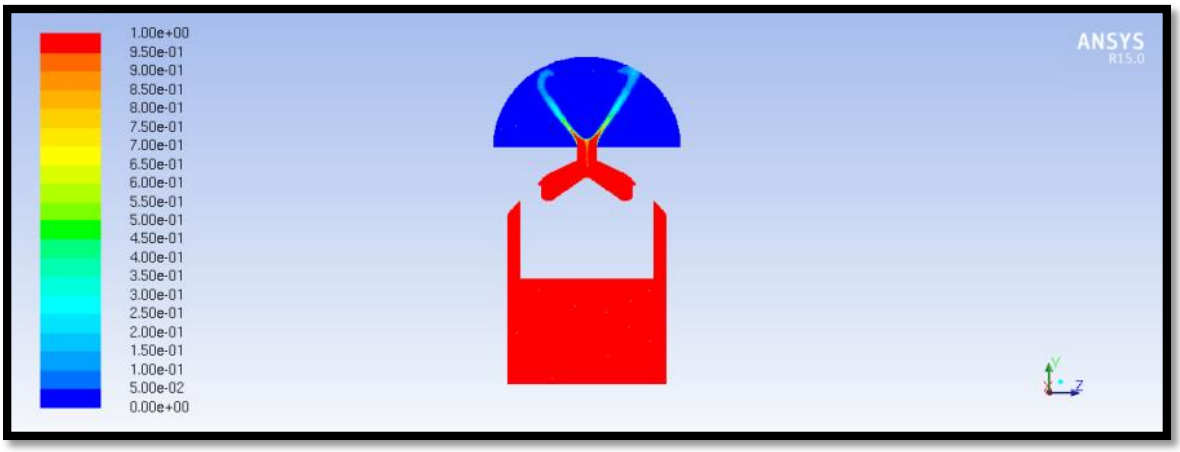

Figure 61: 100 psi, Conventional Atomizer, Volume Fraction

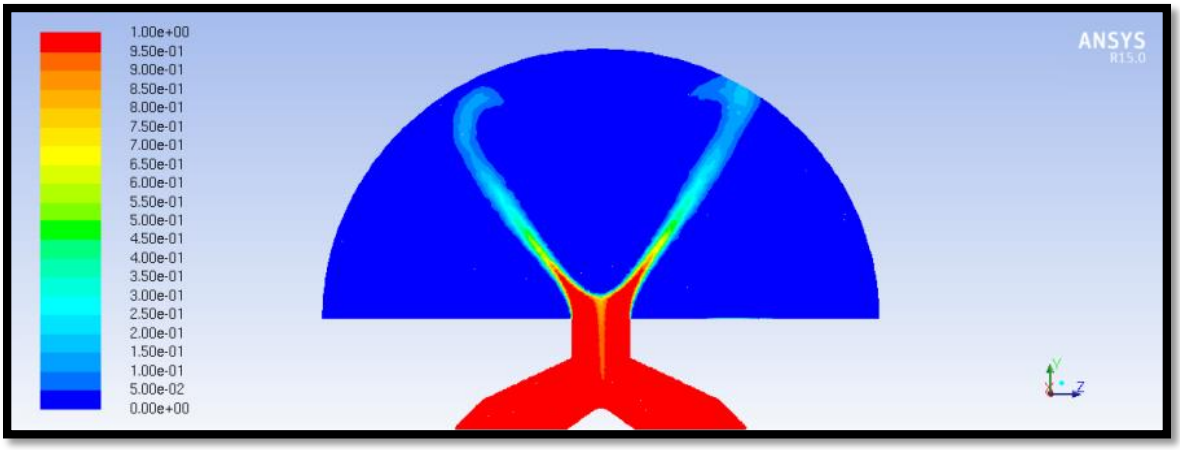

Figure 62: 100 psi, Conventional Atomizer, Volume Fraction, Outlet Domain

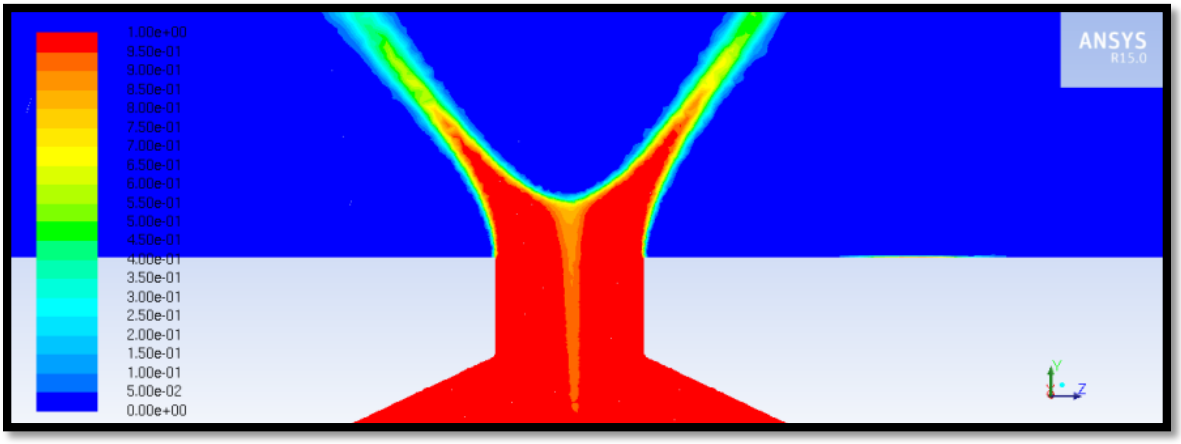

Figure 63: 100 psi, Conventional Atomizer, Volume Fraction, Orifice

Figures 61, 62, and 63 show the volume fraction plots of the simulated nozzle. On the legend, red represents the MILPRF-7024 calibration fluid while blue represents air. All three figures show the air core formation. The air core, while visible, is not as large as expected.

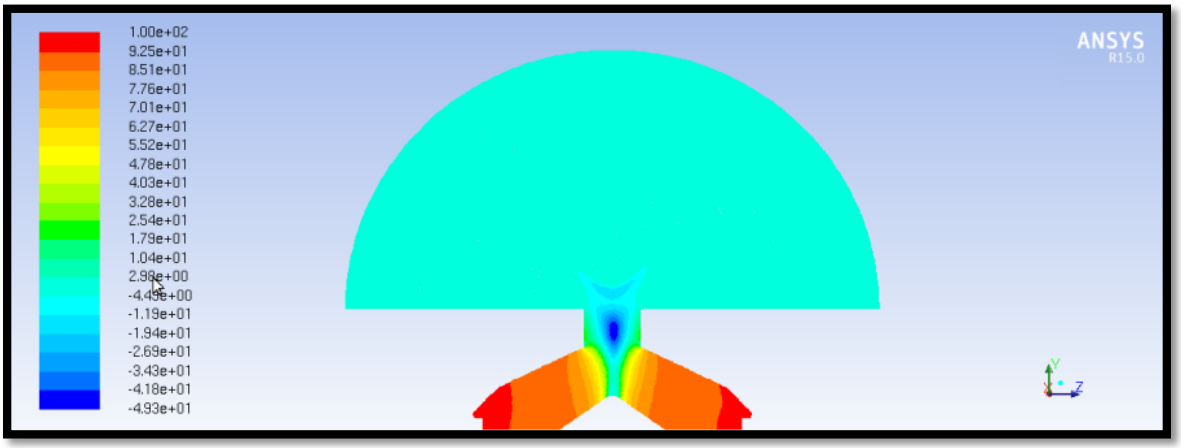

Figure 64: 100 psi, Conventional Atomizer, Pressure Contours, Outlet Domain

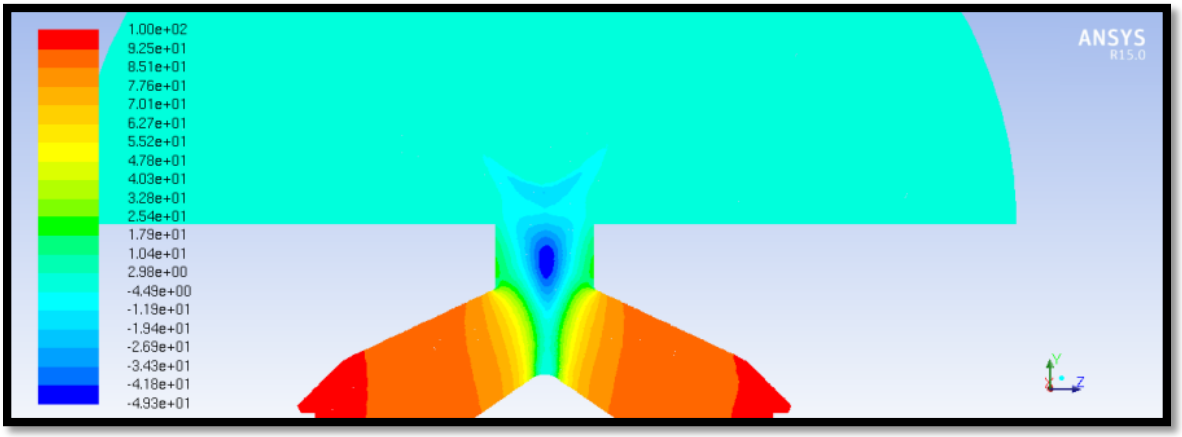

Figure 65: 100 psi, Conventional Atomizer, Pressure Contours, Orifice

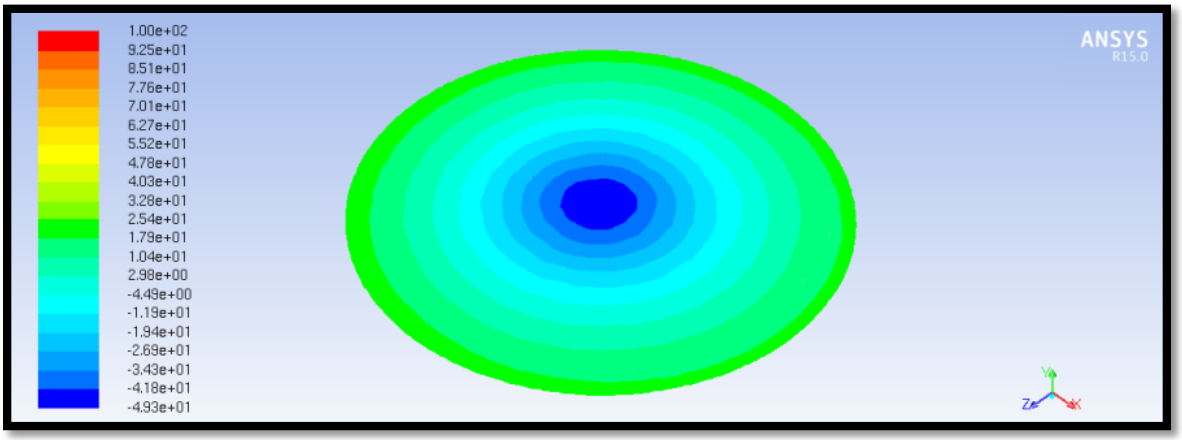

Figure 66: 100 psi, Conventional Atomizer, Pressure Contours, Orifice Cross Section

Figures 64, 65, and 66 show the pressure contours of the conventional atomizer simulation. Figure 66 shows a detailed close up view of the orifice of the nozzle. The low pressure region is indicative of a high velocity flow. This vortex flow is a strong indication of the air core forming in the expected region. A cross sectional cut of the orifice is shown in figure 66. This image further reinforces the low pressure region in the center, indicative of the existence of the air core.

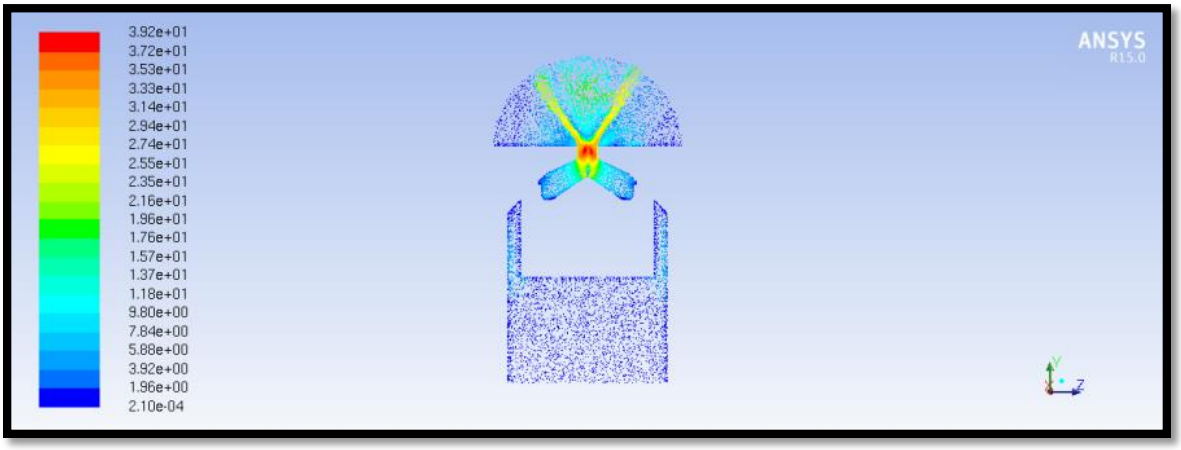

Figure 67: 100 psi, Conventional Atomizer, Velocity Vectors

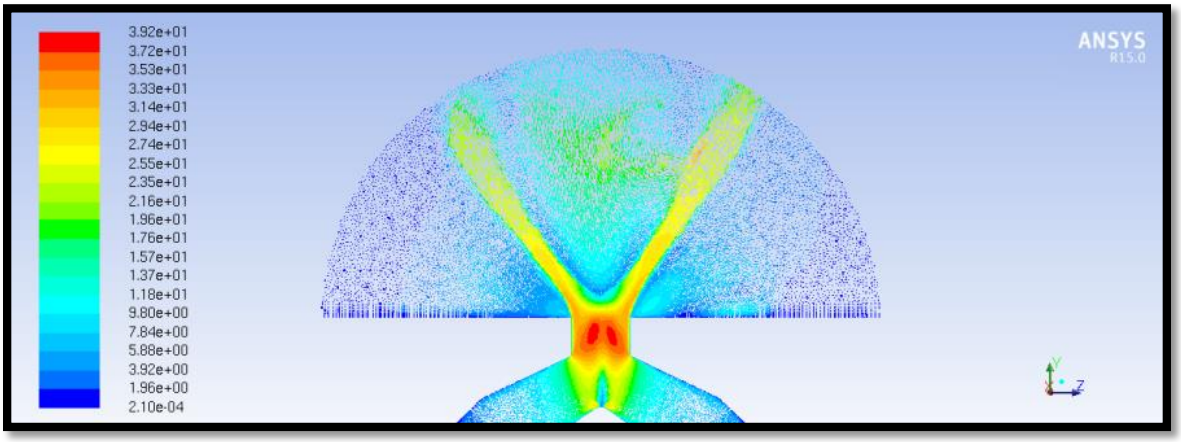

Figure 68: 100 psi, Conventional Atomizer, Velocity Vectors, Outlet Domain

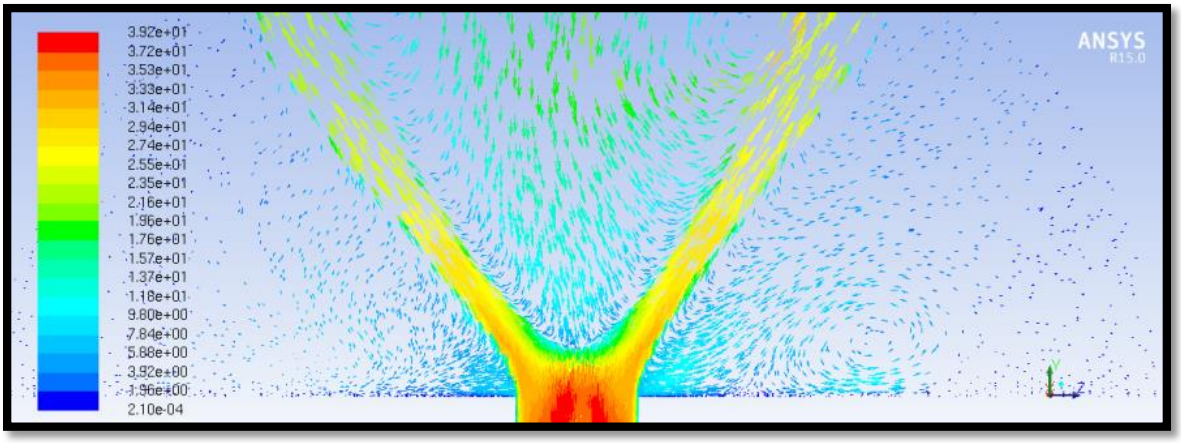

Figure 69: 100 psi, Conventional Atomizer, Velocity Vectors, Air Core

Figures 67, 68, and 69 show the velocity vectors in the model, and show close ups of the downstream outlet region. Here, the high velocity vectors correlate well with the low pressure regions shown in the previous section. Fluid entrainment is seen via the jets exiting from the orifice.

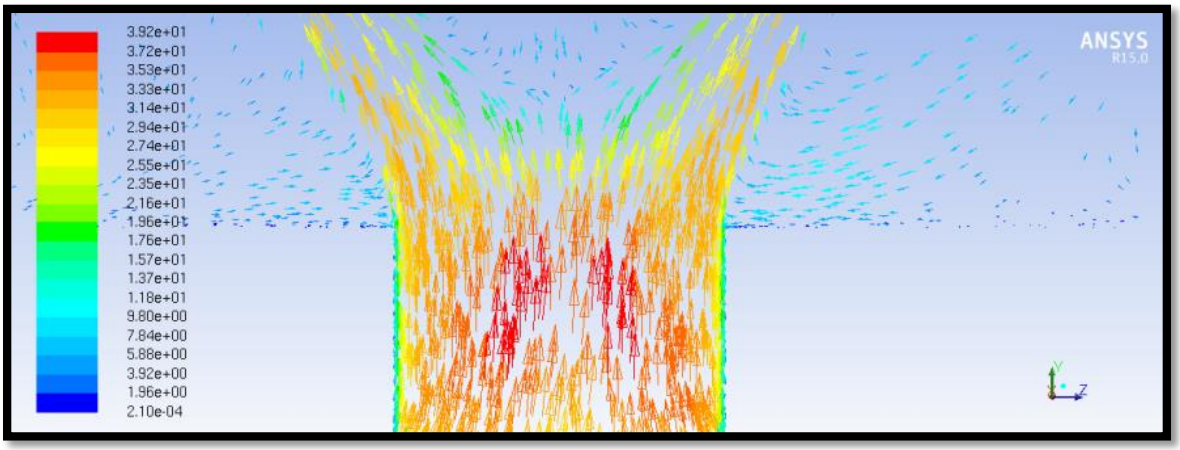

Figure 70: 100 psi, Conventional Atomizer, Velocity Vectors, Orifice

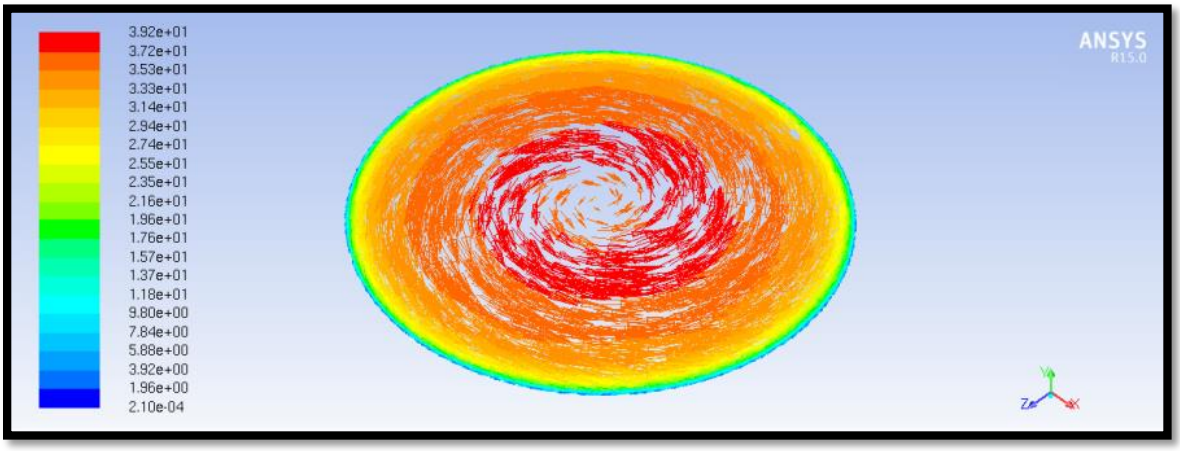

Figure 71: 100 psi, Conventional Atomizer, Velocity Vectors, Orifice Cross Section

The high velocity region in the middle of the exit orifice is easily seen in figures 70 and 71. The rotational direction of the flow shows the swirling motion of the fluid as it rushes

towards the exit orifice. The tangential velocity imparted onto the fluid as it travels through the swirler section results in this velocity distribution.

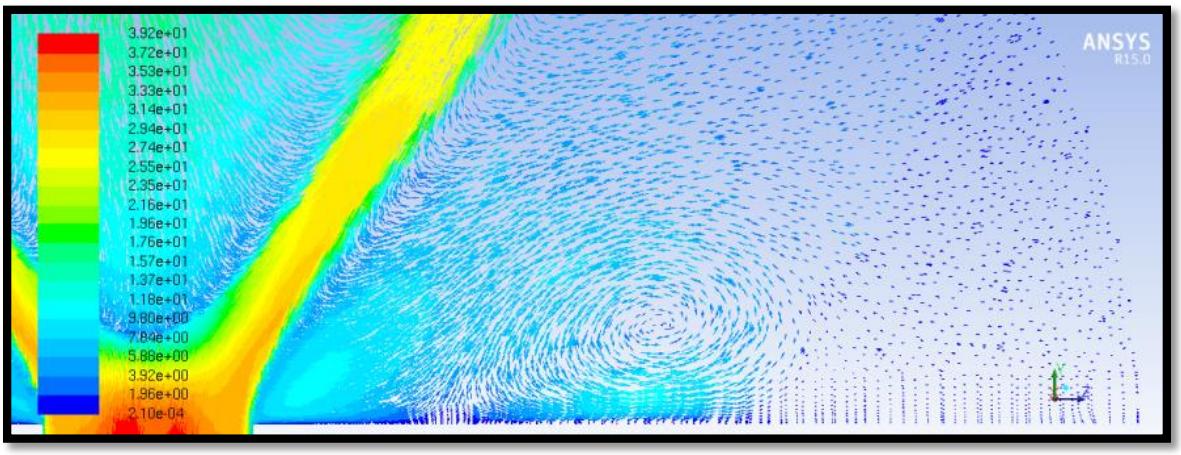

Figure 72: 100 psi, Conventional Atomizer, Velocity Vectors, Recirculation Zones

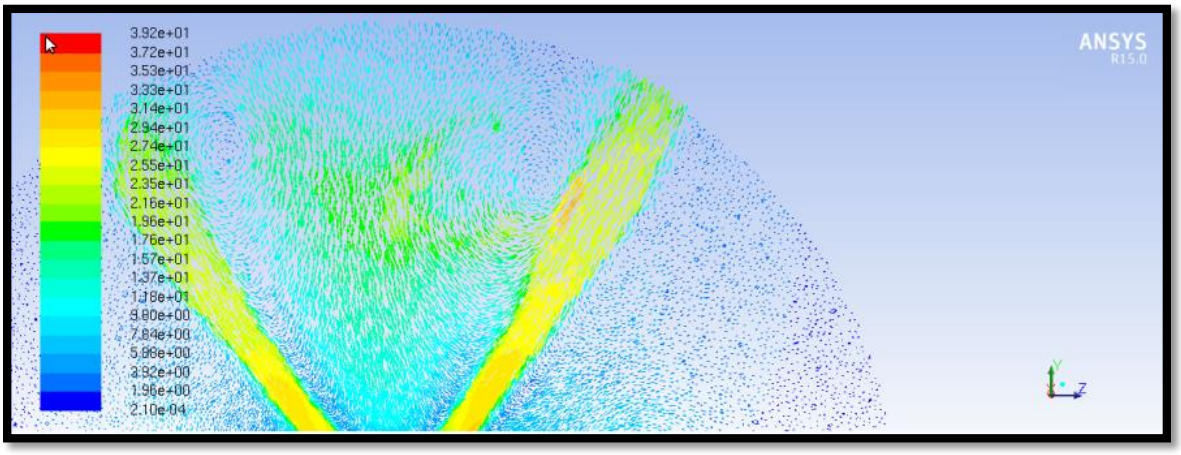

Figure 73: 100 psi, Conventional Atomizer, Velocity Vectors, Jets

Figures 72 and 73 show the fluid entrainment and large recirculation zones occurring immediately downstream of the orifice. The conservation of energy is maintained as the air in the outlet rushes in to fill the void left by the fluid jet.

5.5 Results from Spray Bench Test Stand Experiment, Conventional Atomizer

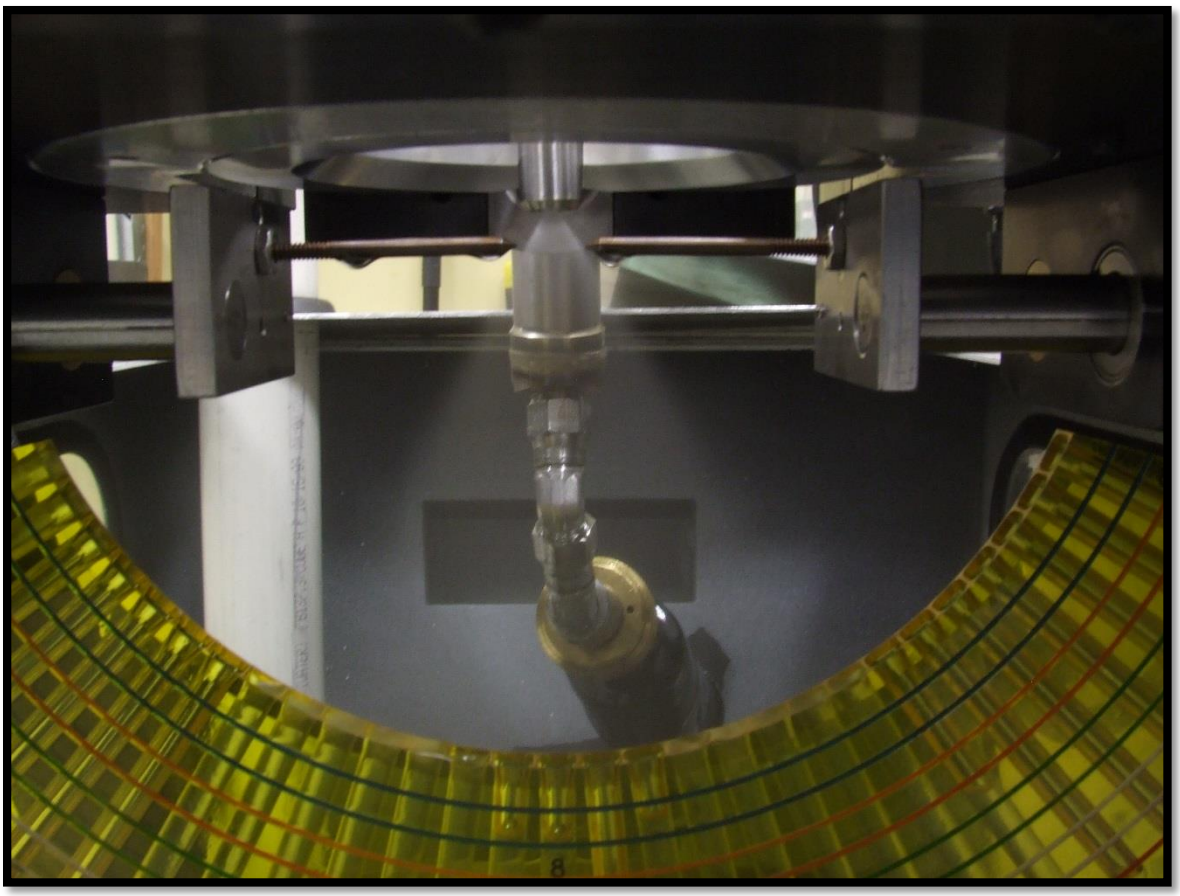

Figure 74: Conventional Atomizer under test, Spray Angle Device (Source: Parker Hannifin Gas Turbine Fuel Systems Division)

Results obtained from the experimental portion of the conventional atomizer showed interesting correlations. The testing document for the nozzle calls for a spray angle in the range of 59° to 65°. This range was not met with the collected data and was instead ranged between 67.7° to 79.1° with an average value of 75.9°. A median value of 76.5° was found. The average value of the data was taken from 30 separate tests. The following table lists the results from testing.

Table 10. Spray Angle Device, Conventional Atomizer, Spray Angle Results

Maximum Angle (Degrees)	**79.1**
Minimum Angle (Degrees)	**67.7**
Average Angle (Degrees)	**75.9**
Median Angle (Degrees)	**76.4**

Table 10 shows the maximum, minimum, median, and average values obtained from the manual angle device experiment of the conventional atomizer. The median and average angles are very close in proximity whereas the minimum angle recorded looks to be an outlier.

5.6 Comparison of Datasets

After collecting all of the data, a deviation and error analysis was conducted to understand how much improvement, if any, was gained through using the CFD and the hot wire test stand for the macrospray atomizer, and the CFD for the conventional atomizer.

5.6.1 Macrospray Atomizer Comparisons

Table 11. Spray Angles for Macrospray Atomizer, All Results

Spray Angles, Macrospray Atomizer				
Type	**Inlet Pressure (psi)**	**Outlet Pressure (psi)**	**Spray Angle (°)**	**% Error from Test Spec.**
Test Specification (30° - 50°)	145	0	44.00	0%
CFD Simulation	10	0	none	-
CFD Simulation	20	0	70.00	59%
CFD Simulation	40	0	47.00	7%
CFD Simulation	80	0	85.00	93%
CFD Simulation	145	0	65.00	48%
Hot Wire Stand, X (Average)	145	0	48.14	9%
Hot Wire Stand, X (Max)	145	0	49.88	13%

Continued from page 98				
Hot Wire Stand, X (Min)	145	0	45.86	4%
Hot Wire Stand, Y (Average)	145	0	48.06	9%
Hot Wire Stand, Y (Max)	145	0	49.68	13%
Hot Wire Stand, Y (Min)	145	0	45.26	3%
Angle Device (Average)	145	0	41.85	-5%
Angle Device (Max)	145	0	47.30	7%
Angle Device (Min)	145	0	34.40	-22%

Table 11 lists the spray angles for the macrospray atomizer from the CFD simulations, hot wire test stand experiment, spray angle device experiment, and the test specification tolerance. The percentage of error the values deviate from the test specification, or the control, are also listed. From the table, it is easily seen that the CFD over predicts the spray angle by almost 50%. The hot wire stand maintains a closer tolerance band gap and is consistent between the x and y axes of the stand. The angle device is shown to have a higher spread across the maximum angle and minimum angles measured.

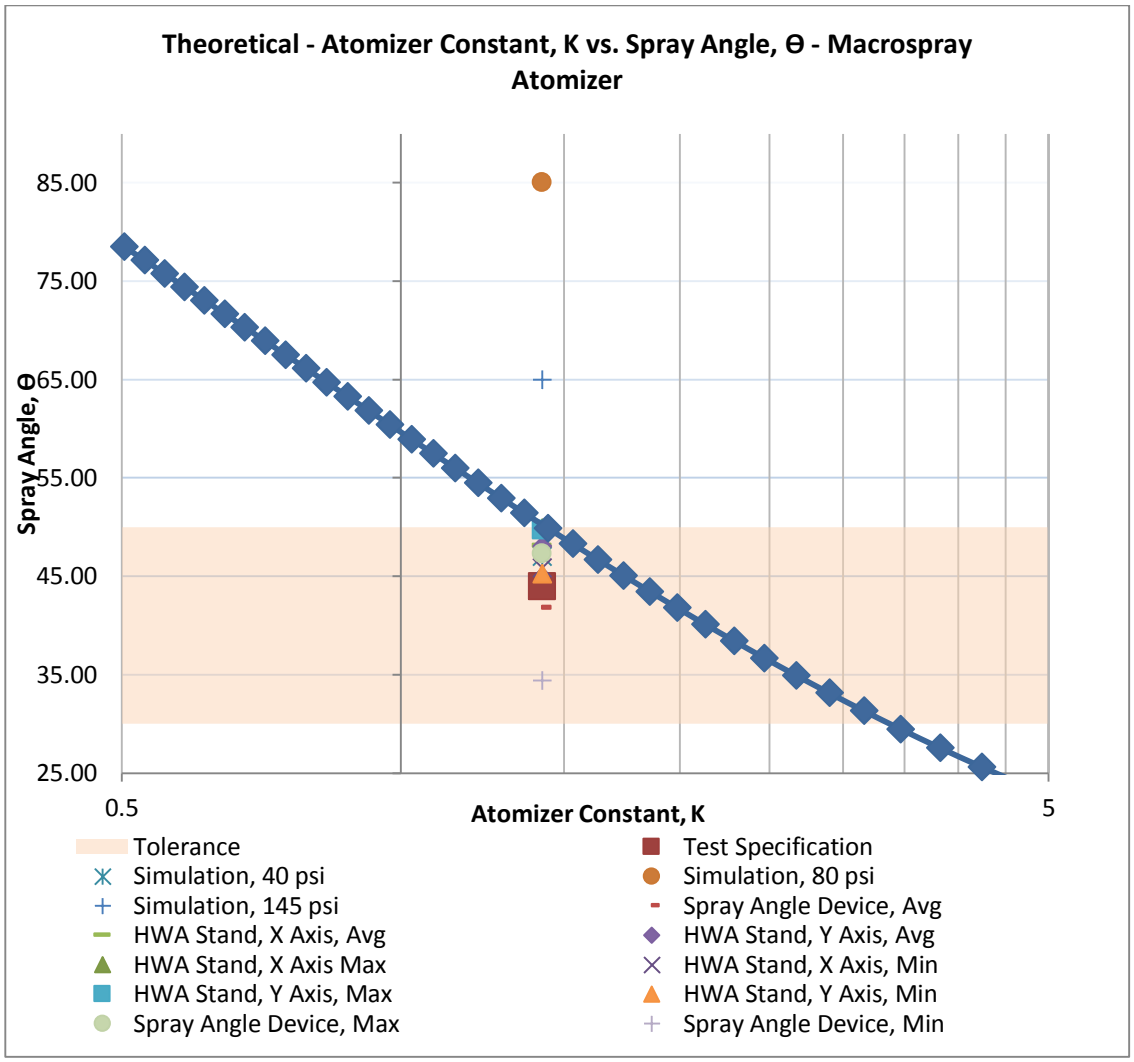

Figure 75: Atomizer Constant versus Spray Angle Results, Macrospray Atomizer

Figure 75 is a plot of the spray angle versus the atomizer constant. The X axis has been shortened, when compared to other atomizer constant versus spray angle plots, to more clearly display the data. All of the atomizers, have the same atomizer constant, but as the plot shows, many of the simulations resulted in spray angles higher than the theoretical or highest possible angle. The only resultant spray angles at or below the theoretical threshold were both axes of the hot wire stand, the test specification for the macrospray atomizer, and the 40 psi inlet condition simulation of the macrospray atomizer.

Table 12. Dimensionless Numbers for Macrospray Atomizer

Macrospray Atomizer Dimensionless Parameters	
Maximum Fluid Velocity (m/s)	42
Reynolds Number	11,945.60
Weber Number (based on maximum velocity)	8,405.00
Atomizer Constant	1.42
Flow Number (Test Specification)	0.93
Flow Number (Simulation, 10 psi inlet)	1.23
Flow Number (Simulation, 20 psi inlet)	0.96
Flow Number (Simulation, 40 psi inlet)	1.26
Flow Number (Simulation, 80 psi inlet)	1.14
Flow Number (Simulation, 145 psi inlet)	1.11
Flow Number (Hot Wire Stand, Average)	-
Flow Number (Hot Wire Stand, Maximum)	-
Flow Number (Hot Wire Stand, Minimum)	-
Flow Number (Angle Device, Average)	0.95
Flow Number (Angle Device, Maximum)	0.95
Flow Number (Angle Device, Minimum)	0.95

Table 12 lists the maximum local fluid velocity of the atomizer. This 42 m/s was seen through the orifice section via the CFD simulation. The Reynolds number of almost 12,000 is far past the threshold of what would be considered laminar flow, meaning turbulent flow travels through the orifice. The Weber number, or the ratio of inertial momentum to surface tension, of 8,405 means that as the fluid exits the orifice, the flow is more influenced by inertial momentum. No flow numbers were calculated for the hot wire stand results as there was no mass flow measuring device on the stand per the requirements of the stand. The flow numbers can be assumed to be similar to those of the angle device measurements.

5.6.2 Conventional Atomizer Nozzle Comparisons

Table 13. Spray Angles for Conventional Atomizer, All Results

Spray Angles, Conventional Atomizer				
Type	**Inlet Pressure (psi)**	**Outlet Pressure (psi)**	**Spray Angle (°)**	**% Error from Test Spec.**
Test Specification (59 °- 65°)	100	0	62.00	0.00%
CFD Simulation	100	0	73.00	17.74%
Angle Device (Average)	100	0	76.00	22.58%
Angle Device (Max)	100	0	79.10	27.58%
Angle Device (Min)	100	0	67.70	9.19%

Table 13 lists the spray angles for the conventional atomizer from the CFD simulations, spray angle device experiment, and the test specification tolerance in addition to the deviation from the test specification for each angle. Unlike the macrospray atomizer, the conventional atomizer is closer in value to the CFD simulation and the angle device results. However, both values over predict the spray angle by approximately 20%.

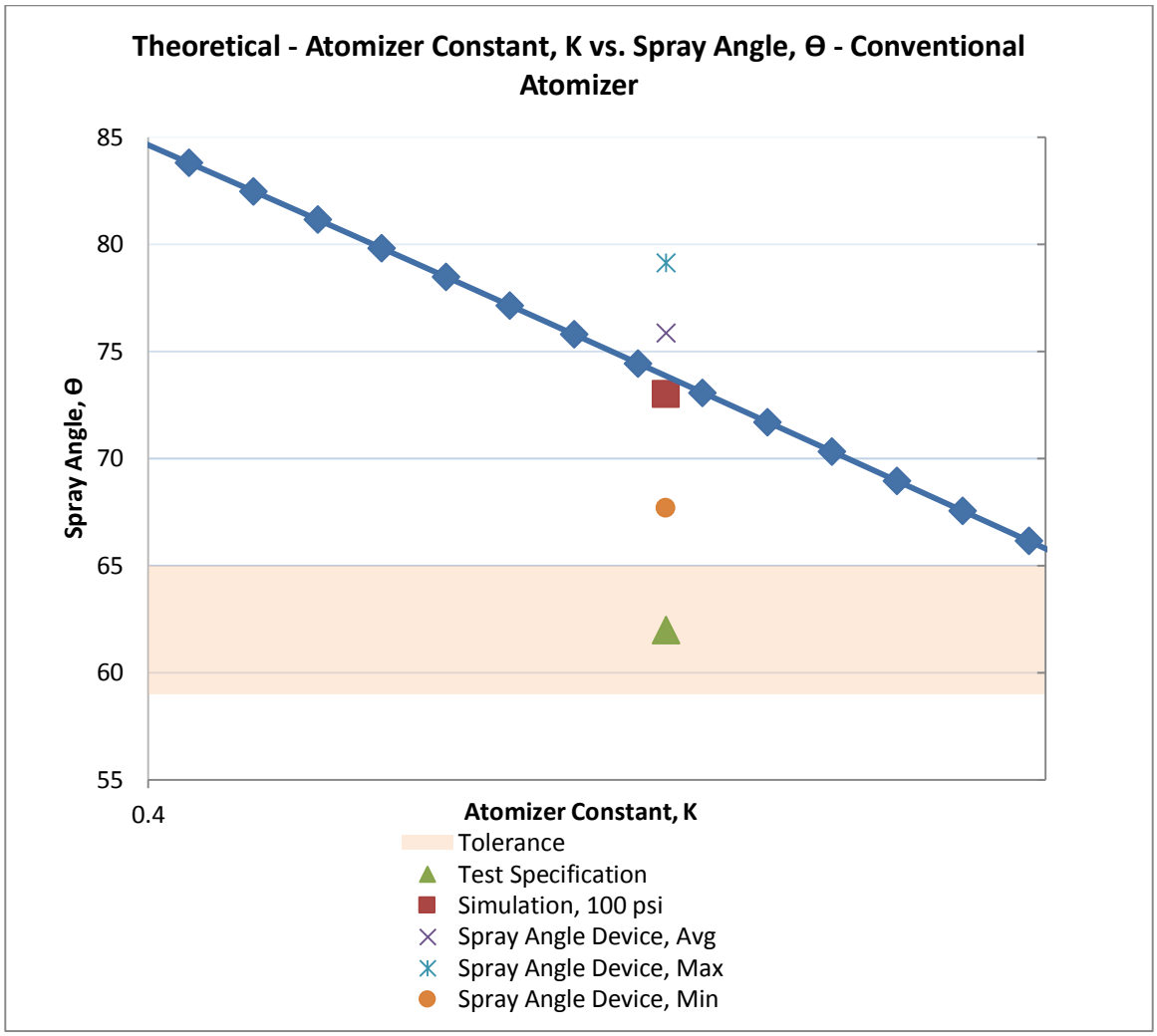

Figure 76: Atomizer Constant versus Spray Angle Results, Conventional Atomizer

Figure 76 is the spray angle versus the atomizer constant for all values obtained for the conventional atomizer. Again, to illustrate the data points more clearly, the X axis has been shortened. The blue curve represents the theoretical maximum spray angle based on Giffen & Muraszew theory. The test specification, minimum angle obtained from the spray angle device, and the simulation all fall under the theoretical curve.

Table 14. Dimensionless Numbers for Conventional Atomizer

Conventional Atomizer Dimensionless Parameters	
Maximum Fluid Velocity (Simulation, m/s)	39
Reynolds Number (Simulation)	18,404.67
Weber Number (based on max velocity) minimum	455.82
Weber Number (based on max velocity) maximum	17,956.58
Atomizer Constant	0.60
Flow Number (Test Specification)	2.09
Flow Number (Simulation, 100 psi)	3.94
Flow Number (Angle Device, Average)	2.81
Flow Number (Angle Device, Maximum)	2.83
Flow Number (Angle Device, Minimum)	2.78

Table 14 shows the highest velocity seen through the atomizer in the orifice, of 39 m/s (via CFD) with a turbulent Reynolds number of approximately 18,400. The Weber number of approximately 18,000 means that the inertial momentum of the fluid droplets influence the spray pattern significantly more than the surface tension.

CHAPTER VI

DISCUSSION

6.1 On the Macrospray Atomizer

The simulation results for the macrospray atomizer were different than initially expected and brought multiple questions to attention. After several iterations and runs of this simulation, the CFD continually predicted the Coanda effect occurring immediately downstream of the exit orifice as seen in figure 49. For the unfamiliar reader, the Coanda effect is the attraction of a flowing fluid to a surface of close proximity due to the low pressure region created by that same surface.

This effect was monitored throughout each of the runs and was seen with each run. To understand what was forcing the spray to adhere to the walls, a CFD simulation was run with the support plates of the atomizer removed. In theory, the removal of the support plates should have no effect on the spray as they are strictly for structural purposes.

After removing the support plates from the model and keeping the simulation parameters constant, the fluid exiting the orifice was a jet, versus the expected spray cone with an arbitrary dispersion angle. Several turbulence models were used to ensure the accuracy of the solution and each consecutive run of the atomizer with no support plates showed that the atomizer was consistently flowing a jet, contrary to what the theory and equations would predict.

This result has implications towards the design process. If this phenomenon is truly occurring during the operation of the atomizer, wasted energy and decreased atomization would be the direct effects. This is undesirable as coarse atomization produces large droplets and the fluid energy required by the operation of the atomizer would potentially be greater (i.e. higher operating pressure) to achieve the desired fine atomization.

In addition, if the Coanda effect is driving fluid to the sides of the support plates and, effectively, is controlling the spray angle, it is not ideal. The support plates have larger dimensions than that of an orifice and can be used as a mating surface. The usage of this surface can wear over time with use. This wear could potentially cause a change in spray angle of the atomizer, if it controls flow.

The experimental results of the macrospray atomizer using the spray angle device reported an angle degree measurement of 41.8°, once averaged out. The requirement of this atomizer calls for an angle within 30°-50°, meaning the averaged angle falls well within limits.

Not documented in this thesis are trial simulations of the macrospray atomizer run with two other turbulence models – the k-omega turbulence model and the k-omega SST (shear stress transport) turbulence model. These models look at the omega (ω) term or the specific rate of kinetic energy dissipation and has a difficult time converging. Both models were used on the macrospray atomizer at operational conditions and upon convergence, both runs resulted in a jet emitting from the orifice. These runs utilized the geometries both with and without the support plates. This result was immediately realized to be inaccurate as pressure swirl atomizers produce spray cones, not jets, which are indicative of a plain orifice atomizer.

6.2 On the Conventional Atomizer

The conventional atomizer nozzle provided a comparative dataset on the differences between the two nozzles studied. An interesting event that occurred during testing was the identification of what the spray cone truly is. As stated earlier in section 2.1.5.2, the edge can be difficult to define. In order to gain an accurate measurement, an operator must first be trained and understand visually what type of spray features make the spray edge the correct edge. In addition, the quality of the spray has a direct effect on how the angle is measured. Identifying how far into the spray the probes were required to be before the edge was considered to be the edge of the cone, was an issue that was frequently ran into throughout the testing of the conventional atomizer.

6.3 On Hot Wire Constant Temperature Anemometry and the Test Stand

Constant temperature anemometry was found to be a very interesting tool to use for spray characterization. While it is possible to identify the spray angle based on the intensity

of fluid droplets impinging upon the hot wire, it may not be the ideal scenario for using this type of device. There are many physical phenomena that may potentially have an effect on the voltage drop of the wire. These events include recirculation zones, leading fluid droplets to recirculate and land back on the wire changing the heat transfer properties of the wire. The primary flow coating the entire wire also changes the heat transfer.

The hot wire can be approximated as a cylinder. In a single phase flow, i.e. only air or water, the fluid has a relatively constant velocity across the wire, meaning a constant source of heat transfer away from the heated wire through convection. However, in the case of two phase flow, i.e. the fluid flow of air (the fluid being measured) is disturbed by the turbulent flow of droplets passing over the wire, changing the heat convected from the wire.

To reiterate the process of how the angle is captured, below are the steps for the angle acquisition -

- Hot wire probes (CTA probes) traverse spray. As the spray is traversed, a voltage drop is recorded from wire voltage throughput. Supply power is increased to compensate for voltage drop and to keep temperature constant.
- Using the voltage drop data, a graph is created (voltage drop versus the linear distance the probe has traveled. Voltage is averaged and normalized to obtain a constant, which all data is matched to.
- Voltage drop curve gives a profile of what the spray angle is and the spray intensity.

Since the hot wire probes are a thermal device, the ambient air in the spray chamber of the stand will have an effect on the calculated angle. The degree to which this effect can be measured is a study that can be conducted in the future. With that said, many calibration tests were run to check how much of an effect the temperature had. During these tests, it was noticed that the temperature of the spraying fluid was of crucial importance when measuring the angle. The temperature rise increased the misting and recirculation of the spray inside of the spray chamber, possibly affecting the probes and giving a false reading of what the spray angle is. Additionally, as temperature rises, density decreases, potentially changing the flow characteristics. Even though the density change in water can be assumed to be negligible, the amount of moisture in the air can have an effect on the heat transfer.

6.4 On Spray Angle Device

The spray angle device, as previously stated, can introduce human error into the spray angle measurement. The test specification for spray angle device usage states that the trained operator shall monitor and count a certain amount of drops per minute or can pass off the nozzle if there is a similar constant stream of droplets from both probes. This can introduce bias as one operator may consider a constant stream of droplets as 10 drops per minute whereas another operator may assume 60 drops per minute as the threshold. Not having an absolute established number of droplets can introduce severe error as the rate of droplets from the probes is directly related to how far into or out of the spray the probes are.

6.5 On CFD Theory

Through the simulation runs, the CFD was found to predict the spray angle very closely to the Rizk/Lefebvre definition, equation 2.5, based on liquid properties and atomizer geometry.

The selected multiphase model, volume of fraction (VoF) is an Euler-Euler approach, meaning both fluids are considered to interpenetrate. These different phases are mathematically treated as interpenetrating with a sum of the volume fractions of the fluids equaling to 1. The conservation equations are solved for each phase. Because of its nature, VoF is a surface tracking model and has its benefits when focusing on the interface between fluids.

The k-epsilon realizable, with enhanced wall treatment model was selected due to its performance during the grid validation study. This model introduces two terms - the turbulent kinetic energy, k, and its corresponding dissipation rate, ε.

The realizable portion of the model strictly means the model satisfies certain constraints with the Reynolds stress model, giving a more realistic view of the physics of a simulated system. The k-epsilon realizable model is more accurate for flows that deal with rotation, have boundary layers with high pressure gradients, recirculation zones, and flow separations.

The enhanced wall treatment enhances solution accuracy and is needed due to the high Reynolds numbers the flow sees in the small passages of the atomizer. Improved accuracy

is attained by refining the mesh of the model in the boundary layer and near the wall. This mesh resolution gives a more accurate representation of how the viscous sublayer affects the flow characteristics.

Due to the additional equations needing to be solved, k-epsilon realizable requires more computational time versus the standard k-epsilon model and the Spalart-Allmaras models. This is a tradeoff that must be considered when wanting to simulate something as closely as possible to its real world operating conditions versus gaining an estimation of a solution.

6.6 On Future Work

There are several tasks that would be of interest to both the author and the designers of the atomizer and nozzle examined in this thesis. The first would be to flow the macrospray atomizer and examine the effect that the support plates have on the spray angle and if there is any impingement of the ejected fluid on the corners of the support plates. The simplest way of testing this would be to manufacture a macrospray atomizer without the support plates and measure both on the hot wire test stand and the spray angle device to measure the spray angle. Any discrepancy will be caught by the measurement, pointing to whether or not the ejected fluid is truly impinging upon the support plates or not.

A qualitative analysis would be of interest as well. Examining the spray quality and how the atomizer flows while under operating conditions would provide a quick check on the effect of the support plates. In addition to this qualitative analysis, more CFD studies would only add to the knowledge acquired through this thesis. A larger CFD matrix could be created, allowing for different turbulence models to be compared. In addition, in an attempt

to fully validate the hot wire test stand, using a high speed camera imaging system to calculate the spray angle of the same parts tested in this thesis would be the most adequate way of qualifying the stand.

It would be of great interest to modify the hot wire test stand to allow for its acceptance of the conventional atomizer in addition to other atomizers and nozzles. Allowing for this redesign would not only give more life to the stand in terms of what families of nozzles and atomizers it can examine, but would also provide more data to pass off the stand as being acceptable or not. However, this would most likely involve a heavy redesign of the entire stand, severely undercutting the benefits of the redesign in the first place.

CHAPTER VII

CONCLUSION

The experimental results versus the simulation test data of both the macrospray atomizer and the conventional atomizer nozzle shows that CFD prediction of spray angles is not necessarily as accurate as one would assume. The largest discrepancies between the calculated angles and the true test values was that of the macrospray atomizer's CFD results versus its test data from both the hot wire stand and the spray angle device. Through the experimentation process, the measured angles varied widely, even when adhering to the test specification guidelines.

There were intriguing results gained from the CFD simulation of the macrospray atomizer. The results obtained from the 40 psi inlet condition give a spray angle close to the angle measured with the spray angle device for the production specification, 44°. This is interesting as the 145 psi inlet does not show these same results and actually over predicts the spray angle by approximately 48%.

It can be stated that at a very minimum, the hot wire stand has eliminated a large amount of human error, allowing for the measured spray angle to be purely a function of the hot wire probes output signal and the flow characteristics of the spray chamber in which the spray angle is measured. As stated previously in chapter 6, more work to validate the stand over more families of macrospray atomizers would give additional confidence in the stand's ability to quantity and qualify the parts that it must validate. As seen in the results chapter, chapter 5, it is seen that the large discrepancy between the spray angle device measurement and that of the hot wire stand calls into the question and stresses the fact that an operator must be trained or have good experience in measuring spray angles with the spray angle device in order to properly pass or fail a nozzle.

In regards to the conventional atomizer, its CFD spray angle was closer to landing in the tolerance gap allotted to it, (73° from CFD versus 59°-65° tolerance) based on the test specification under operational parameters (i.e., 100 psi fluid inlet, discharge to atmospheric pressure).

In conclusion, the hot wire test stand gave repeatable results over the course of experiments. Even with the large discrepancy between the results of the hot wire test stand and the spray angle device, the hot wire test stand utilizes the more dependable measurement technique due to the removal of the bias introduced by human operators. Furthermore, the large discrepancy shows the error can and will greatly influence the measurements obtained from the spray angle device, if not eliminated. The smaller error between the CFD data for the conventional atomizer and the spray angle device data versus

that of the conventional atomizer shows that the CFD data can give a good estimate of the spray angle. This case shows that results obtained from CFD can be used but must be interrogated to understand how the fluid domain used for the simulation is affecting or could affect the results.

BIBLIOGRAPHY

ANSYS Help Viewer. 2013. Version 15.0.0. SAS IP, Inc.

Comte-Bellot, Geneviève. "Hot-Wire Anemometry." *Annual Review Fluid Mechanics* 8 (1976): 209-31. Web. Jan. 2015. <arjournals.annualreviews.org>.

DeCorso, S. M., and A. Kemeny. *Effect of Ambient and Fuel Pressure on Nozzle Spray Angle*. Proc. of Gas Turbine Power Division Conference, Washington D.C. N.p.: n.p., 1956. 607-15. Print.

Giffen, Edmund, and A. Muraszew. *The Atomisation of Liquid Fuels*. New York: Wiley, 1953. Print.

"How to Measure Turbulence (Practical Guide)." *How to Measure Turbulence (Practical Guide)*. N.p., n.d. Web. Jan. 2015. <http://www.dantecdynamics.com/how-to-measure-turbulence-practical-guide>.

Jorgenson, Finn E. *How to Measure Turbulence with Hot Wire Anemometers - A Basic Guide*. 2004. Dantec Dynamics.

Joyce, J. R. "The Atomization of Liquid Fuels for Combustion." *Journal of the Institute of Fuel* February (1949): 650-63. Web.

King, Louis Vessot. *On the Convection of Heat from Small Cylinders in a Stream of Fluid: Determination of the Convection Constants of Small Platinum Wires with Applications to Hot-Wire Anemometry*. Diss. McGill U, 1914. N.p.: n.p., n.d. Print.

Kutty, P. Shankaran, M. V. Narasimhan, and K. Narayanaswamy. *Design and Prediction of Discharge Rate, Cone Angle and Aircore Diameter of Swirl*

Chamber Atomisers. Proc. of ICLASS 78. Vol. 1978. N.p.: n.p., n.d. 93-100. Print.

Lefebvre, Arthur H. *Atomization and Sprays*. New York: Taylor & Francis, 1989. Print.

"Measurement Principles of PDA." *Phase Doppler Anemometry Measurement Principles*. N.p., n.d. Web. Jan. 2015. <http://www.dantecdynamics.com/measurement-principles-of-pda>.

"Measurement Principles of Planar-LIF." *Laser-Induced Liquid Fluorescence Measurement Principles*. N.p., n.d. Web. Jan. 2015. <http://www.dantecdynamics.com/measurement-principles-of-planar-lif>.

Rizk, N. K., and A. H. Lefebvre. *Internal Flow Characteristics of Simplex Swirl Atomizers*. Proc. of Journal of Propulsion and Power. 3rd ed. Vol. 1. N.p.: n.p., n.d. 193-99. Print. Ser. 1985.

Rizk, N. K., and A. H. Lefebvre. *Prediction of Velocity Coefficient and Spray Cone Angle for Simplex Swirl Atomizers*. Proc. of International Journal of Turbo and Jet-Engines. N.p.: n.p., 1987. 65-73. Print.

Rizk, N. K., and A. H. Lefebvre. *Spray Characteristics of Simplex Swirl Atomizers*. Proc. of 9th ICODERS, France, Poitiers. N.p.: American Institute of Aeronautics and Astronautics, 1984. 563-80. Print.

Simmons, Harold C. *The Atomization of Liquids, Principles & Methods*. Cleveland: Parker Hannifin Corporation, Gas Turbine Fuel Systems Division, 1979. Print.

Steinthorssen, Erlendur, Ph.D. *CFD Analysis of Flow and Erosion Characteristics in ML Single Point Atomizer*. ER MEN11-013. N.p.: n.p., 2011. Print.

Taylor, G. I. "The Boundary Layer in the Converging Nozzle of a Swirl Atomizer." *Quarterly Journal of Mechanics & Applied Mathematics* 3.2 (n.d.): 129-39. Web. Feb. 2015. <http://qjmam.oxfordjournals.org/content/3/2/129.full.pdf+html>.

Taylor, G. I. *The Mechanics of Swirl Atomisers*. Proc. of Seventh International Congress for Applied Mechanics. Vol. 2. N.p.: n.p., 1948. 280-85. Print.

"Techniques." *LaVision* -. N.p., n.d. Web. Jan. 2015. <http://www.lavision.de/en/techniques/index.php>.

APPENDICES

Appendix A

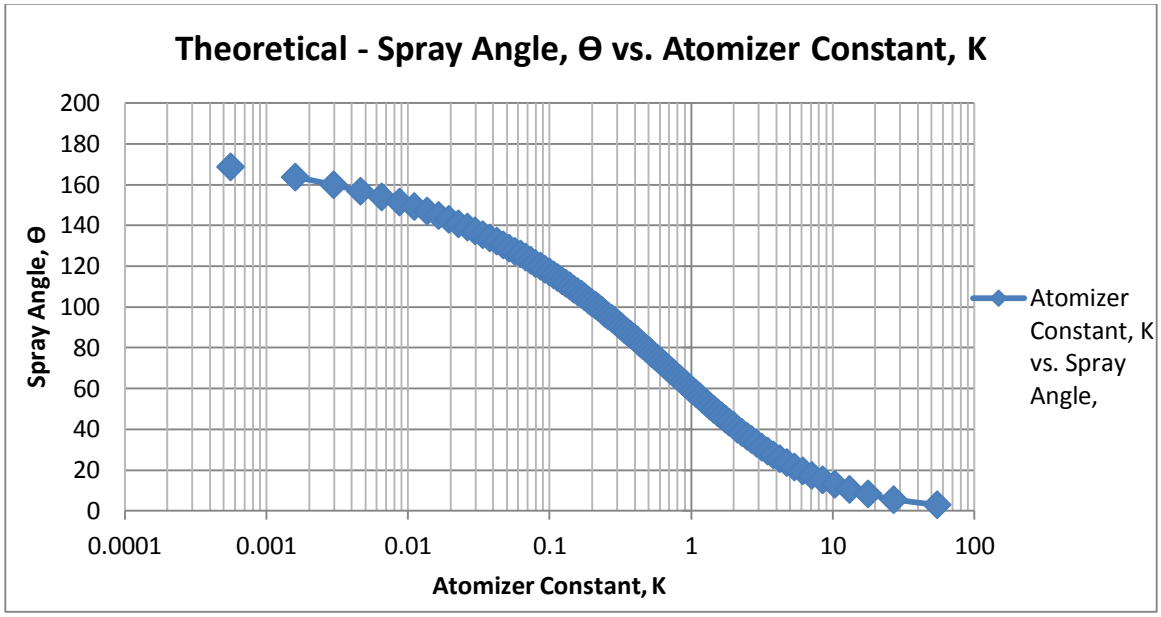

Figure 77: Theoretical Atomizer Constant versus Spray Angle

Appendix B

Table 15. Macrospray Atomizer, Liquid Properties

Macrospray Atomizer	***Liquid (English Units)***	***Liquid (Metric Units)***
	WATER	WATER
Number of ports, N	3	3
Density (lbm/ft^3) (kg/m^3)	1000.00	62.43
Viscosity, liquid (lbf-s/ft^2) (Pa-s)	1.00E-03	2.09E-05
Pressure drop (psi) (Pa)	482,632.99	70.00
Surface Tension (lbf/ft) (N/m)	0.0049	0.0720

Table 16. Conventional Atomizer, Liquid Properties

Conventional Atomizer	***Liquid (English Units)***	***Liquid (Metric Units)***
	MILPRF7024C	MILPRF7024C
Number of ports, N	4	4
Density (lbm/ft^3) (kg/m^3)	770.00	48.07
Viscosity, liquid (lbf-s/ft^2) (Pa-s)	9.16E-04	1.91E-05
Pressure drop (psi) (Pa)	689,475.70	100.00
Surface Tension (lbf/ft) (N/m)	0.0018	0.02595

Appendix C

Table 17. Spray Angle Based on Giffen & Muraszew Theory versus Rizk & Lefebvre Definition

GIFFEN & MURASZEW THEORY					RIZK & LEFEBVRE DEFINITION	
X (air core/area ratio)	Cd, discharge coefficient	K, atomizer constant	Cone angle (2Ɵm)	Cd, corrected	Conventional Atomizer (2Ɵm)	Macrospray Atomizer (2Ɵm)
1.00	0.00	0.00	-	0.00	0.00	0.00
0.99	0.00	0.00	168.51	0.00	17.93	14.18
0.98	0.00	0.00	163.71	0.00	23.51	18.60
0.97	0.00	0.00	159.99	0.00	27.56	21.80
0.96	0.01	0.00	156.84	0.01	30.85	24.40
0.95	0.01	0.01	154.04	0.01	33.68	26.64
0.94	0.01	0.01	151.48	0.01	36.18	28.62
0.93	0.01	0.01	149.11	0.02	38.45	30.42
0.92	0.02	0.01	146.89	0.02	40.53	32.06
0.91	0.02	0.02	144.78	0.02	42.47	33.59
0.90	0.02	0.02	142.77	0.03	44.28	35.03
0.89	0.03	0.02	140.85	0.03	45.99	36.38
0.88	0.03	0.03	138.99	0.04	47.61	37.66
0.87	0.03	0.03	137.20	0.04	49.15	38.88
0.86	0.04	0.03	135.45	0.04	50.63	40.05
0.85	0.04	0.04	133.76	0.05	52.05	41.17
0.84	0.05	0.04	132.10	0.06	53.41	42.25
0.83	0.05	0.05	130.48	0.06	54.73	43.29
0.82	0.06	0.05	128.90	0.07	56.00	44.30
0.81	0.06	0.06	127.34	0.07	57.23	45.27
0.80	0.07	0.06	125.81	0.08	58.43	46.22
0.79	0.07	0.07	124.31	0.08	59.60	47.14
0.78	0.08	0.07	122.83	0.09	60.73	48.04
0.77	0.08	0.08	121.36	0.10	61.84	48.92
0.76	0.09	0.09	119.92	0.10	62.92	49.77
0.75	0.09	0.09	118.49	0.11	63.98	50.61
0.74	0.10	0.10	117.07	0.12	65.01	51.43
0.73	0.11	0.11	115.67	0.12	66.03	52.23
0.72	0.11	0.11	114.28	0.13	67.02	53.02
0.71	0.12	0.12	112.91	0.14	68.00	53.79
0.70	0.13	0.13	111.54	0.15	68.95	54.54
0.69	0.13	0.14	110.18	0.16	69.89	55.29
0.68	0.14	0.15	108.83	0.16	70.82	56.02
0.67	0.15	0.16	107.49	0.17	71.73	56.74
0.66	0.15	0.17	106.15	0.18	72.63	57.45

Continued from page 122						
0.65	0.16	0.18	104.82	0.19	73.51	58.15
0.64	0.17	0.19	103.50	0.20	74.38	58.84
0.63	0.18	0.20	102.17	0.21	75.24	59.52
0.62	0.18	0.21	100.86	0.22	76.09	60.19
0.61	0.19	0.22	99.54	0.22	76.92	60.85
0.60	0.20	0.23	98.23	0.23	77.75	61.50
0.59	0.21	0.25	96.92	0.24	78.57	62.15
0.58	0.22	0.26	95.61	0.25	79.37	62.79
0.57	0.23	0.27	94.30	0.26	80.17	63.42
0.56	0.23	0.29	93.00	0.27	80.96	64.04
0.55	0.24	0.30	91.69	0.28	81.74	64.66
0.54	0.25	0.32	90.38	0.29	82.52	65.27
0.53	0.26	0.34	89.07	0.30	83.28	65.88
0.52	0.27	0.36	87.76	0.32	84.04	66.48
0.51	0.28	0.37	86.44	0.33	84.79	67.07
0.50	0.29	0.39	85.13	0.34	85.54	67.66
0.49	0.30	0.41	83.81	0.35	86.27	68.25
0.48	0.31	0.43	82.48	0.36	87.01	68.82
0.47	0.32	0.46	81.16	0.37	87.73	69.40
0.46	0.33	0.48	79.82	0.38	88.45	69.97
0.45	0.34	0.50	78.49	0.40	89.17	70.53
0.44	0.35	0.53	77.14	0.41	89.88	71.10
0.43	0.36	0.56	75.80	0.42	90.58	71.65
0.42	0.37	0.58	74.44	0.43	91.28	72.21
0.41	0.38	0.61	73.08	0.45	91.98	72.76
0.40	0.39	0.65	71.71	0.46	92.67	73.30
0.39	0.40	0.68	70.33	0.47	93.35	73.85
0.38	0.42	0.71	68.95	0.49	94.03	74.38
0.37	0.43	0.75	67.55	0.50	94.71	74.92
0.36	0.44	0.79	66.15	0.51	95.39	75.45
0.35	0.45	0.83	64.73	0.53	96.06	75.98
0.34	0.46	0.88	63.30	0.54	96.72	76.51
0.33	0.48	0.92	61.87	0.56	97.39	77.04
0.32	0.49	0.97	60.42	0.57	98.05	77.56
0.31	0.50	1.03	58.96	0.59	98.71	78.08
0.30	0.51	1.08	57.48	0.60	99.36	78.60
0.29	0.53	1.15	55.99	0.62	100.01	79.11
0.28	0.54	1.21	54.49	0.63	100.66	79.63
0.27	0.55	1.28	52.97	0.65	101.31	80.14
0.26	0.57	1.36	51.43	0.66	101.95	80.65
0.25	0.58	1.44	49.88	0.68	102.59	81.15
0.24	0.59	1.53	48.30	0.70	103.23	81.66

Continued from page 123						
0.23	0.61	1.63	46.71	0.71	103.87	82.16
0.22	0.62	1.74	45.10	0.73	104.50	82.67
0.21	0.64	1.86	43.47	0.75	105.14	83.17
0.20	0.65	1.99	41.81	0.76	105.77	83.67
0.19	0.67	2.13	40.13	0.78	106.40	84.16
0.18	0.68	2.29	38.42	0.80	107.02	84.66
0.17	0.70	2.47	36.69	0.82	107.65	85.16
0.16	0.71	2.67	34.93	0.84	108.28	85.65
0.15	0.73	2.90	33.14	0.85	108.90	86.14
0.14	0.75	3.16	31.32	0.87	109.52	86.63
0.13	0.76	3.47	29.46	0.89	110.14	87.13
0.12	0.78	3.82	27.56	0.91	110.76	87.62
0.11	0.80	4.24	25.62	0.93	111.38	88.11
0.10	0.81	4.74	23.65	0.95	112.00	88.59
0.09	0.83	5.36	21.62	0.97	112.62	89.08
0.08	0.85	6.13	19.54	0.99	113.23	89.57
0.07	0.87	7.12	17.41	1.01	113.85	90.06
0.06	0.89	8.44	15.22	1.04	114.46	90.55
0.05	0.90	10.28	12.95	1.06	115.08	91.03
0.04	0.92	13.06	10.61	1.08	115.69	91.52
0.03	0.94	17.69	8.17	1.10	116.31	92.00
0.02	0.96	26.94	5.63	1.12	116.92	92.49
0.01	0.98	54.71	2.93	1.15	117.54	92.98

Appendix D

Grid Independence Plots

Grid Independence | Macrospray Atomizer | 1 million cells, Meshed Volume Fraction

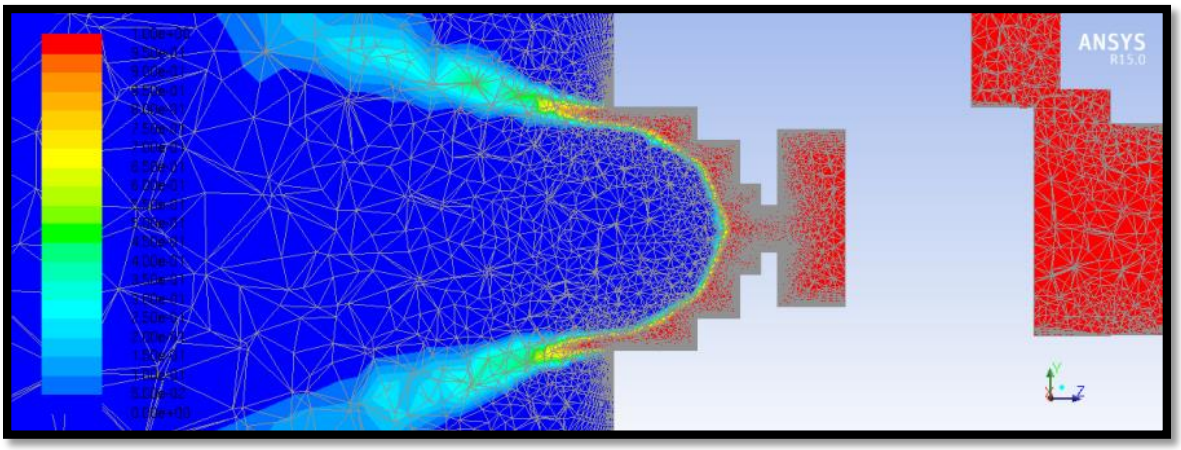

Figure 78: Meshed Volume Fraction, Macrospray Atomizer, 1 million cells

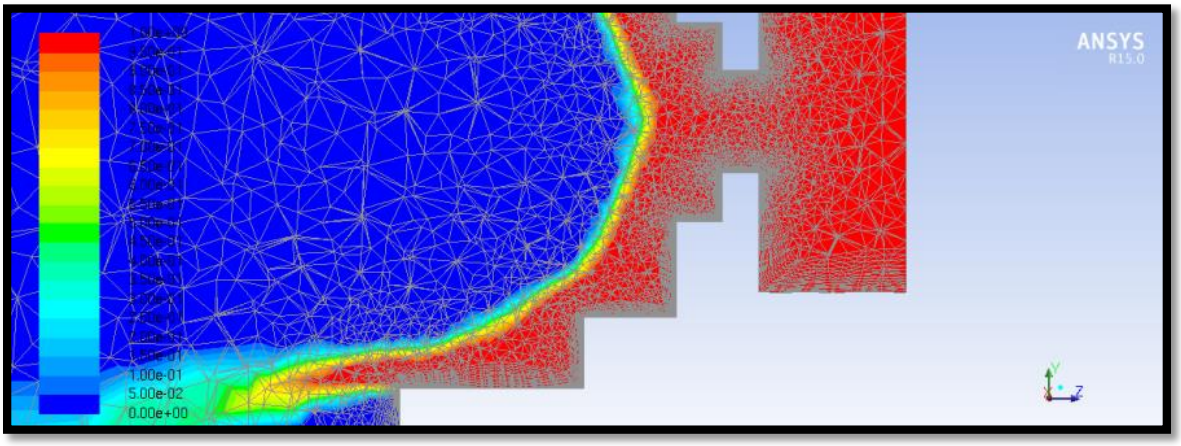

Figure 79: Meshed Volume Fraction, Macrospray Atomizer, 1 million cells, Orifice

Grid Independence | Macrospray Atomizer | 3.5 million cells, Meshed Volume Fraction

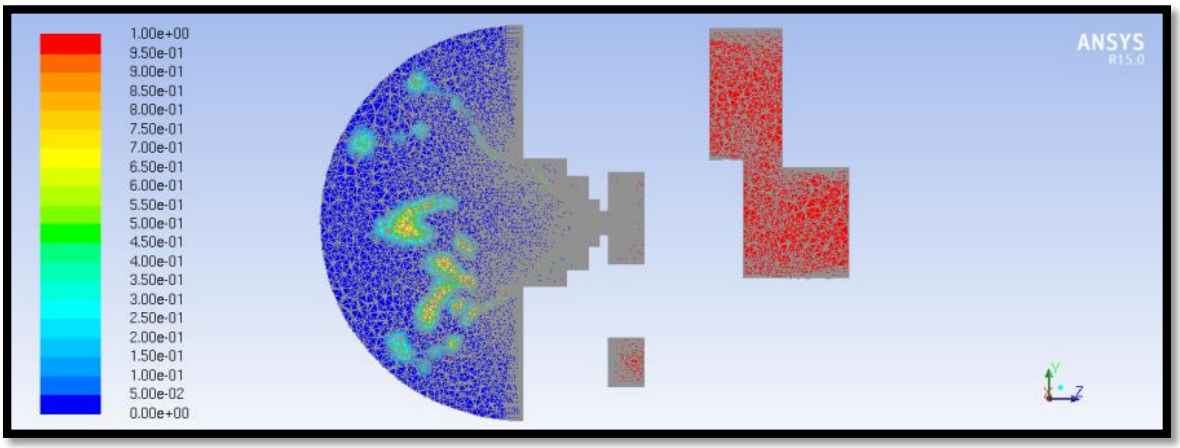

Figure 80: Meshed Volume Fraction, Macrospray Atomizer, 3.5 million cells

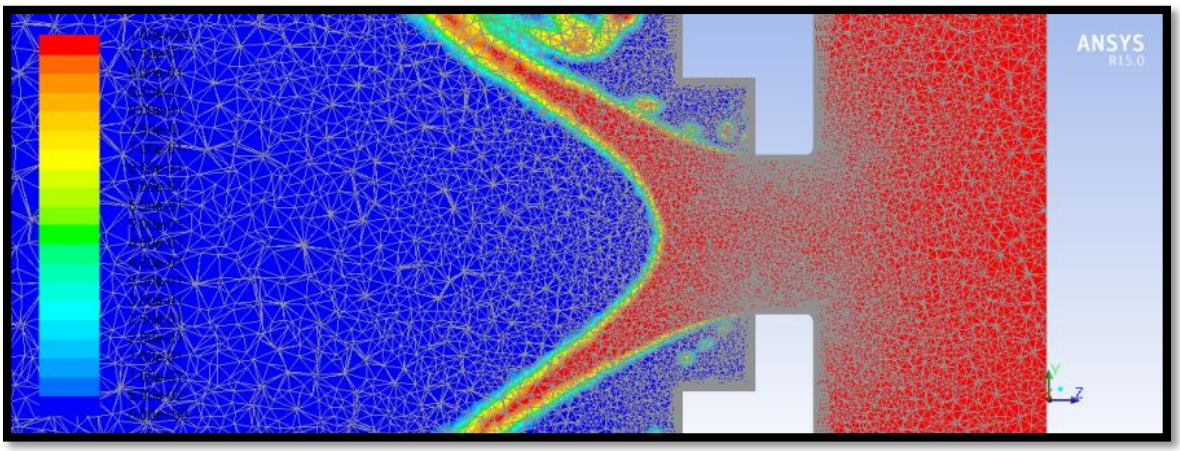

Figure 81: Meshed Volume Fraction, Macrospray Atomizer, 3.5 million cells, Orifice

Grid Independence | Macrospray Atomizer | 7 million cells, Meshed Volume Fraction

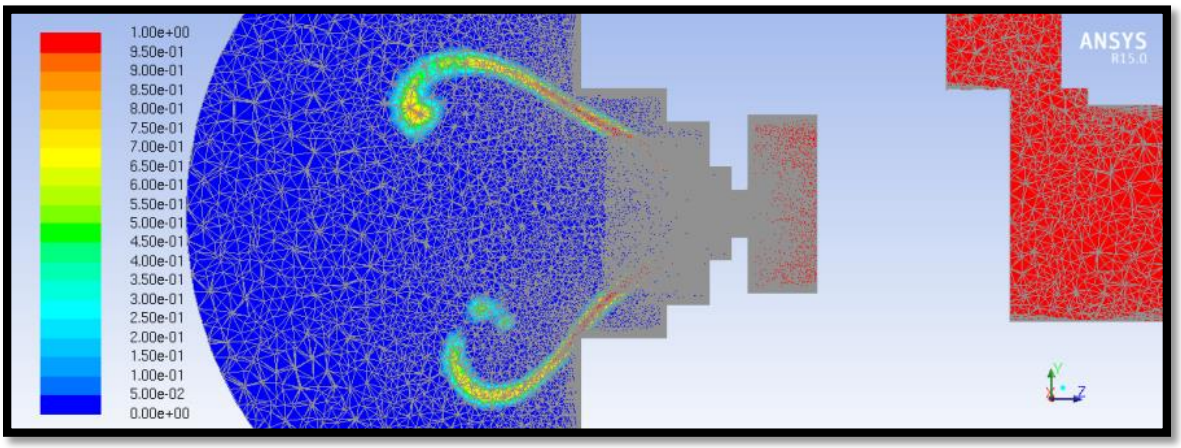

Figure 82: Meshed Volume Fraction, Macrospray Atomizer, 7 million cells

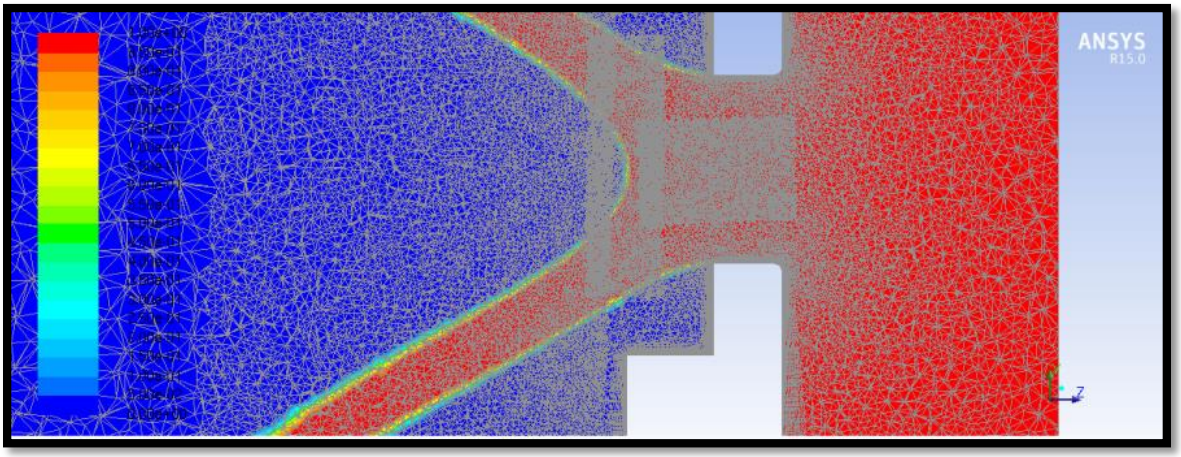

Figure 83: Meshed Volume Fraction, Macrospray Atomizer, 7 million cells, Orifice

Grid Independence | Conventional Atomizer | 1.5 million cells, Meshed Volume Fraction

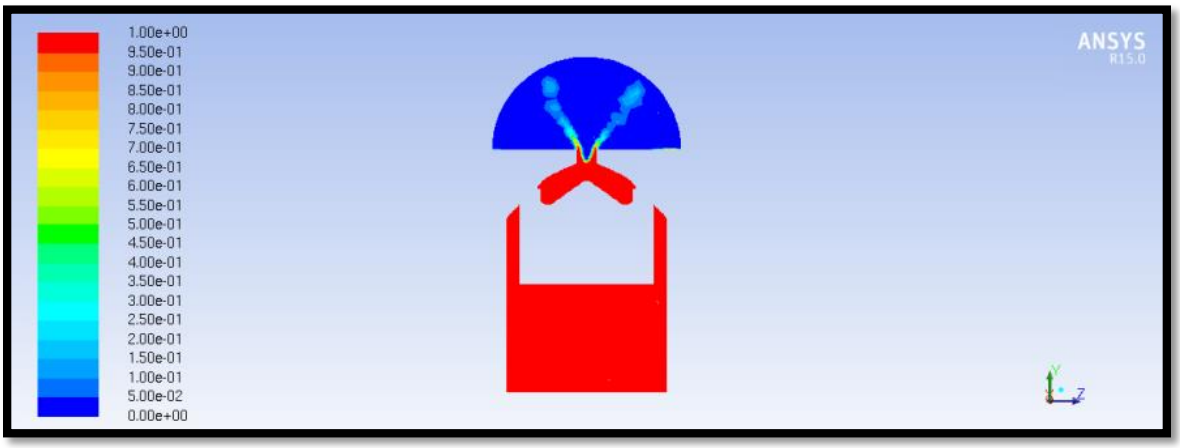

Figure 84: Volume Fraction, Conventional Atomizer, 1.5 million cells

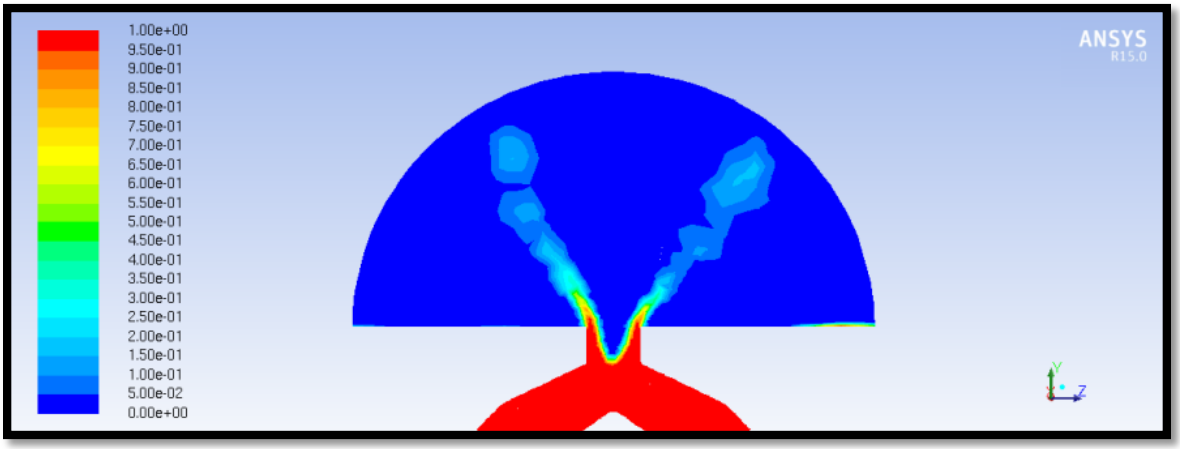

Figure 85: Volume Fraction, Conventional Atomizer, 1.5 million cells, Outlet

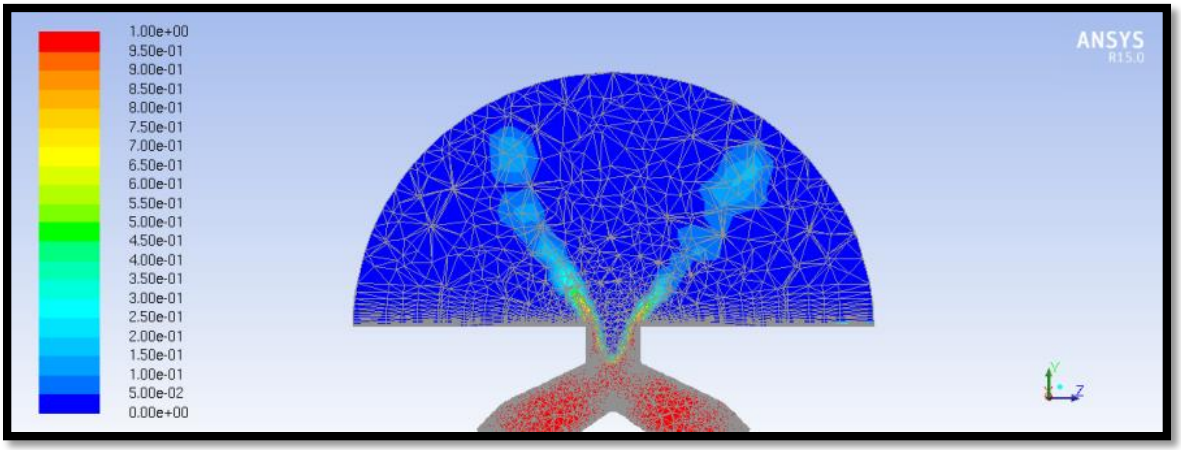

Figure 86: Meshed Volume Fraction, Conventional Atomizer, 1.5 million cells, Outlet

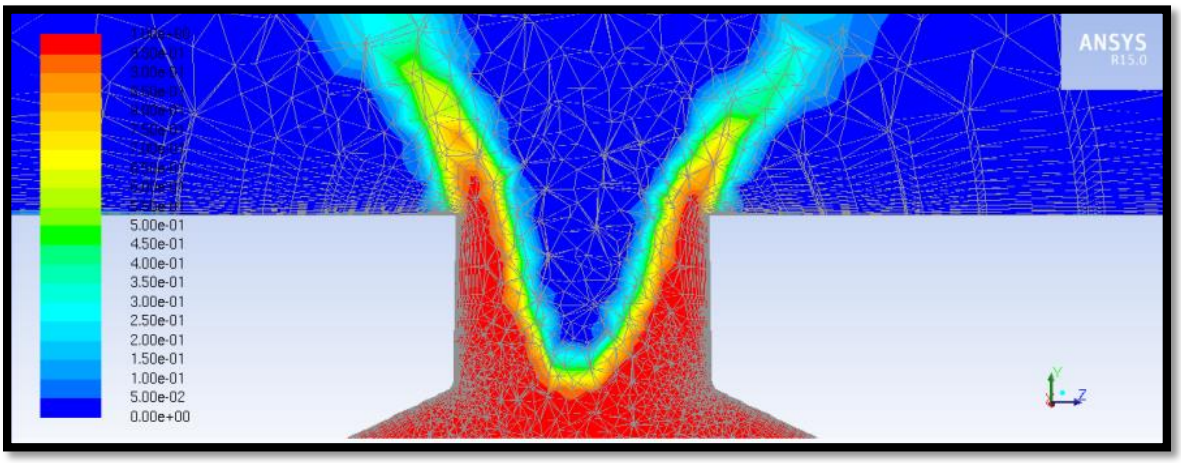

Figure 87: Meshed Volume Fraction, Conventional Atomizer, 1.5 million cells, Orifice

Grid Independence | Conventional Atomizer | 2.8 million cells, Meshed Volume Fraction

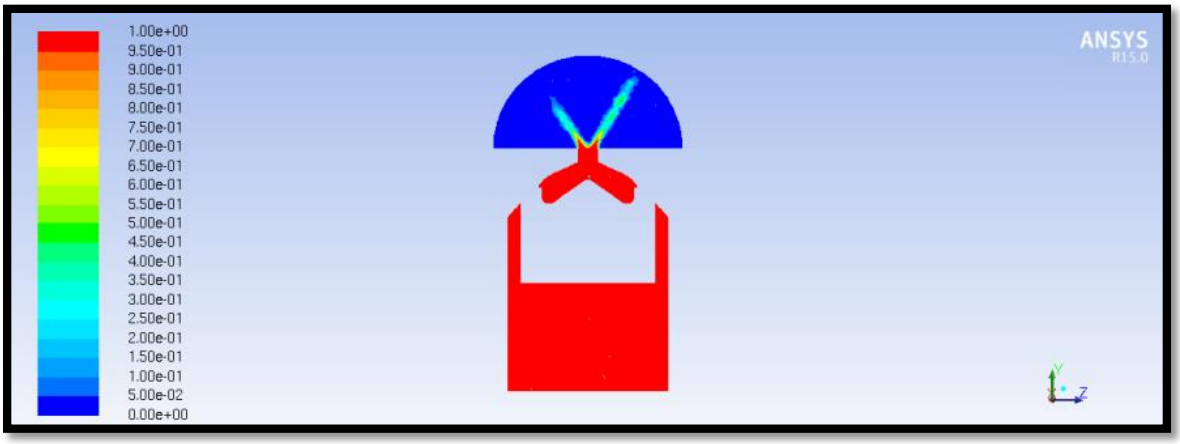

Figure 88: Volume Fraction, Conventional Atomizer, 2.8 million cells

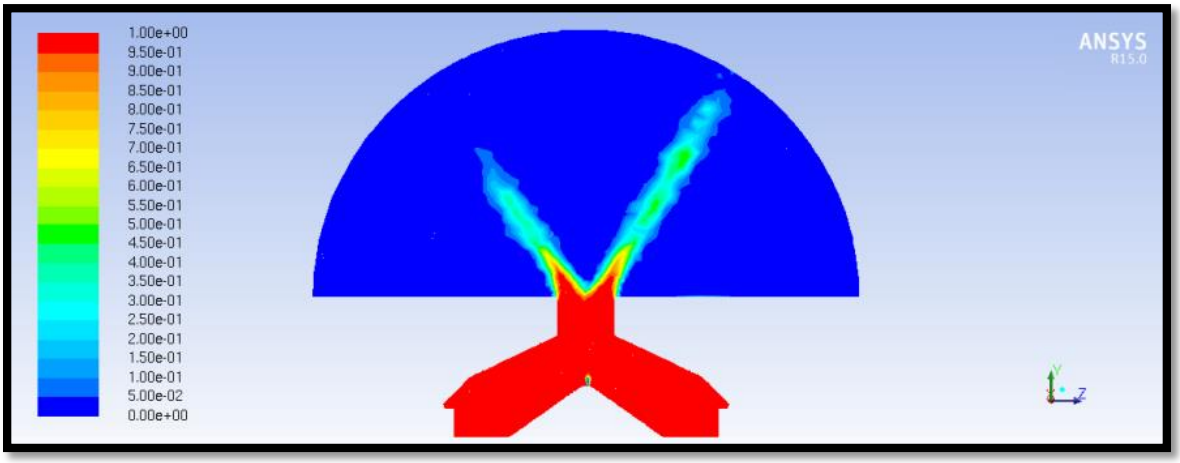

Figure 89: Volume Fraction, Conventional Atomizer, 2.8 million cells, Outlet

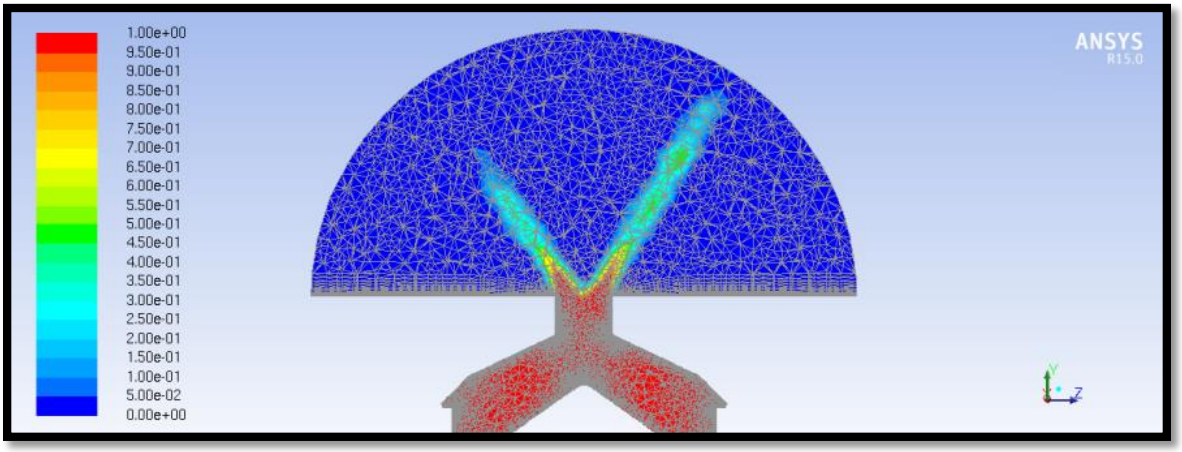

Figure 90: Meshed Volume Fraction, Conventional Atomizer, 2.8 million cells, Outlet

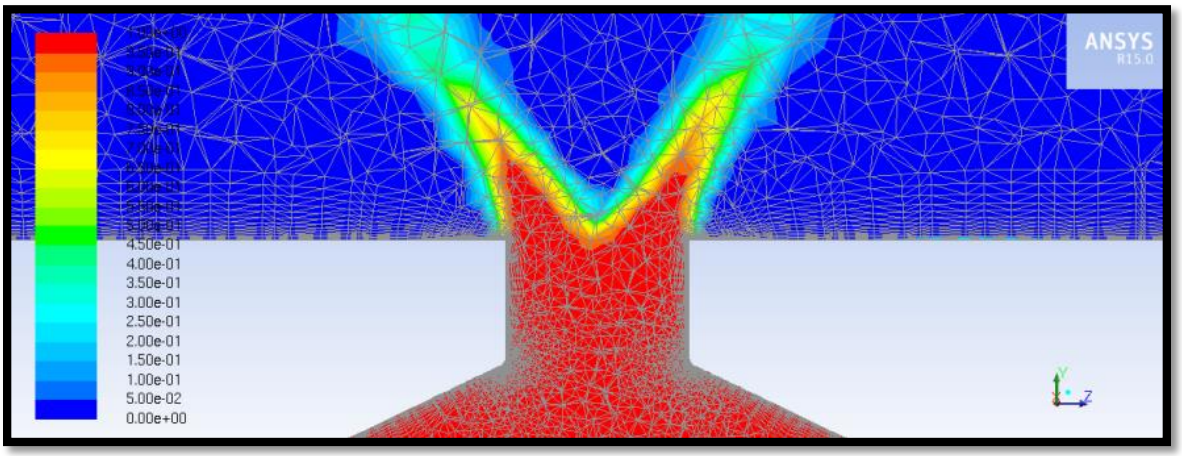

Figure 91: Meshed Volume Fraction, Conventional Atomizer, 2.8 million cells, Orifice

Grid Independence | Conventional Atomizer | 3.7 million cells, Meshed Volume Fraction

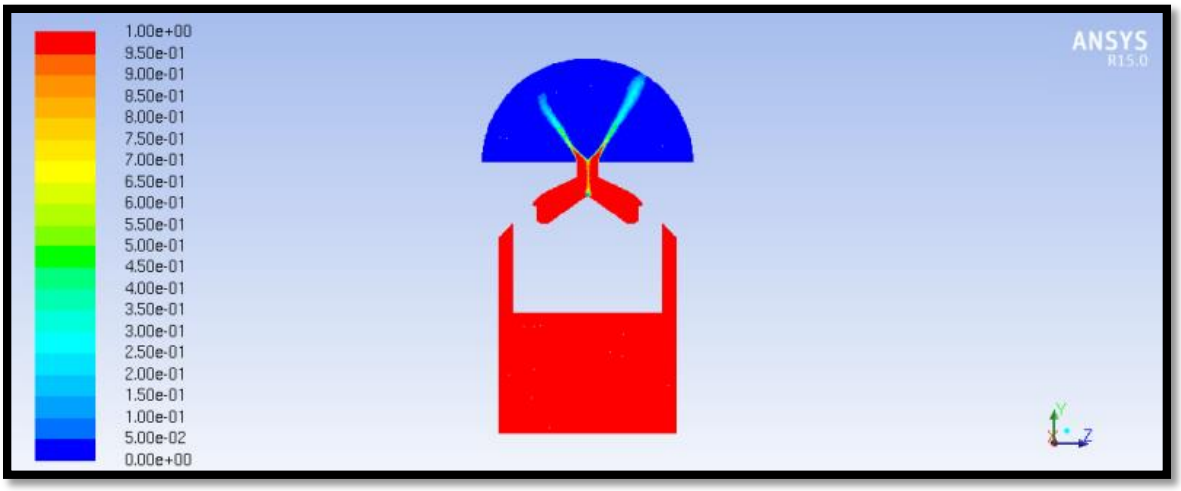

Figure 92: Volume Fraction, Conventional Atomizer, 3.7 million cells

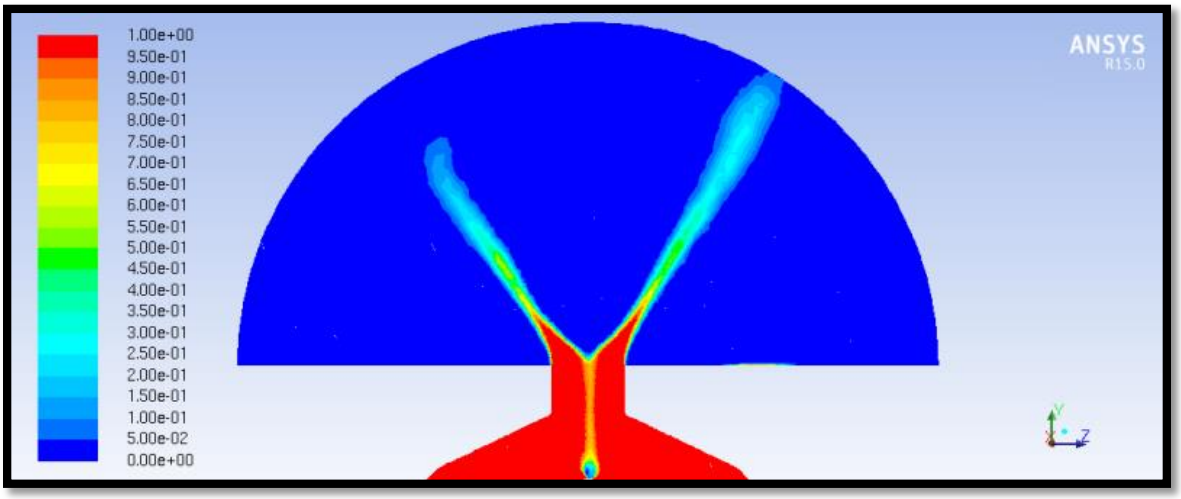

Figure 93: Volume Fraction, Conventional Atomizer, 3.7 million cells, Outlet

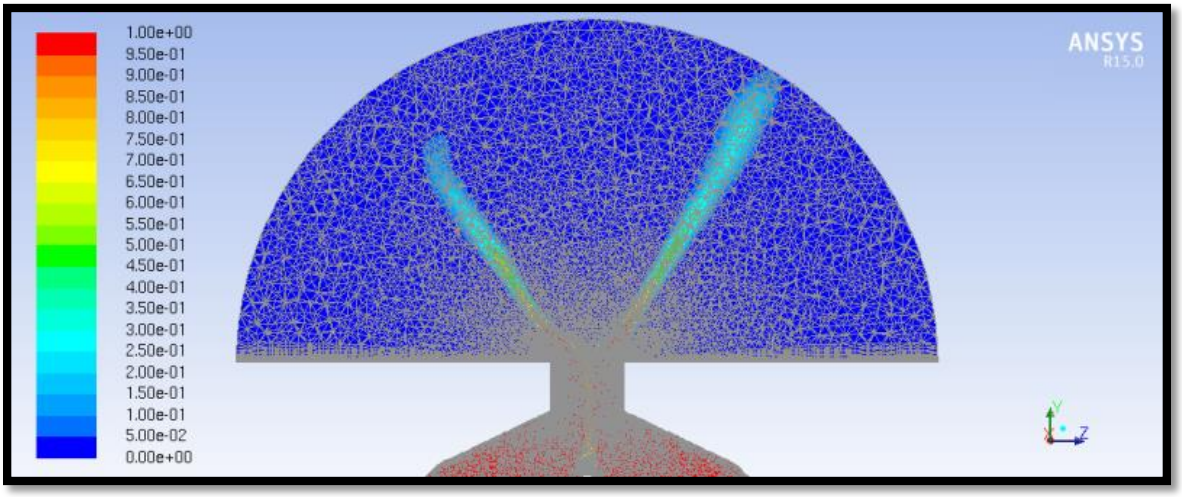

Figure 94: Meshed Volume Fraction, Conventional Atomizer, 3.7 million cells, Outlet

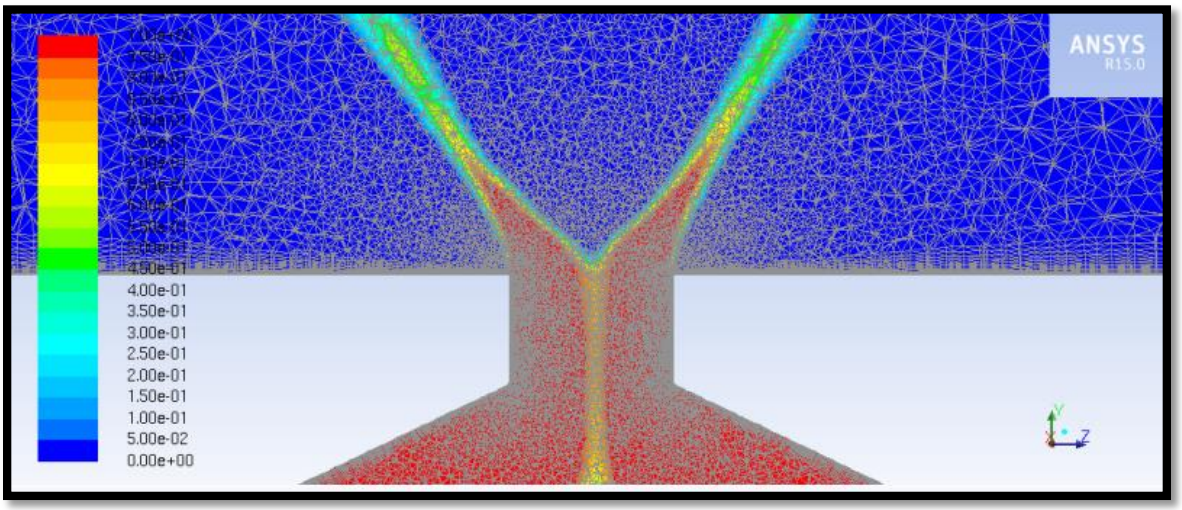

Figure 95: Meshed Volume Fraction, Conventional Atomizer, 3.7 million cells, Orifice

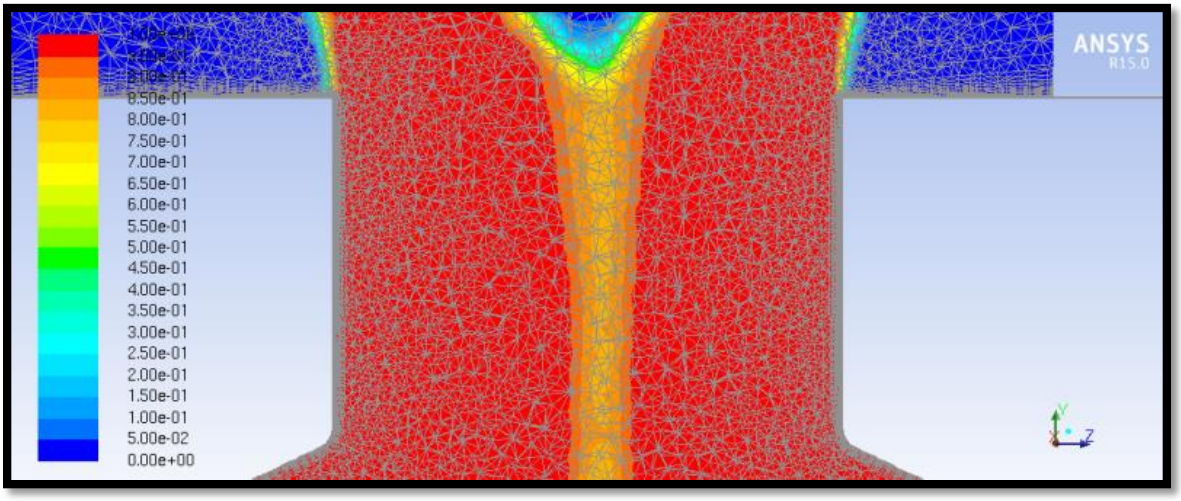

Figure 96: Meshed Volume Fraction, Conventional Atomizer, 3.7 million cells, Air Core

Grid Independence | Conventional Atomizer | 3.8 million cells, Meshed Volume Fraction

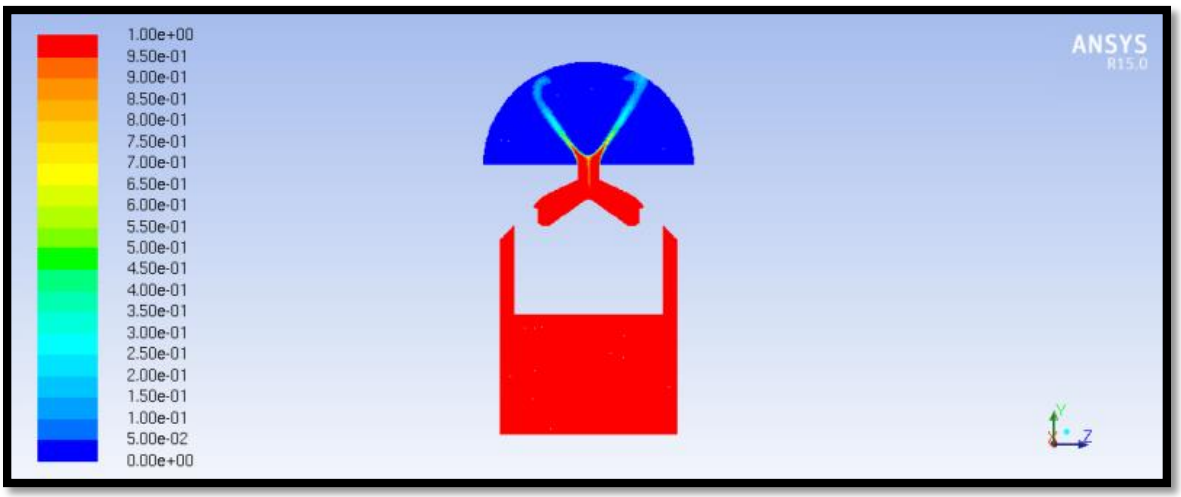

Figure 97: Volume Fraction, Conventional Atomizer, 3.8 million cells

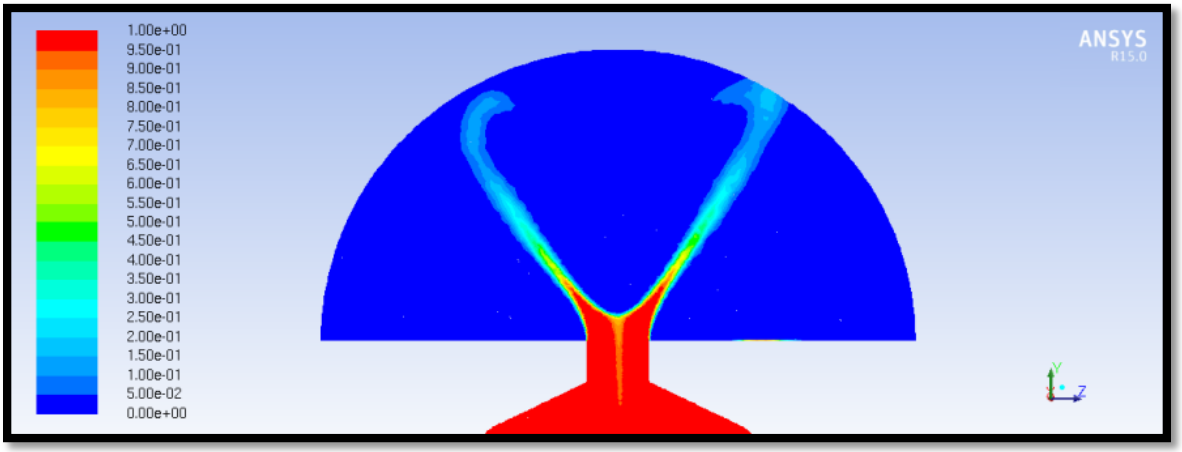

Figure 98: Volume Fraction, Conventional Atomizer, 3.8 million cells, Outlet

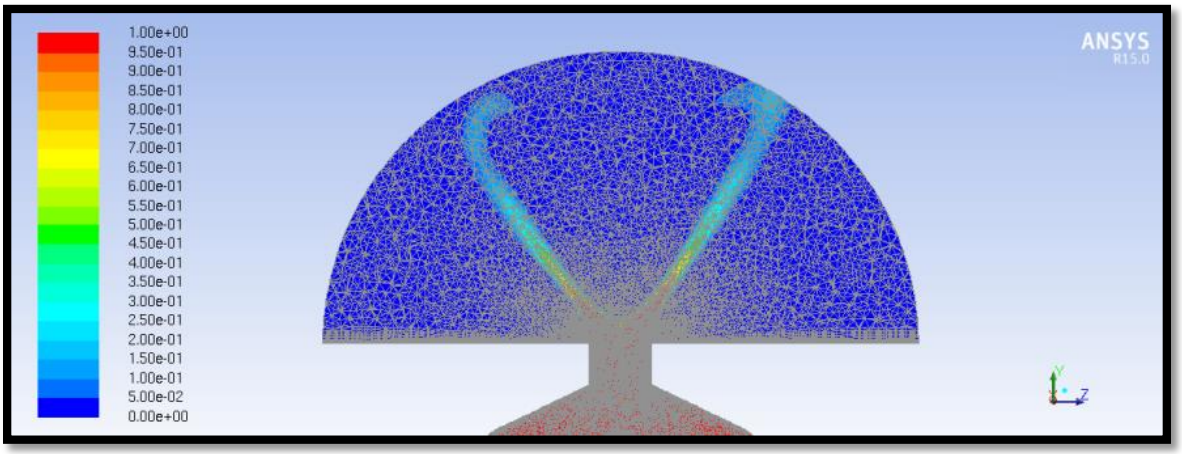

Figure 99: Meshed Volume Fraction, Conventional Atomizer, 3.8 million cells, Outlet

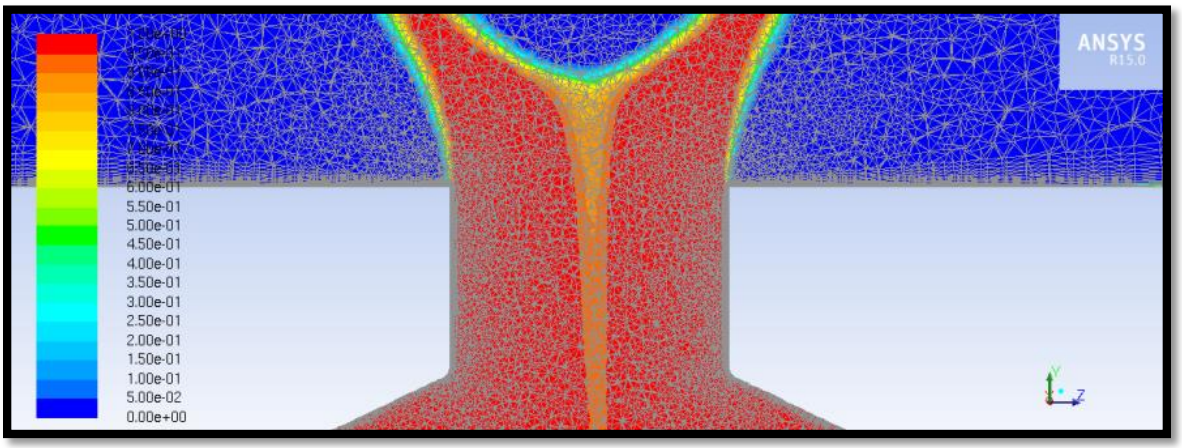

Figure 100: Meshed Volume Fraction, Conventional Atomizer, 3.8 million cells, Air Core

Appendix E

Pressure Stages for Simulation of Macrospray Atomizer

10 psi Inlet Condition

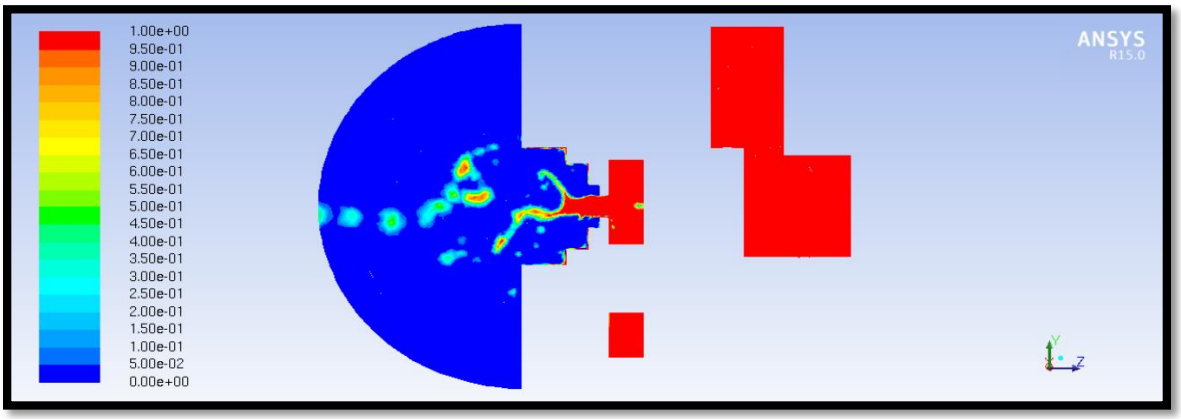

Figure 101: 10 psi, Macrospray Atomizer, Volume Fraction

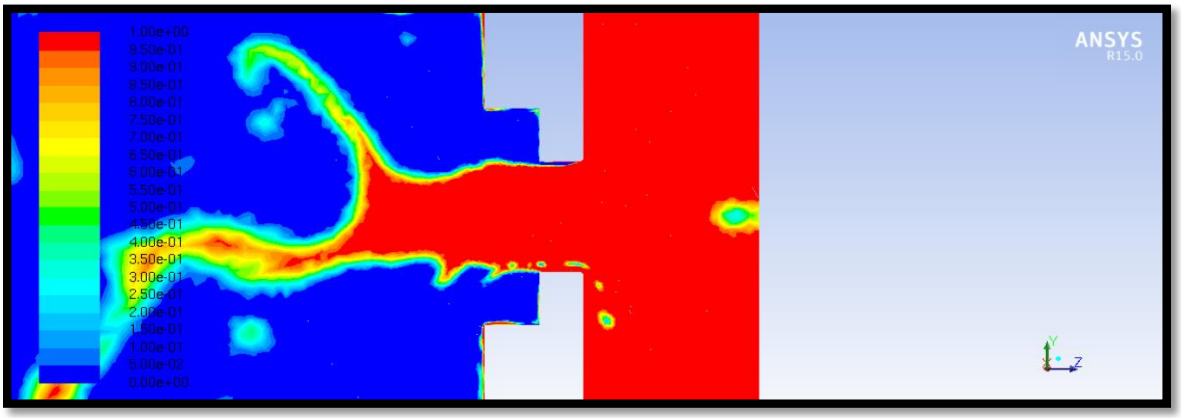

Figure 102: 10 psi, Macrospray Atomizer, Volume Fraction, Orifice

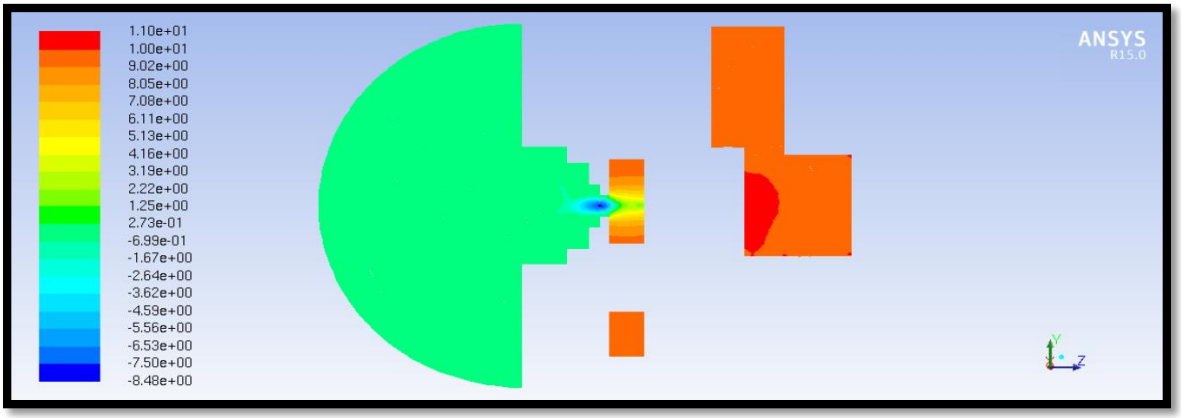

Figure 103: 10 psi, Macrospray Atomizer, Pressure Contours

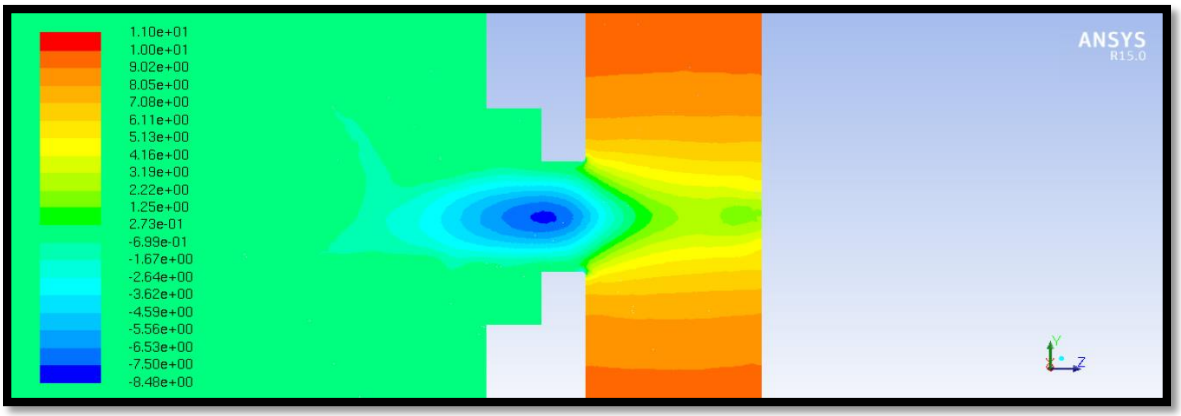

Figure 104: 10 psi, Macrospray Atomizer, Pressure Contours, Orifice

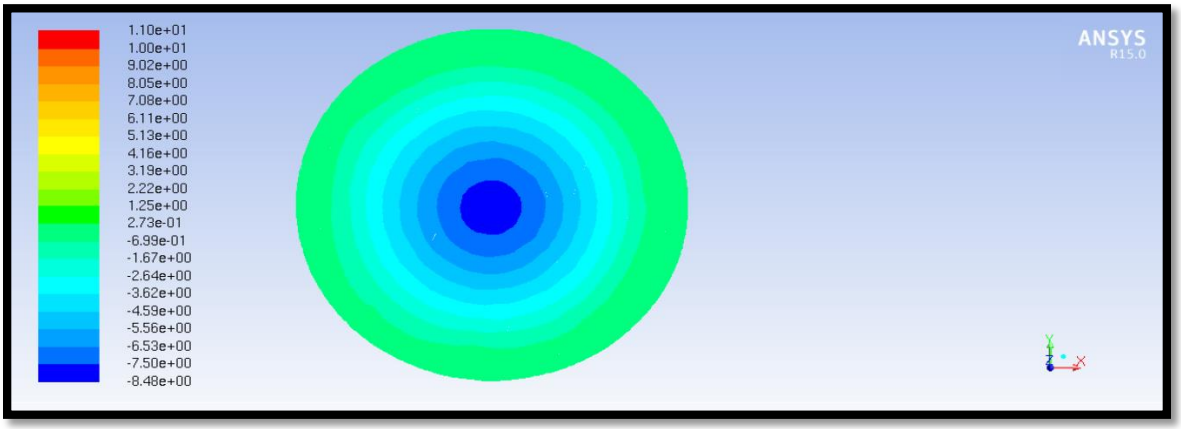

Figure 105: 10 psi, Macrospray Atomizer, Pressure Contours, Orifice Cross Section Velocity Vectors

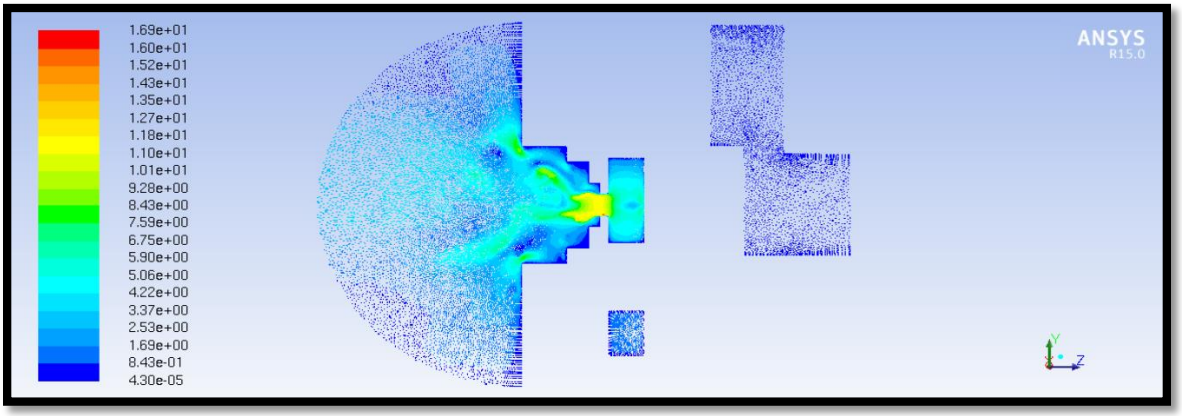

Figure 106: 10 psi, Macrospray Atomizer, Velocity Vectors

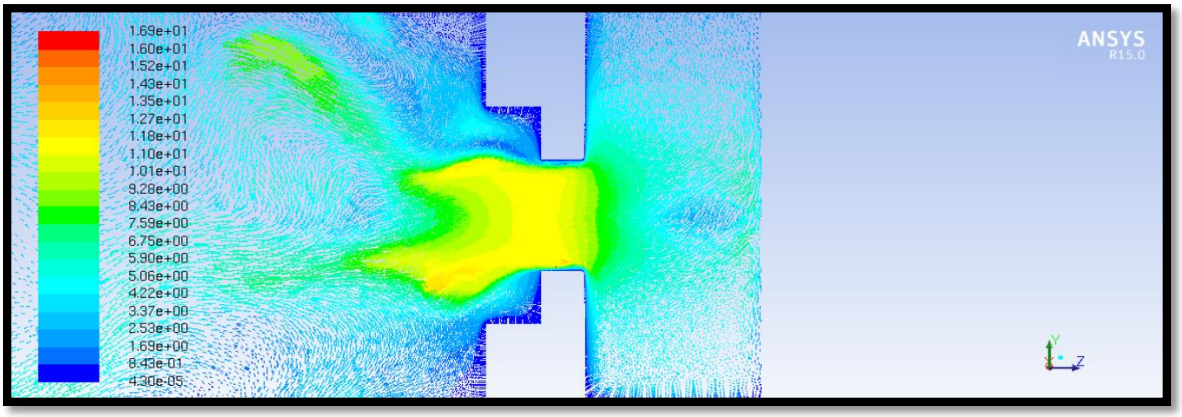

Figure 107: 10 psi, Macrospray Atomizer, Velocity Vectors, Orifice

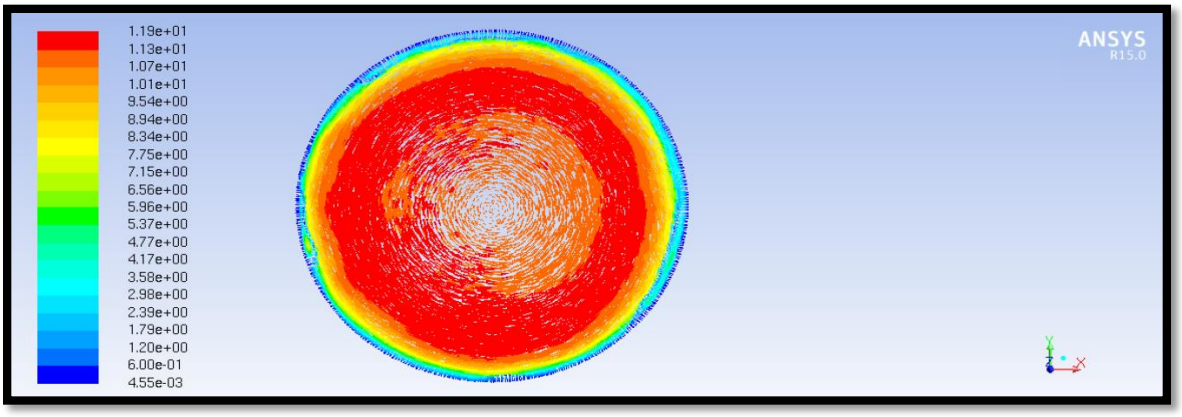

Figure 108: 10 psi, Macrospray Atomizer, Velocity Vectors, Orifice Cross Section

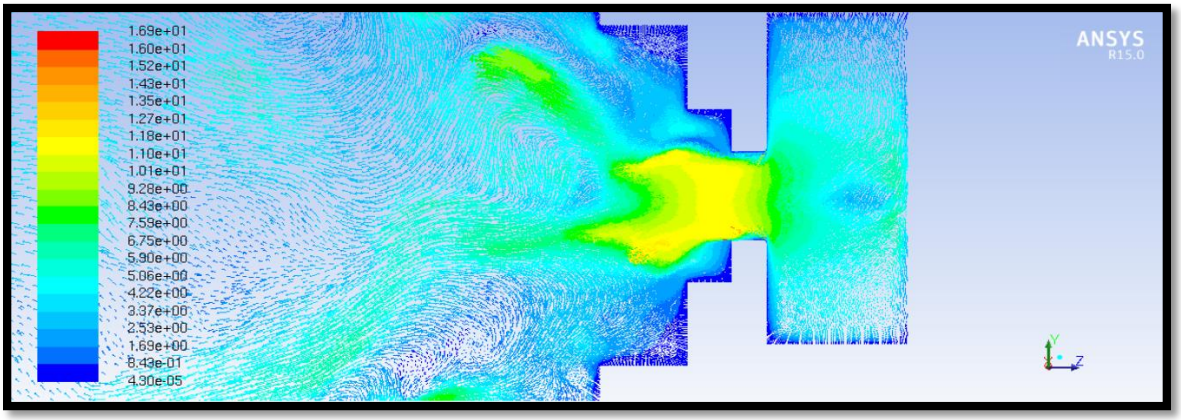

Figure 109: 10 psi, Macrospray Atomizer, Velocity Vectors, Air Core

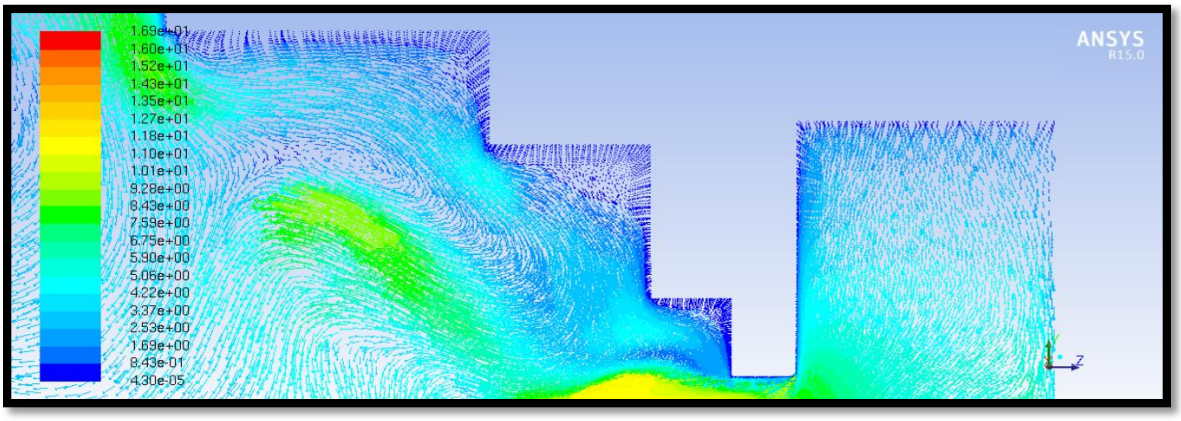

Figure 110: 10 psi, Macrospray Atomizer, Velocity Vectors, Recirculation Zones

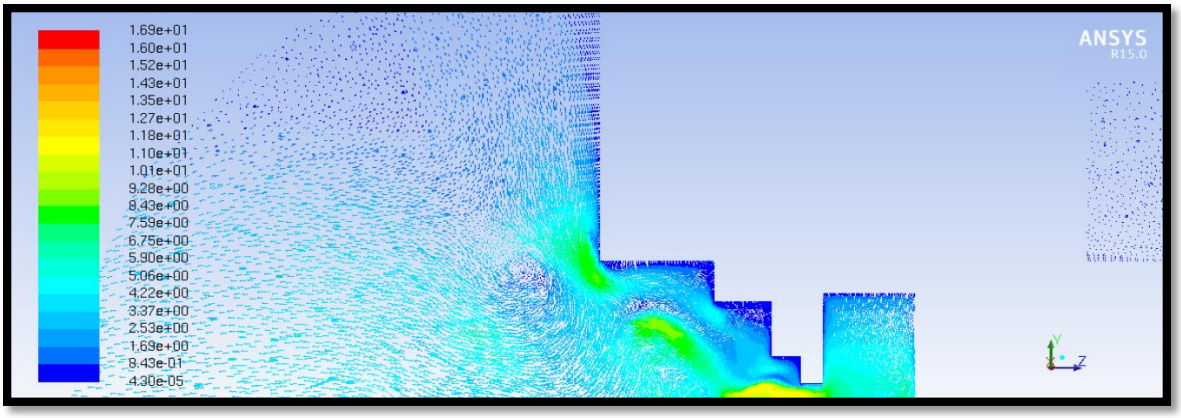

Figure 111: 10 psi, Macrospray Atomizer, Velocity Vectors, Jetstream Top

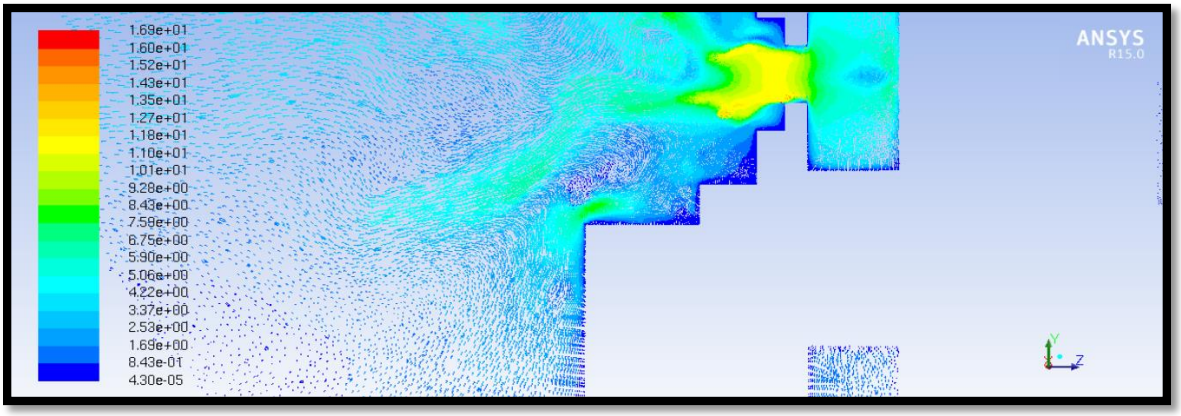

Figure 112: 10 psi, Macrospray Atomizer, Velocity Vectors, Jetstream Bottom

20 psi Inlet Condition

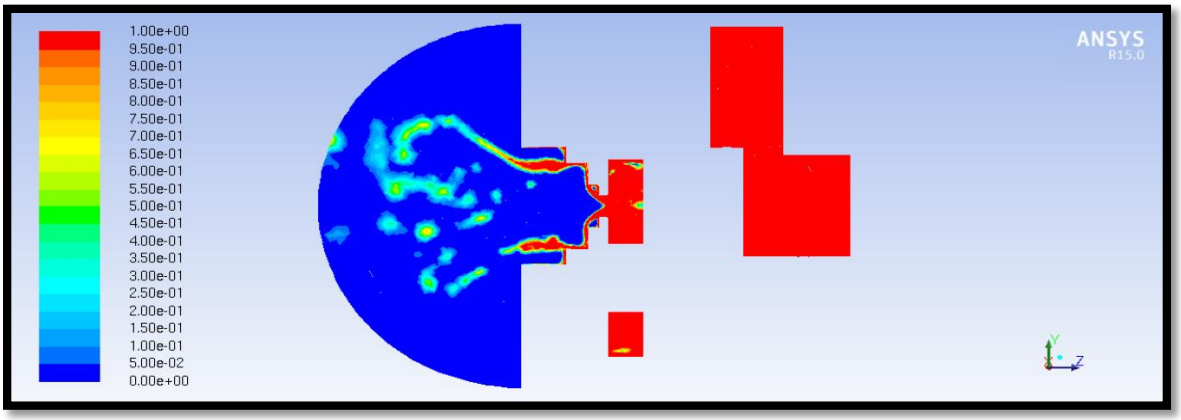

Figure 113: 20 psi, Macrospray Atomizer, Volume Fraction

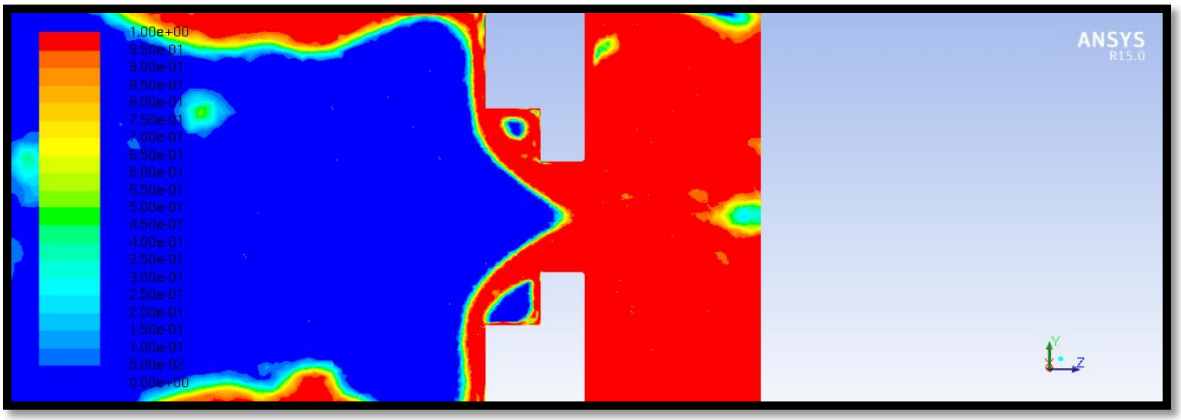

Figure 114: 20 psi, Macrospray Atomizer, Volume Fraction, Orifice

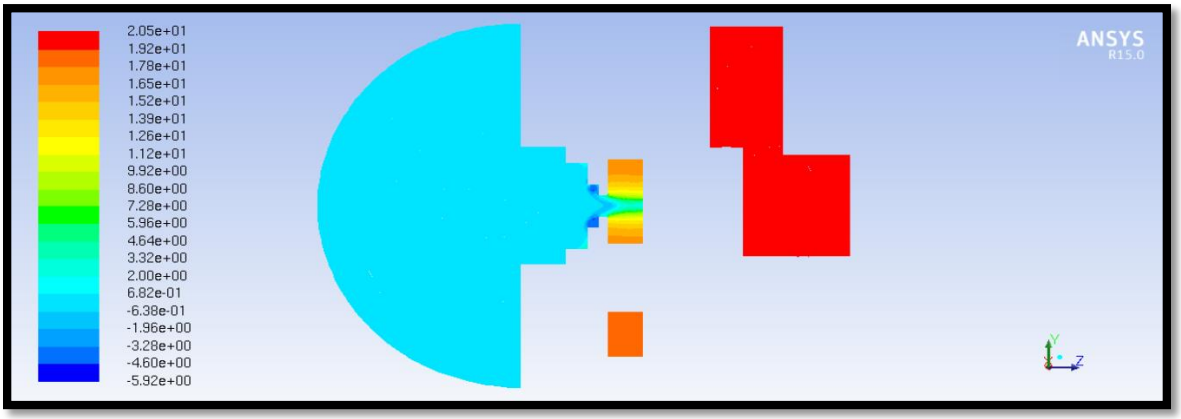

Figure 115: 20 psi, Macrospray Atomizer, Pressure Contours

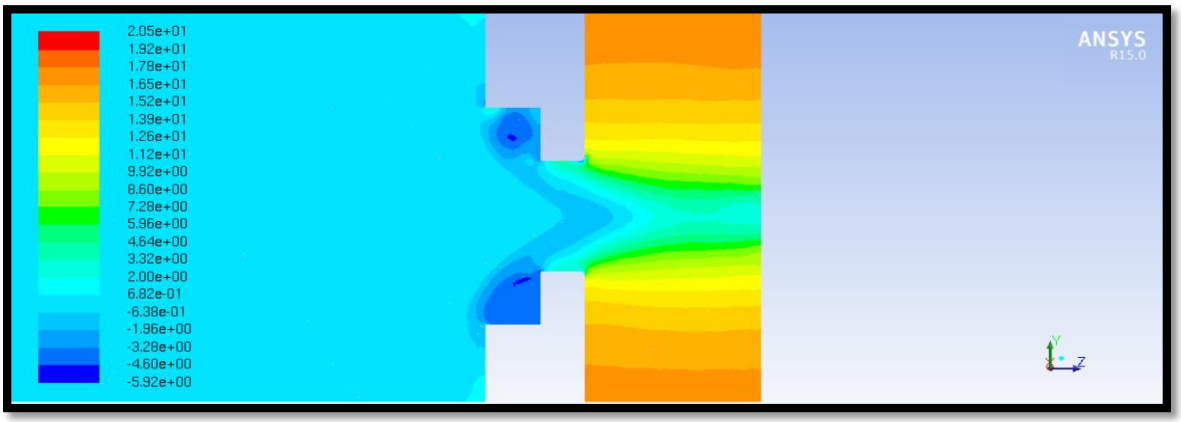

Figure 116: 20 psi, Macrospray Atomizer, Pressure Contours, Orifice

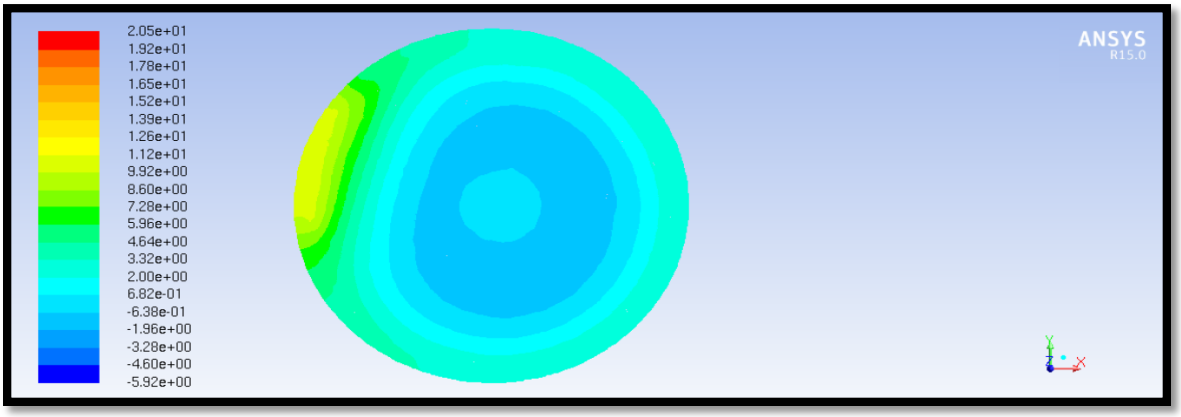

Figure 117: 20 psi, Macrospray Atomizer, Pressure Contours, Orifice Cross Section

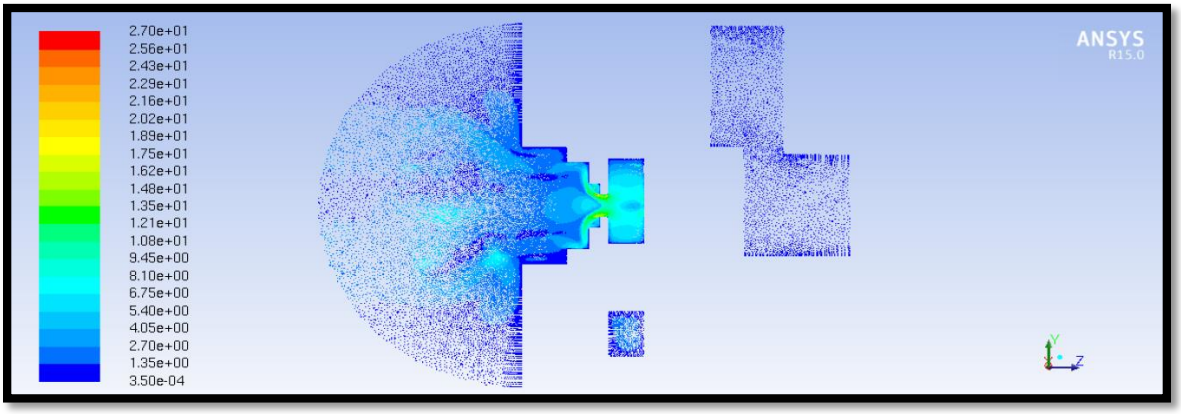

Figure 118: 20 psi, Macrospray Atomizer, Velocity Vectors

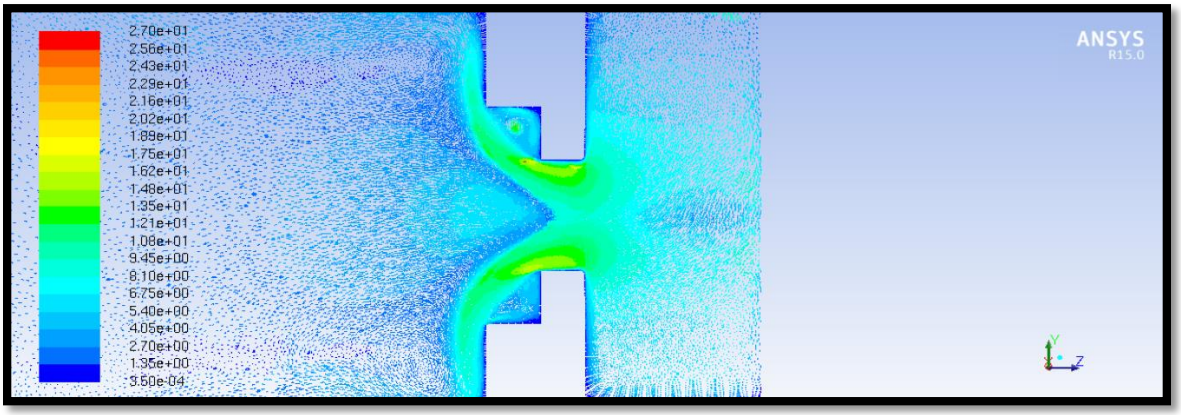

Figure 119: 20 psi, Macrospray Atomizer, Velocity Vectors, Orifice

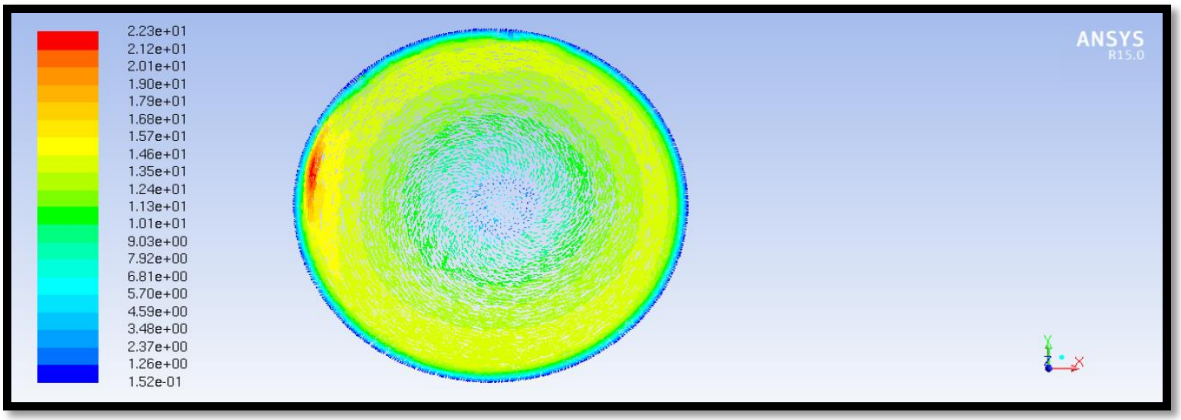

Figure 120: 20 psi, Macrospray Atomizer, Velocity Vectors, Orifice Cross Section

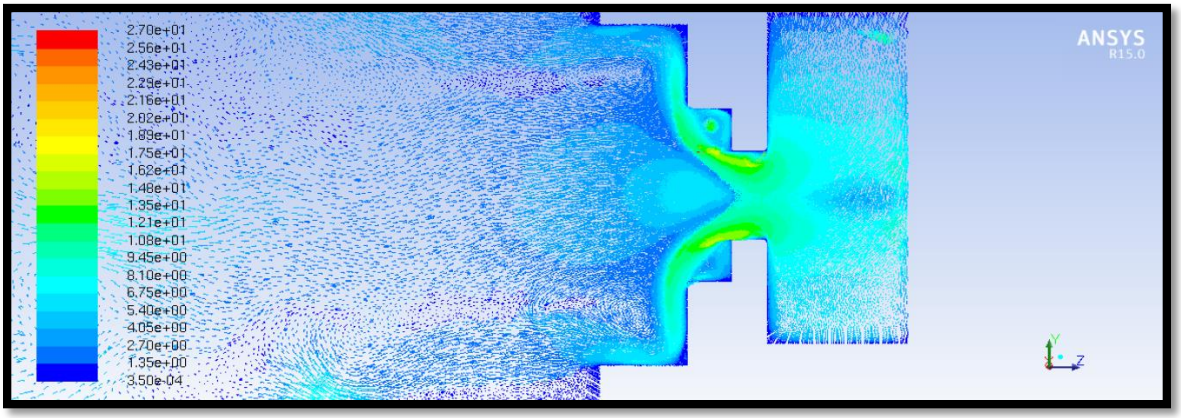

Figure 121: 20 psi, Macrospray Atomizer, Velocity Vectors, Air Core

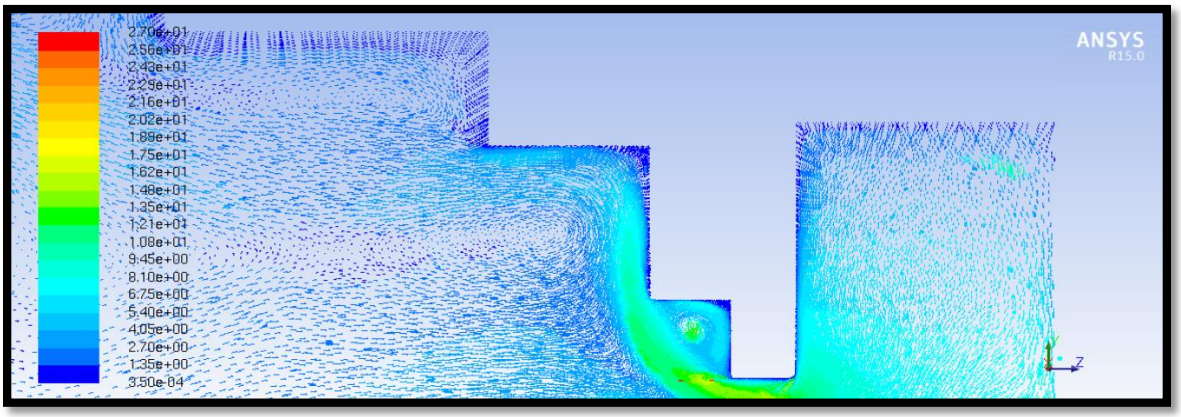

Figure 122: 20 psi, Macrospray Atomizer, Velocity Vectors, Recirculation Zones

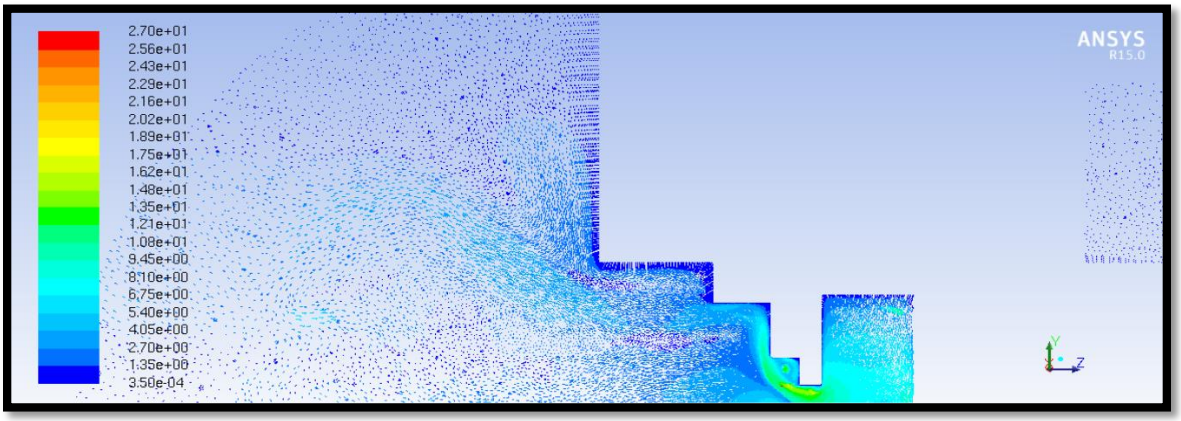

Figure 123: 20 psi, Macrospray Atomizer, Velocity Vectors, Jetstream Top

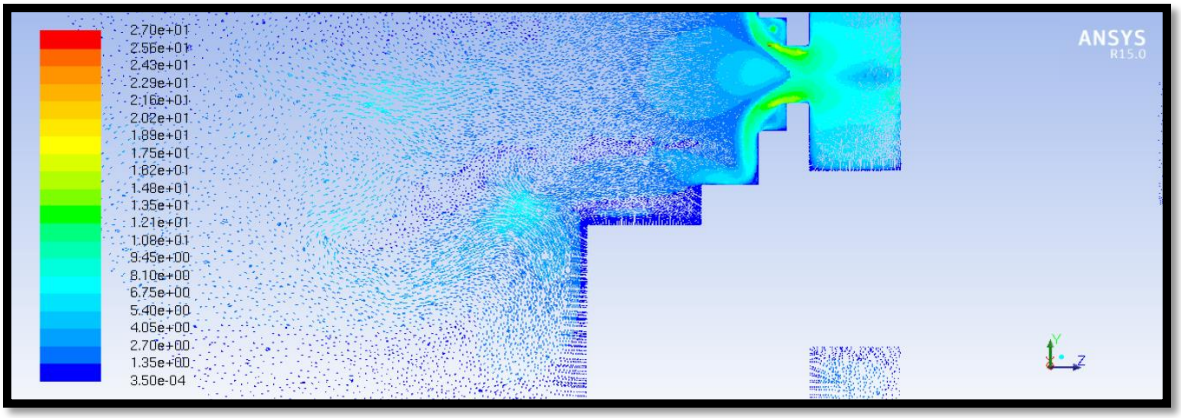

Figure 124: 20 psi, Macrospray Atomizer, Velocity Vectors, Jetstream Bottom

40 psi Inlet Condition

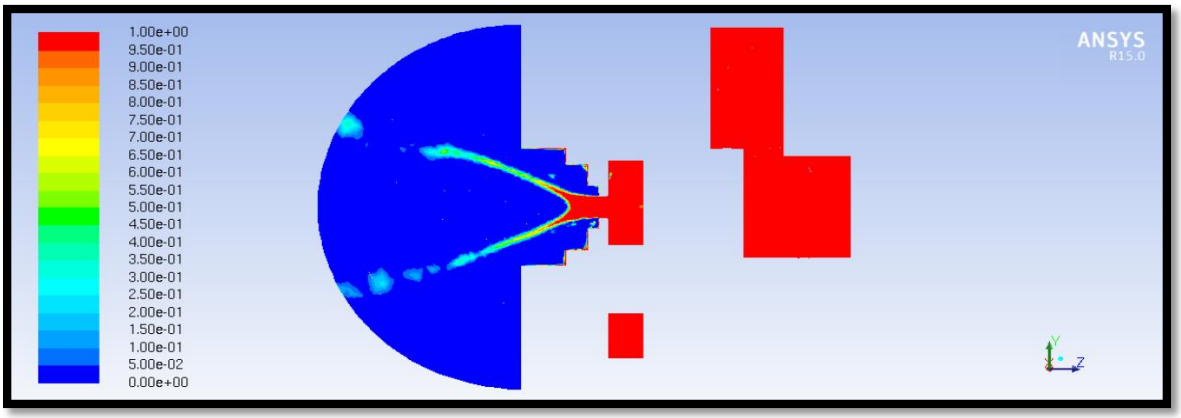

Figure 125: 40 psi, Macrospray Atomizer, Volume Fraction

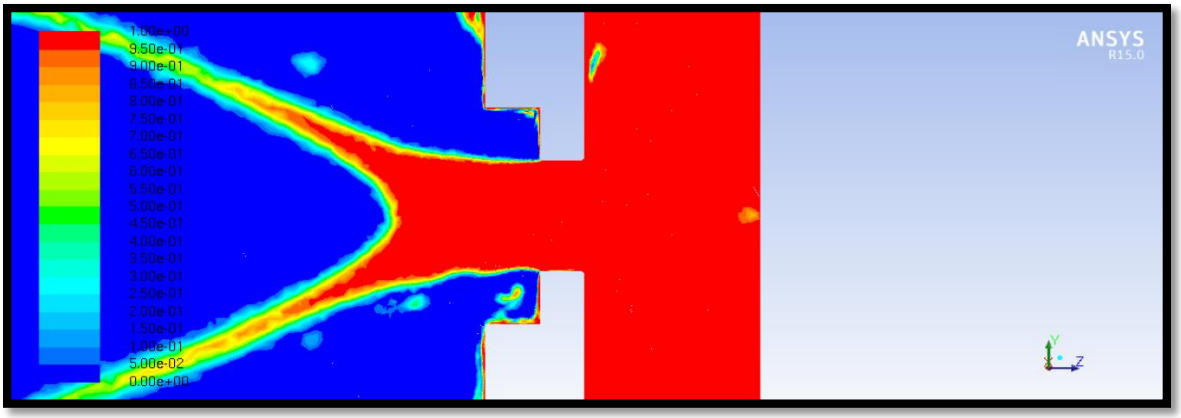

Figure 126: 40 psi, Macrospray Atomizer, Volume Fraction, Orifice

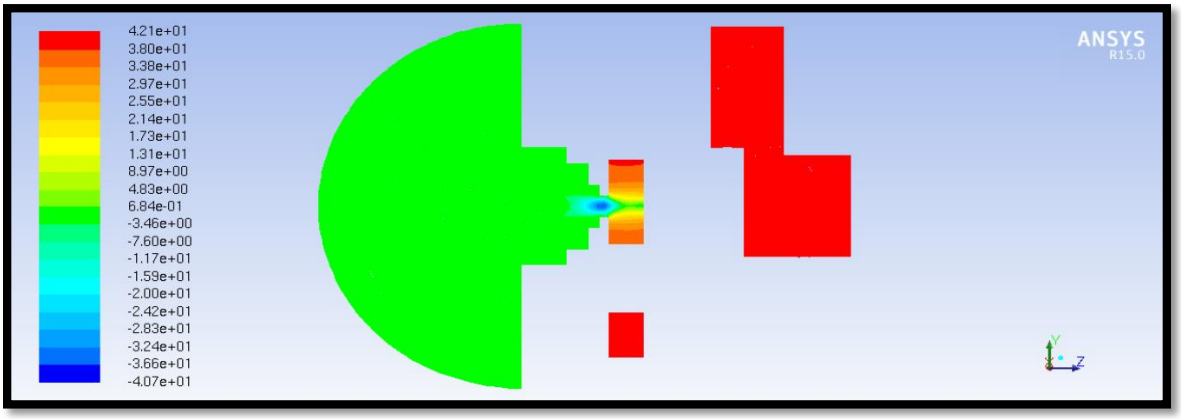

Figure 127: 40 psi, Macrospray Atomizer, Pressure Contours

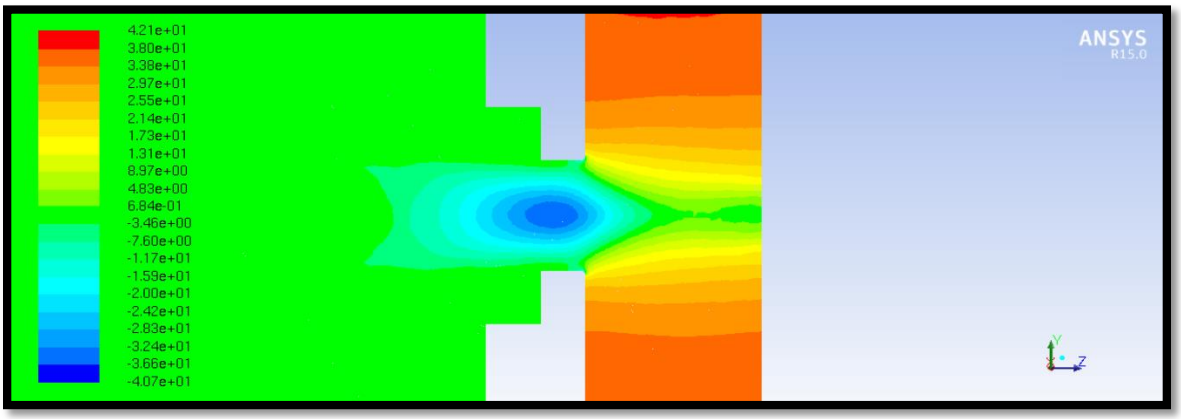

Figure 128: 40 psi, Macrospray Atomizer, Pressure Contours, Orifice

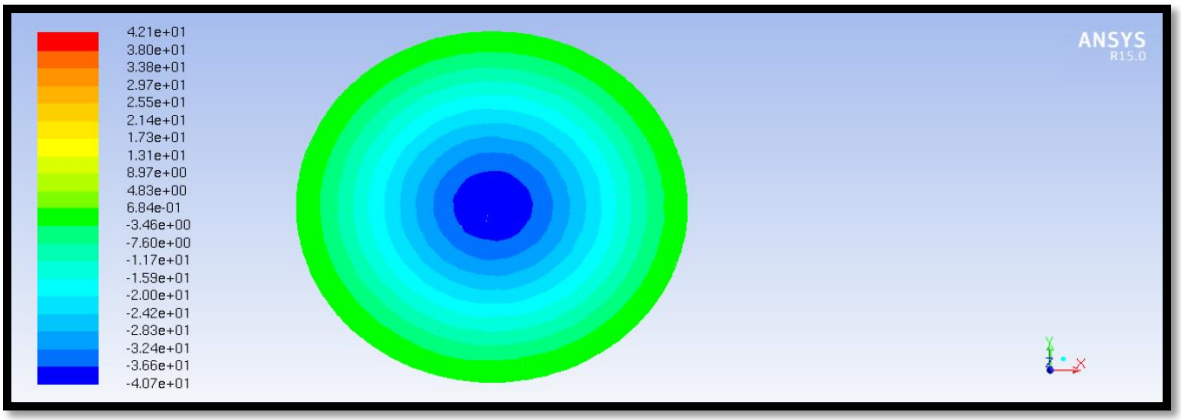

Figure 129: 40 psi, Macrospray Atomizer, Pressure Contours, Orifice Cross Section

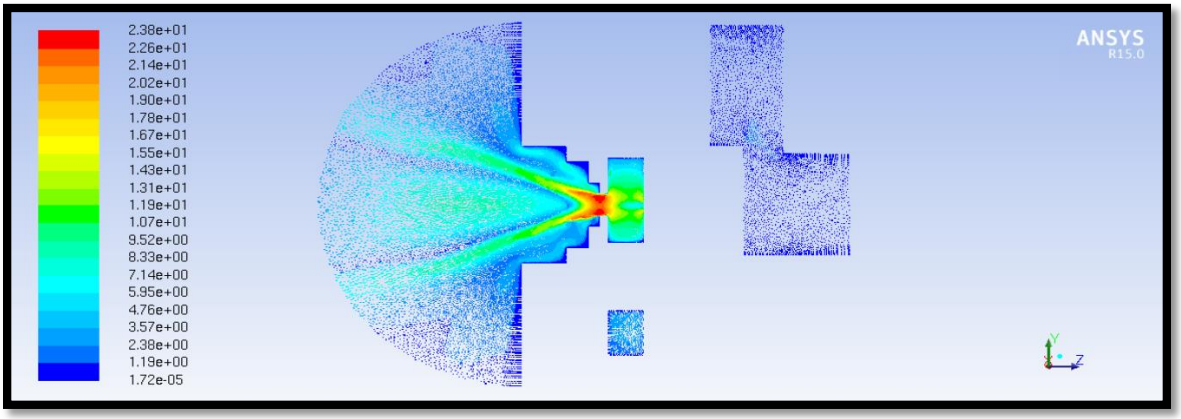

Figure 130: 40 psi, Macrospray Atomizer, Velocity Vectors

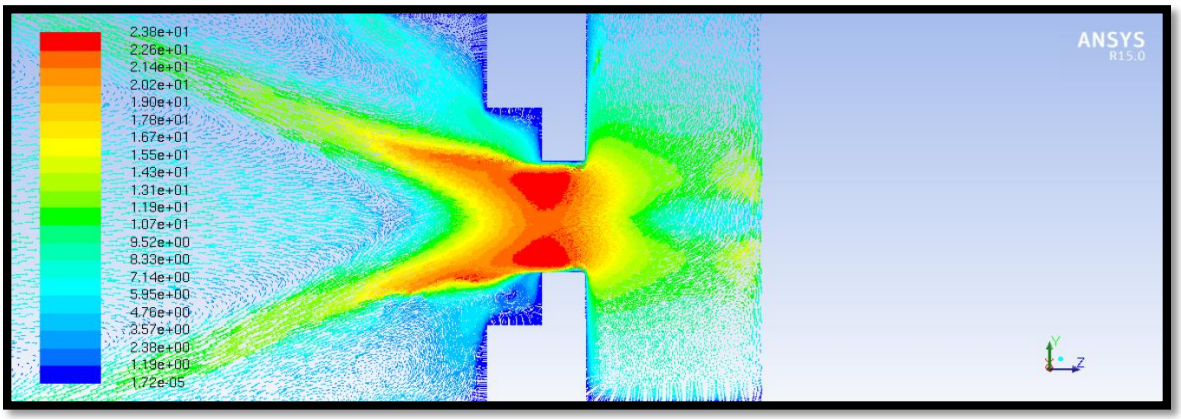

Figure 131: 40 psi, Macrospray Atomizer, Velocity Vectors, Orifice

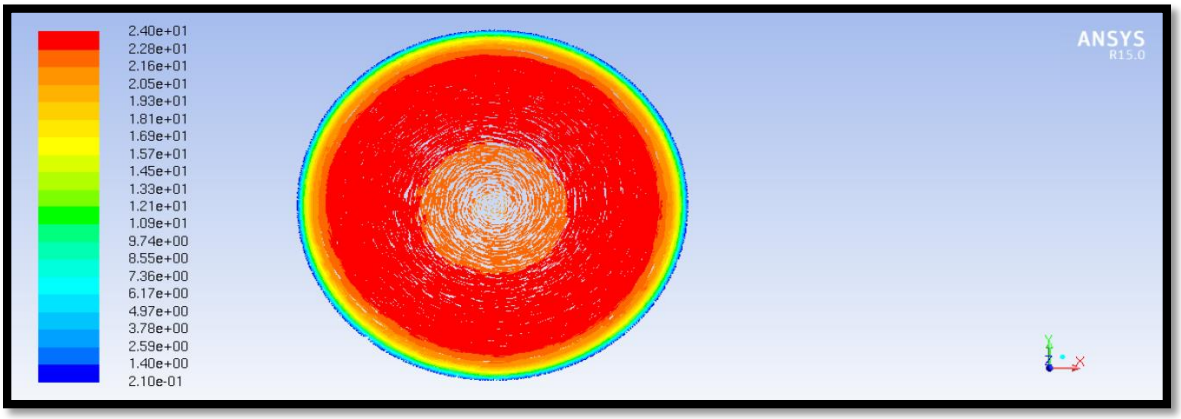

Figure 132: 40 psi, Macrospray Atomizer, Velocity Vectors, Orifice Cross Section

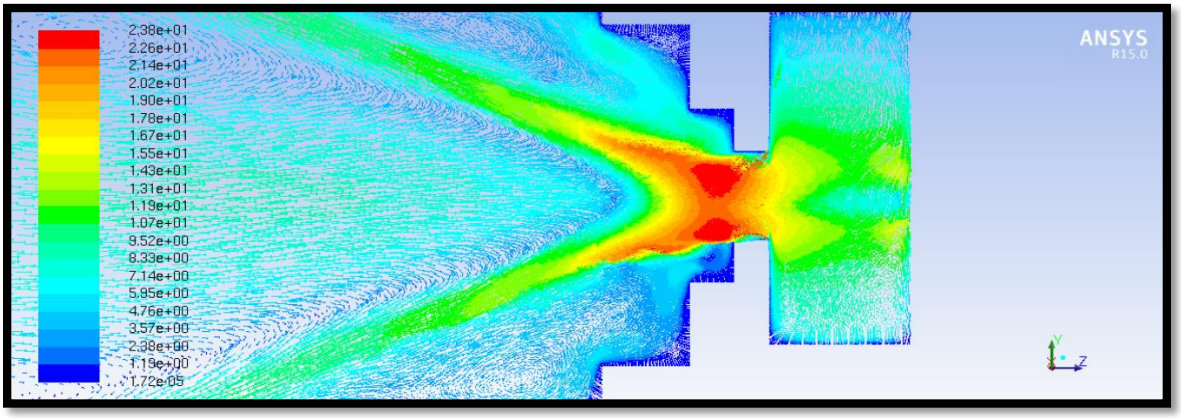

Figure 133: 40 psi, Macrospray Atomizer, Velocity Vectors, Air Core

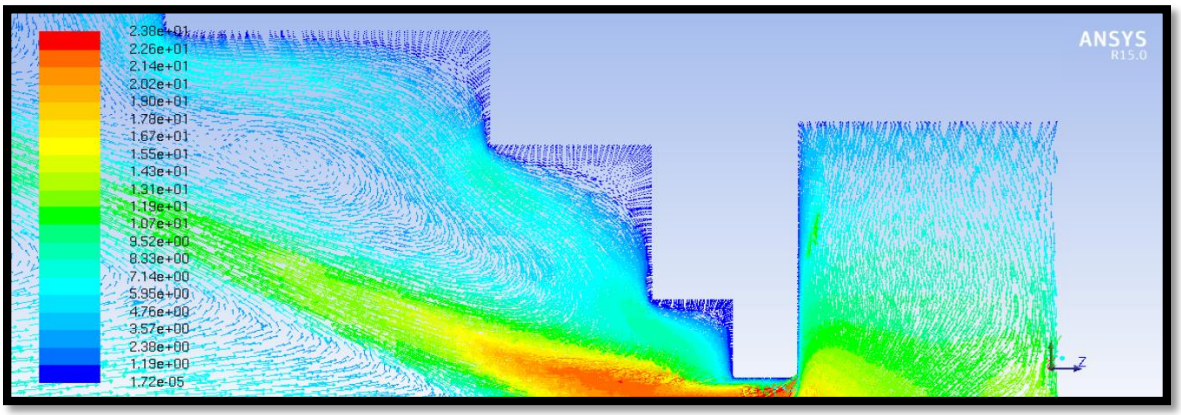

Figure 134: 40 psi, Macrospray Atomizer, Velocity Vectors, Recirculation Zones

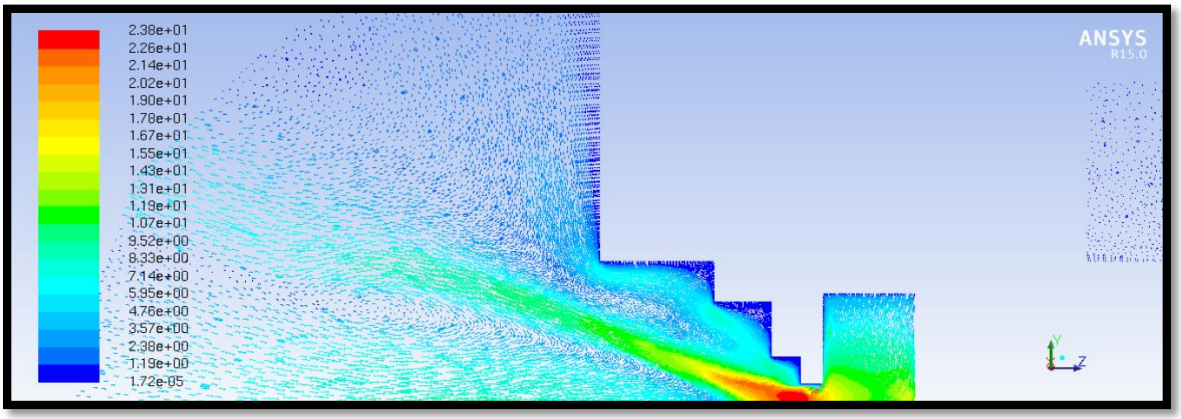

Figure 135: 40 psi, Macrospray Atomizer, Velocity Vectors, Jetstream Top

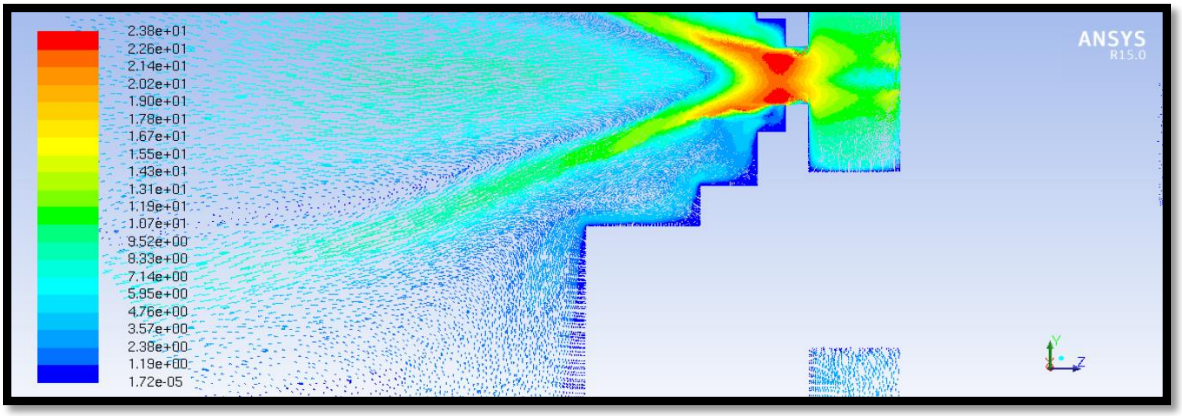

Figure 136: 40 psi, Macrospray Atomizer, Velocity Vectors, Jetstream Bottom

80 psi Inlet Condition

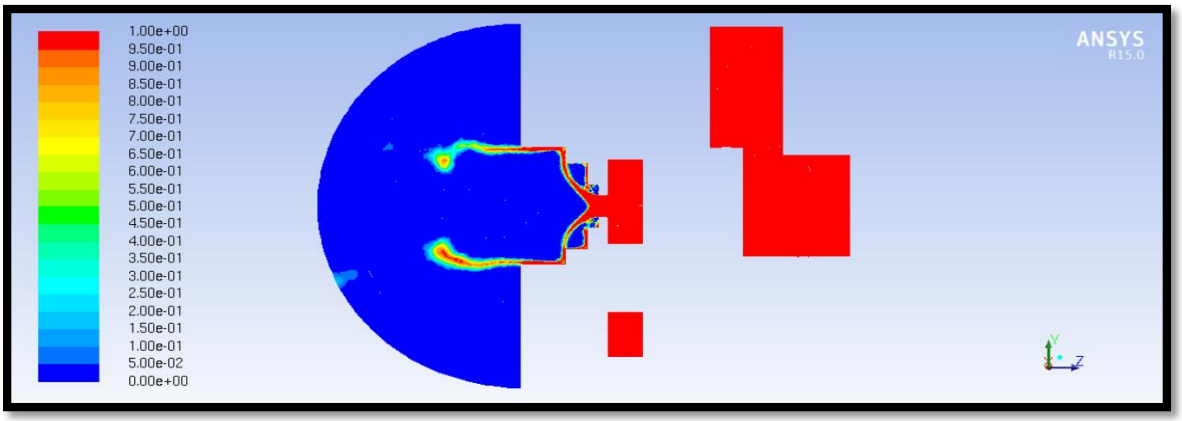

Figure 137: 80 psi, Macrospray Atomizer, Volume Fraction

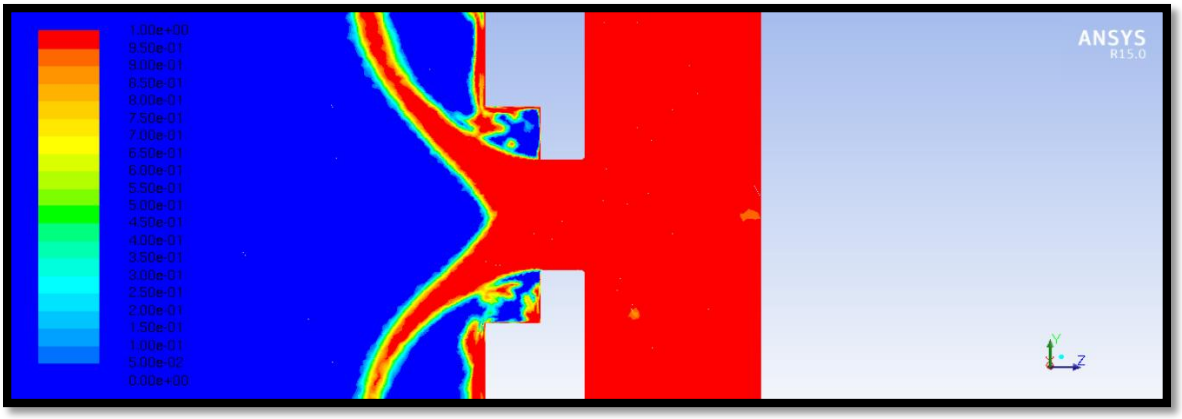

Figure 138: 80 psi, Macrospray Atomizer, Volume Fraction, Orifice

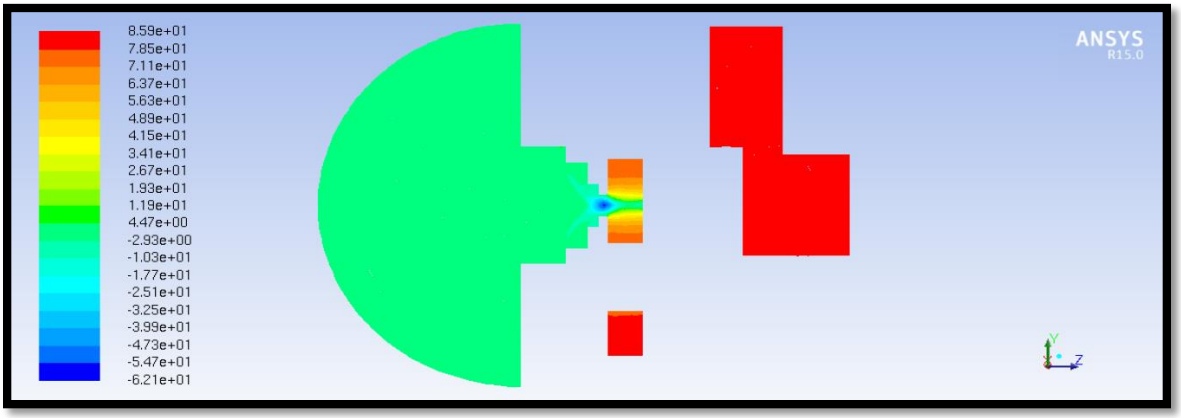

Figure 139: 80 psi, Macrospray Atomizer, Pressure Contours

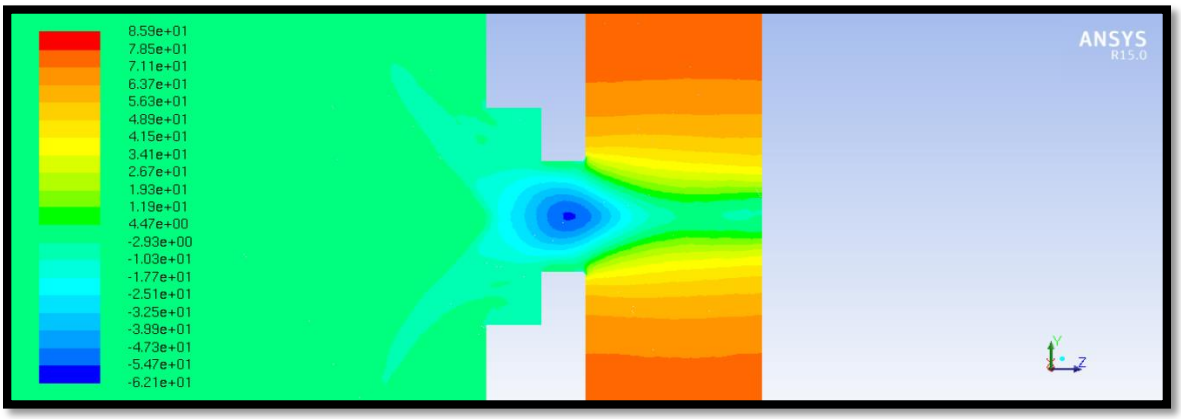

Figure 140: 80 psi, Macrospray Atomizer, Pressure Contours, Orifice

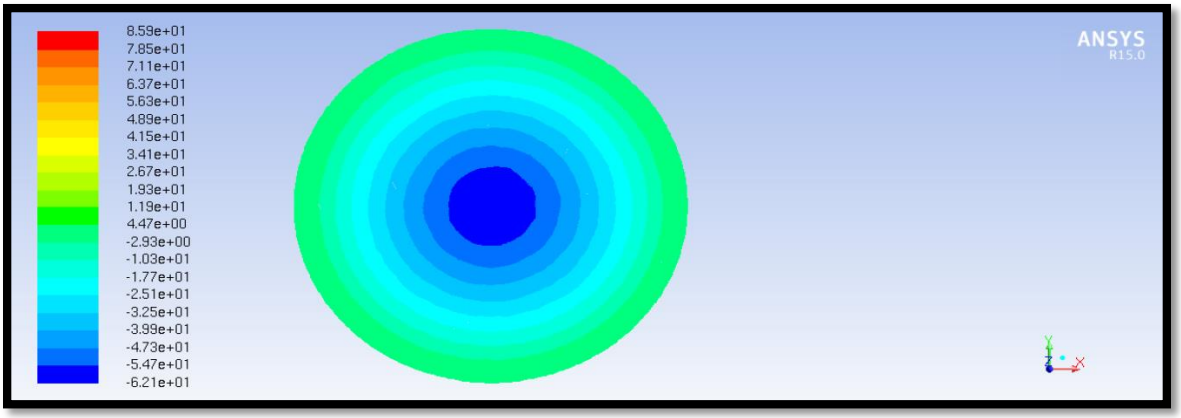

Figure 141: 80 psi, Macrospray Atomizer, Pressure Contours, Orifice Cross Section

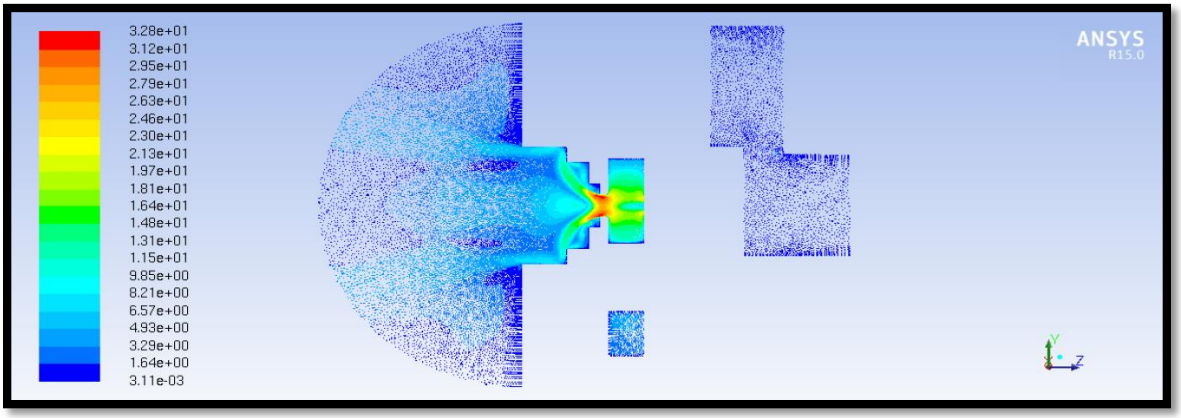

Figure 142: 80 psi, Macrospray Atomizer, Velocity Vectors

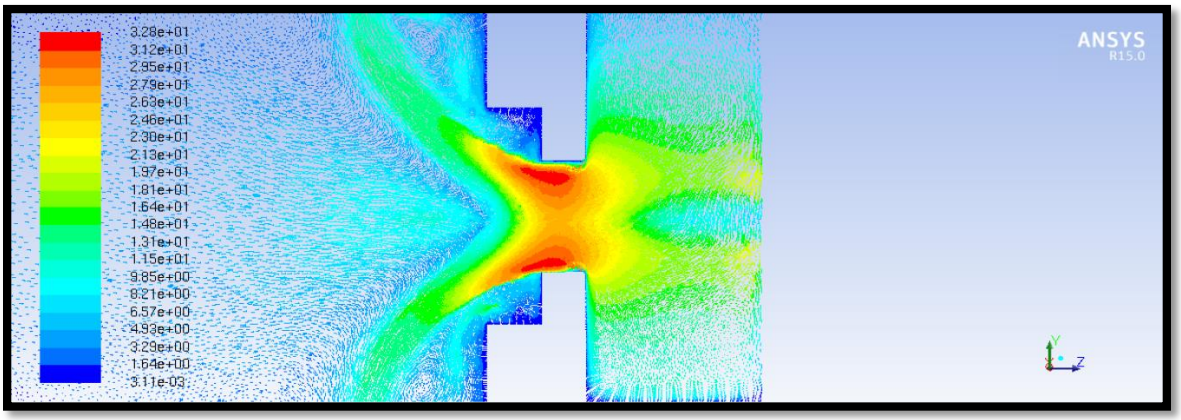

Figure 143: 80 psi, Macrospray Atomizer, Velocity Vectors, Orifice

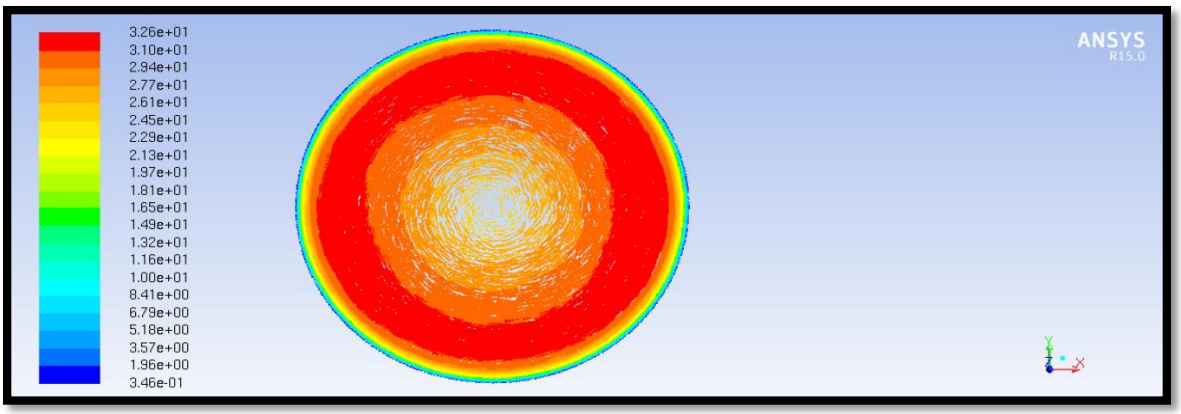

Figure 144: 80 psi, Macrospray Atomizer, Velocity Vectors, Orifice Cross Section

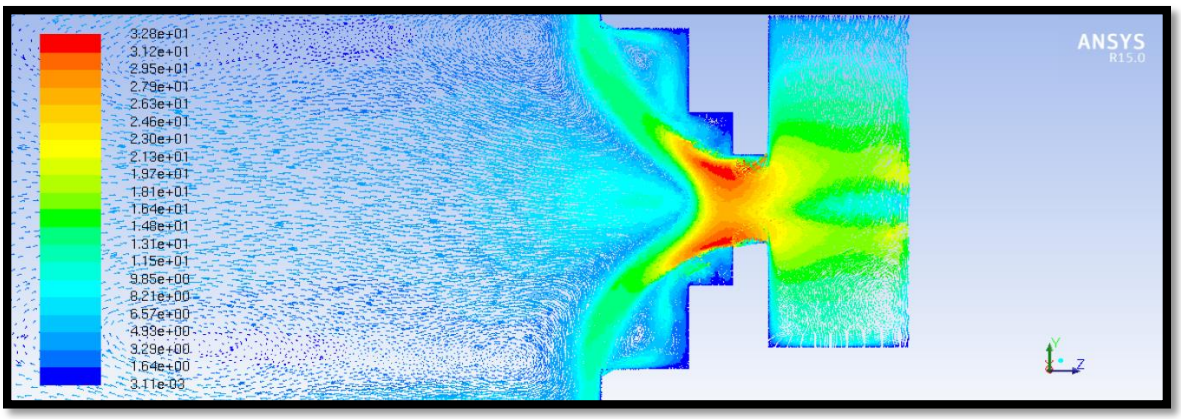

Figure 145: 80 psi, Macrospray Atomizer, Velocity Vectors, Air Core

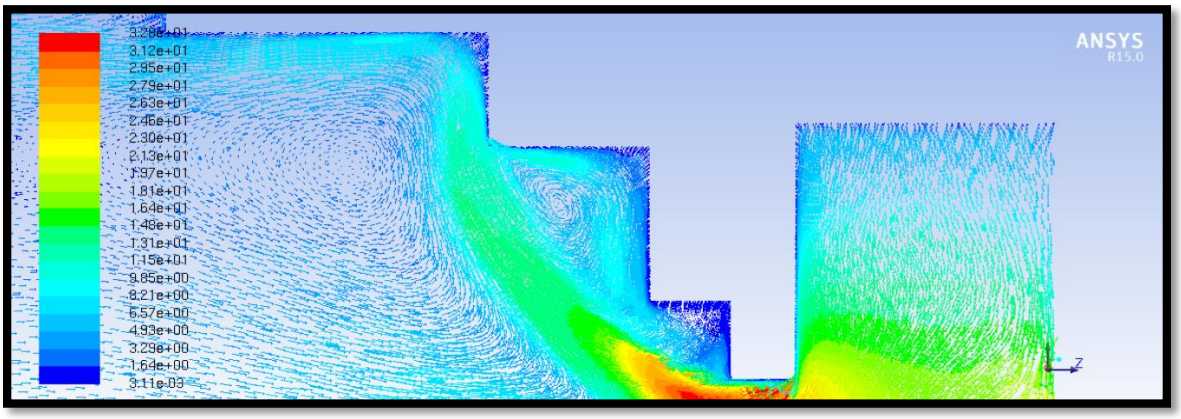

Figure 146: 80 psi, Macrospray Atomizer, Velocity Vectors, Recirculation Zones

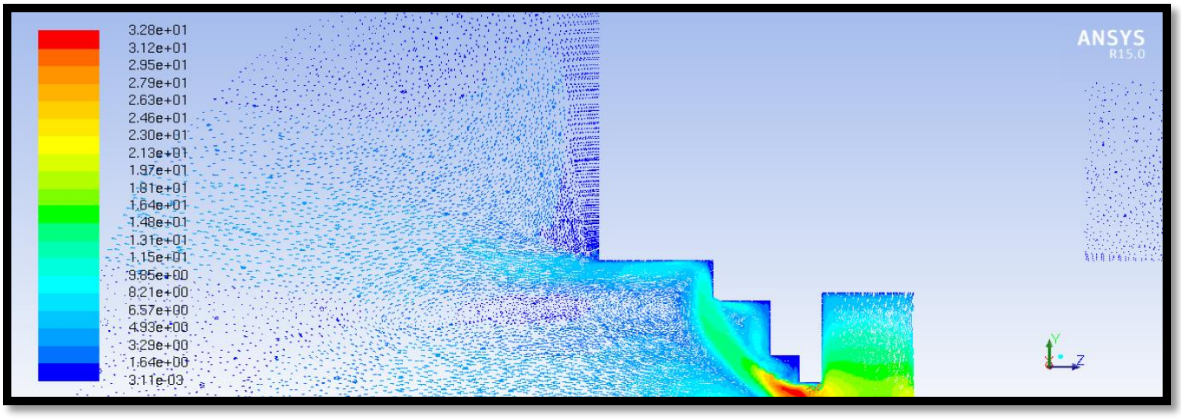

Figure 147: 80 psi, Macrospray Atomizer, Velocity Vectors, Jetstream Top

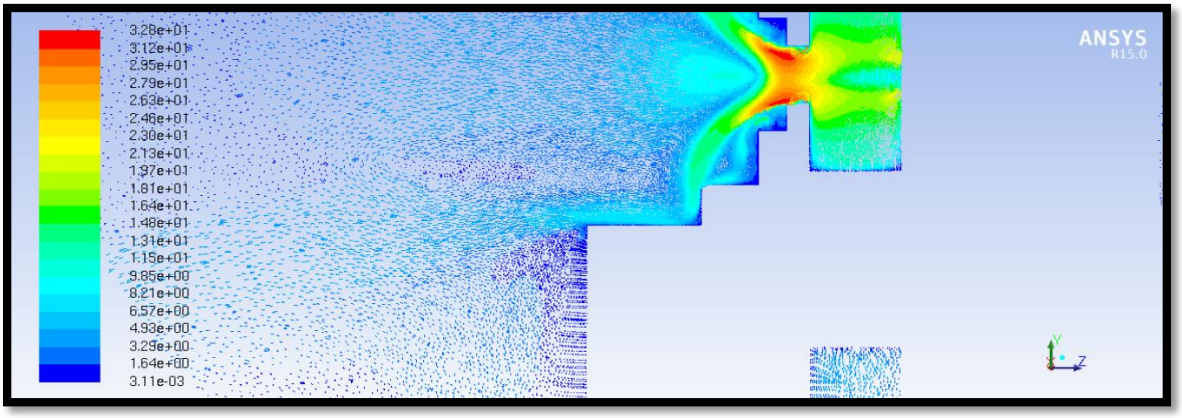

Figure 148: 80 psi, Macrospray Atomizer, Velocity Vectors, Jetstream Bottom

Appendix F

Experimental Data, Conventional Atomizer, Spray Angle Device

Table 18. Raw Experimental Data for Conventional Atomizer, Spray Angle Device

Run	Absolute Probe 1 X Value	Probe 1, X (in)	Probe 1, Y (in)	Probe 2, X (in)	Probe 2, Y (in)	Vertex, X (in)	Vertex, Y (in)
1	0.154	-0.154	0	0.182	0	0	0.25
2	0.187	-0.187	0	0.207	0	0	0.25
3	0.184	-0.184	0	0.221	0	0	0.25
4	0.163	-0.163	0	0.204	0	0	0.25
5	0.182	-0.182	0	0.209	0	0	0.25
6	0.181	-0.181	0	0.219	0	0	0.25
7	0.178	-0.178	0	0.222	0	0	0.25
8	0.177	-0.177	0	0.222	0	0	0.25
9	0.171	-0.171	0	0.207	0	0	0.25
10	0.181	-0.181	0	0.21	0	0	0.25
11	0.182	-0.182	0	0.224	0	0	0.25
12	0.181	-0.181	0	0.235	0	0	0.25
13	0.174	-0.174	0	0.21	0	0	0.25
14	0.169	-0.169	0	0.198	0	0	0.25
15	0.173	-0.173	0	0.221	0	0	0.25
16	0.187	-0.187	0	0.223	0	0	0.25
17	0.176	-0.176	0	0.219	0	0	0.25
18	0.185	-0.185	0	0.225	0	0	0.25
19	0.17	-0.17	0	0.207	0	0	0.25
20	0.168	-0.168	0	0.212	0	0	0.25
21	0.186	-0.186	0	0.212	0	0	0.25
22	0.183	-0.183	0	0.215	0	0	0.25
23	0.19	-0.19	0	0.222	0	0	0.25
24	0.184	-0.184	0	0.217	0	0	0.25
25	0.168	-0.168	0	0.194	0	0	0.25
26	0.171	-0.171	0	0.218	0	0	0.25
27	0.174	-0.174	0	0.215	0	0	0.25
28	0.187	-0.187	0	0.217	0	0	0.25

Continued from page 153							
29	0.168	-0.168	0	0.212	0	0	0.25
30	0.187	-0.187	0	0.222	0	0	0.25

Appendix G

Calculated Data for Spray Angle, Conventional Atomizer

Table 19. Law of cosines values for calculating spray angle

Run	A	B	C	Angle (radians)	Angle (degrees)
1	0.293626	0.309231	0.336	1.1814	67.7
2	0.3122	0.324575	0.394	1.3338	76.4
3	0.310413	0.333678	0.405	1.3584	77.8
4	0.298444	0.32267	0.367	1.2622	72.3
5	0.309231	0.325854	0.391	1.3256	76.0
6	0.308644	0.332357	0.40	1.3460	77.1
7	0.306894	0.334341	0.40	1.3449	77.1
8	0.306315	0.334341	0.399	1.3422	76.9
9	0.302888	0.324575	0.378	1.2915	74.0
10	0.308644	0.326497	0.391	1.3253	75.9
11	0.309231	0.335672	0.406	1.3599	77.9
12	0.308644	0.343111	0.416	1.3811	79.1
13	0.304592	0.326497	0.384	1.3067	74.9
14	0.301763	0.318911	0.367	1.2643	72.4
15	0.304021	0.333678	0.394	1.3292	76.2
16	0.3122	0.335006	0.41	1.3706	78.5
17	0.305738	0.332357	0.395	1.3328	76.4
18	0.311006	0.336341	0.41	1.3699	78.5
19	0.302324	0.324575	0.377	1.2888	73.8
20	0.301204	0.327787	0.38	1.2950	74.2
21	0.311602	0.327787	0.398	1.3430	76.9
22	0.309821	0.329735	0.398	1.3422	76.9
23	0.314006	0.334341	0.412	1.3760	78.8
24	0.310413	0.331042	0.401	1.3493	77.3
25	0.301204	0.316443	0.362	1.2516	71.7
26	0.302888	0.331699	0.389	1.3170	75.5
27	0.304592	0.329735	0.389	1.3183	75.5
28	0.3122	0.331042	0.404	1.3571	77.8
29	0.301204	0.327787	0.38	1.2950	74.2
30	0.3122	0.334341	0.409	1.3684	78.4